Missouri S&T Library and Learning Resources

Scholars' Mine

Doctoral Dissertations | Student Theses and Dissertations

1977

Theoretical and experimental investigation of oil recovery by the electrothermic technique

Samy Abdel-Hakeem El-Feky

Follow this and additional works at: https://scholarsmine.mst.edu/doctoral_dissertations

 Part of the Petroleum Engineering Commons

Department: Geosciences and Geological and Petroleum Engineering

Recommended Citation

El-Feky, Samy Abdel-Hakeem, "Theoretical and experimental investigation of oil recovery by the electrothermic technique" (1977). *Doctoral Dissertations*. 637.
https://scholarsmine.mst.edu/doctoral_dissertations/637

This thesis is brought to you by Scholars' Mine, a service of the Missouri S&T Library and Learning Resources. This work is protected by U. S. Copyright Law. Unauthorized use including reproduction for redistribution requires the permission of the copyright holder. For more information, please contact scholarsmine@mst.edu.

THEORETICAL AND EXPERIMENTAL INVESTIGATION OF OIL RECOVERY BY THE ELECTROTHERMIC TECHNIQUE

By

SAMY ABDEL-HAKEEM EL-FEKY, 1941-

A DISSERTATION

Presented to the Faculty of the Graduate School of the

UNIVERSITY OF MISSOURI-ROLLA

In Partial Fulfillment of the Requirement for the Degree

DOCTOR OF PHILOSOPHY

in

PETROLEUM ENGINEERING

1977

T4429
C. 1, 205 pages

Bound By AMERICAN BINDERY, Topeka, Kansas.

A. Helen Haney
Advisor

Charles A. Holungan

P. F. Kosky

M. D. Arnold

S. Marshall

ABSTRACT

This work investigates the feasibility of increasing oil recovery from petroleum reservoirs by the electrothermic technique. A mathematical model was developed for the prediction of reservoir response to heating by alternating electric current flow through the oil-bearing formations. The mathematical model was programmed in FORTRAN for solution on the IBM 370/168. The model used the finite difference technique to represent the differential equations that describe the system, and the sets of difference equations were solved by the Strongly Implicit Procedure (SIP) and Successive Overrelaxation (SOR).

In order to verify the mathematical model, a set of experiments was conducted to determine oil recovery from a five-spot laboratory model by cold waterflood and the electrothermic technique. The experimental data were compared with the numerically calculated responses. Agreement between calculated and experimental responses supports the assumptions of the mathematical model and the numerical solution procedure.

The mathematical model was utilized to predict the response of single layer and double layer oil reservoirs to the electrothermic process. The results indicate that the approaches described in U.M.R. Patent Disclosure No. 75-P-UMR-003 might be used for selectively heating the relatively undepleted portions of oil reservoirs.

ACKNOWLEDGMENT

This research was supported by the Egyptian Government for which thanks is given. I wish to thank Dr. L. F. Koederitz for his help with equipment. A special thanks goes to Dr. A. H. Harvey, my advisor, for his time and effort in making this research possible. I also wish to express my gratitude to Dr. M. D. Arnold, Dr. S. V. Marshall, and Dr. C. A. Johnson for having served on my graduate committee.

I wish to thank my parents, Mr. and Mrs. Abdel-Hakeem El-Feky, for their patience and encouragement.

I am greatly indebted to my wife, Asha, for her love, patience and help in the preparation of this dissertation.

TABLE OF CONTENTS

LIST OF ILLUSTRATIONS

Figure Page

Figure Page

Figure Page

Photographs

LIST OF TABLES

I. INTRODUCTION

The existence of large reserves of high viscosity oil and the increased demand for domestic crude petroleum have generated considerable interest in thermal methods of oil recovery during the past decade. Generally, in reservoirs containing heavy, viscous oil, conventional secondary recovery methods are ineffective. In contrast, thermal methods are most effective when used with heavy oils with extremely temperature-sensitive viscosities. The required thermal energy can be supplied by moving a combustion front through the reservoir, hot fluid injection, or flow of electricity through the reservoir. The latter method, which has been termed the electrothermic technique, is the subject of the present research.

The electrothermic technique applies electric current into an oil reservoir through specially designed electrodes. The electric current is dissipated by resistance of the oil-bearing formation, producing 3,413 B.T.U. per kilowatt hour. Since connate water is the current carrier and resistance heating element, brine with an appropriate salinity can be injected into the oil-bearing formation in order to maintain the resistivity of the water through which current flows at the desired level. Several plans for applying the electrothermic technique have been described (1,2,3,4). However, the details of the process are still not worked out to a definitive state. An approach for selectively heating the relatively undepleted portions of oil reservoirs is described in U.M.R. Patent Disclosure No. 75-P-UMR-003 (5). The technique involves the injection of water prior to electric heating. Resistivity of this water is selected so that heating occurs

primarily in those portions of the reservoir that were not contacted by the injected water.

In order to investigate the feasibility of applying the electrothermic technique to increase production from oil reservoirs, a prediction is made of the behavior in a five-spot reservoir pattern. The analysis falls naturally into three parts: developing a theoretical model of the system behavior, verifying the theoretical approach with a laboratory study, and utilizing the mathematical model to study the possibility of commercial use of the process.

The theoretical model consists of four partial differential equations plus appropriate equations of state for the fluid density, specification of the system transport properties, and appropriate boundary conditions. The basic fluid flow equations are developed from continuity and velocity equations for each phase, with fluid velocity represented by Darcy's Law. The effect of the nonisothermal reservoir condition on the basic multiphase flow equations is considered. The electric flow equation is developed from the continuity equation for current and Ohm's Law, and the thermal energy equation is developed from basic thermodynamic considerations. A mass balance is used to describe the distribution of salt concentration. The system of nonlinear partial differential equations is approximated by implicit finite difference equations and solved numerically. Although this technique does not give exactly the results as solutions to the original differential equations, there is evidence suggesting that the results are reliable and truncation errors are negligible. The laboratory investigation is considered in Part V.

II. LITERATURE REVIEW

The petroleum literature is almost devoid of theoretical and experimental reports which are directly related to reservoir heating by electric current flow. However, published studies of other thermal recovery processes are relatively numerous and are useful in the development of a mathematical model for the electrothermic process. Thermal recovery process models, as well as the present state of knowledge about reservoir rock and fluid properties will be reviewed briefly.

A. THERMAL RECOVERY PROCESS MODELS

As early as 1840, two French mathematicians, Fourier and Poisson, (6) derived an equation for heat transfer in the presence of fluid motion. Since that time, interest in heat transfer in porous media has been centered almost exclusively in the relevant chemical and mechanical engineering literature. A variety of materials has been used as porous media, including glass beads and sand. Much of the data collected have been for gases flowing through unconsolidated media. One of the first attempts in the petroleum industry to analyze mathematically the problem of hot fluid injection was carried out by Lauwerier (7). This study motivated a number of more recent investigations of temperature behavior during hot fluid injection (8,9,10). There are three basic components to the unsteady-state heat transfer during hot fluid injection into a porous medium:

1. Forced convection--transfer of heat by fluid motion from one location to another.

2. Conduction--transfer of heat by grain to grain conduction.

3. Convective transfer of heat between fluid and solid through a film.

Radiation has shown to be neglibile at reservoir conditions (56).

The bulk of research and published data indicates two fundamental schools of thought. For illustrative purposes, these can be categorized as Model I and Model II. In Model I, postulated by Klinkenberg (11), and Preston, et al (12), conduction is negligible and the dominant factors are forced convection and the transfer of heat between fluid and solid through a film. Their model may be described mathematically as:

$$V \frac{\partial T}{\partial X} + V \frac{\partial T}{\partial Y} + \tilde{h} (T_w - T_s) = \frac{\partial T}{\partial t} \qquad (1)$$

where: V = fluid velocity

$\tilde{h}$ = heat transfer film coefficient

T_s = temperature of sand grain

T_w = temperature of water

The first two terms on the left account for the fluid movement, while the third term accounts for the surface transfer coefficient between the fluid and sand particles.

In Model II, first postulated by French mathematicians Fourier and Poisson (6), the differential equation governing heat flow in the presence of fluid motion can be expressed as:

$$K_{te} \nabla^2 T = [\phi \rho_f C_f + (1-\phi) \rho_s C_s] \frac{\partial T}{\partial t} + [\rho_f C_f \frac{\partial T}{\partial x} V_x + \rho_f C_f \frac{\partial T}{\partial y} V_y] \qquad (2)$$

where: K_{te} = thermal conductivity of porous medium, Btu/hr/^{o}F/ft

∇ = Laplacian operator

ϕ = porosity, fraction

ρ = density, lb/ft^{3}

C = heat capacity, Btu/lb/^{o}F

V_x = velocity in X direction, ft/hr

V_y = velocity in y direction, ft/hr

In this model, heat conduction is evidenced by the term on the left; heat convection is given by the second term on the right. The rock and fluid temperatures are assumed equal.

The study conducted by Preston and Hazen (12) suggests that Model I is not a realistic representation of the heat flow in oil reservoirs. Model II, however, seems to be adequate for this purpose.

B. RESERVOIR ROCK AND FLUID PROPERTIES

Reservoir rock and fluid properties that are pertinent to this research are considered below.

1. Electric Properties of Hydrocarbon Reservoirs. When an alternating current circulates through a rock, the current flow can be divided into two main components: an ohmic current which flows in phase with the applied voltage and is independent of frequency; and a displacement current which is 90^{o} out-of-phase with the applied voltage and is directly proportional to frequency. Thus in order to specify the behavior of porous rocks under the action of an e.m.f., we must have a knowledge of two parameters:

i. a parameter determining the conduction current. The electric conductivity of the medium serves this purpose.

ii. a parameter determining the electric displacement. The specific inductive capacity or the dielectric constant of the medium serves this purpose.

a. Electrical Conductivity. Conduction of electricity in most porous rocks is almost entirely through the water contained in the pores. Water resistivity (the reciprocal of conductivity) has been found to depend primarily on salinity and temperature. The resistivity of the rock depends on water resistivity, water saturation, and the way in which the water is distributed in the rock. Various formulas have been proposed to relate the rock resistivity to the connate water resistivity. The generally accepted form of high porosity sand is that of Humble and Archie (13).

$$R_r = \frac{0.62 R_w}{\phi^{2.15} S_w^2} \tag{3}$$

where: R_r = rock resistivity, ohm-m

R_w = water resistivity, ohm-m

S_w = water saturation, fraction

The dependence of resistivity on temperature for either an electrolyte or a rock saturated with an electrolyte is given by the equation:

$$(R_r)_T = \frac{(R_r)_{18}}{1 + \alpha(T - 18)} \tag{4}$$

where: $(R_r)_T$ = rock resistivity at temperature T° C

$(R_r)_{18}$ = rock resistivity at 18° C

$\alpha = 0.025$

T = temperature, $^\circ$ C.

b. Dielectric Constant. Media have been classified as conductors or dielectrics according to the ratio $\sigma/(\omega\varepsilon)$, which is the ratio between the magnitude of the conduction and the displacement currents in the medium under the action of an e.m.f. In this relationship:

σ = conductivity, mhos/meter

ε = permittivity, farad/meter

$\omega = 2\pi f$

f = frequency in cycles per second.

Water, which is the current carrying element in most porous rocks, is made up of molecules in which the geometric center of the negative charges does not coincide with the geometric center of the positive charges. When an electric field is applied across such a material, these molecules tend to rotate about their centers of gravity until the negative side faces the positive pole of the field and the positive side faces the negative pole. The rotation of these molecules constitutes an electric current. If the molecules have rotated into alignment with the electric field, the alignment results in a net charge or polarization. Water molecules become aligned with an electric field in about a thirtieth of a microsecond. Water has a relative dielectric constant of about 81. Table 1 shows the electrical properties of water, oil, and quartz.

The average power dissipated per cubic meter in quartz with a relative permittivity of 5 and a power factor of 0.0003 under the action of an e.m.f. of 1000 volt/meter and frequency of 60 cycles/second is found to be 5.0×10^{-6} watts/m^3.

TABLE I

ELECTRICAL PROPERTIES OF WATER, OIL, AND QUARTZ
AT 20° C

Substance	Relative Permittivity	Conductivity mhos/meter
Water (distilled)	81.0	10^{-4}
Oil (mineral)	2.2	10^{-14}
Quartz	5.0	10^{-17}
Sea water	81.0	4

Permittivity of vacuum (dielectric constant) = 8.85×10^{-12} farad/meter.

Media have been classified as belonging to conductors or dielectrics according to the ratio $\frac{\sigma}{\omega\varepsilon}$

dielectrics: $\frac{\sigma}{\omega\varepsilon} < 100$

conductors: $\frac{\sigma}{\omega\varepsilon} > 100$

2. Thermal Properties of Hydrocarbon Reservoirs. A theoretical analysis of the mechanisms involved in the displacement of immiscible fluids was originally established by Buckley and Leverett (14). An important part of this frontal displacement theory is that the flooding behavior is largely dependent upon the mobility of the displacing phase (K_{rw}/μ_w) relative to that of the displaced phase (K_{ro}/μ_o). Heat affects both of these parameters and must be considered in a noniso-thermal flow process.

Certain properties of the overall reservoir system or of its phases are strongly influenced by temperature variation. For purposes of discussion, it will be convenient to divide the pertinent properties into fluid properties and rock properties.

a. Thermal Properties of Fluids. This discussion will be limited to the temperature dependent behavior of viscosity, heat capacity, and thermal conductivity of reservoir fluids and fluid mixtures.

The variation with temperature of the viscosity of water is well known (15). However, data on the sensitivity of the viscosity of hydrocarbon liquids to temperatures are more limited. A relatively early publication by Beal (16) and Schild's more recent investigation (17) are the sources of data employed in this study. Suitable empirical formulas for the heat capacities of water and reservoir hydrocarbon liquids are also available (18).

Data on the thermal conductivity of reservoir fluids and fluid mixtures are incomplete. Correlations of this property with temperature are not available for reservoir liquids. One model of the thermal conductivity of liquid mixtures is given in a study by Grover and

Knudsen (19). Their investigation of heat transfer effects associated with two-phase turbulent flow experiments led to the development of an expression for the thermal conductivity of a mixture of two immiscible liquids.

b. Thermal Properties of Rocks. A number of important rock properties are influenced by temperature variation. Information is available on the relationship of this effect to the heat capacity, thermal conductivity, and absolute permeability of the rock.

An experimental investigation by Somerton (20) indicated that the heat capacity of reservoir solids increases linearly and fairly rapidly with temperature within the range of temperatures encountered in hot fluid injection processes. Somerton also showed that the heat capacity increases as the rock silica-alumina ratio declines. Data published by Hougen, Watson, and Ragatz confirm this conclusion. Generalized expressions for this property are still not available.

A large number of investigations of the effective thermal conductivity of a porous system have been made (20,21,22,23,24,25,26,27,28,29). Somerton (20) presented a general expression developed by Asaad (24) for the behavior of reservoir rock thermal conductivity. The equation is substantiated by Somerton's experimental results. The relationship may be written:

$$K_{te} = K_{ts} \left(K_{tf}/_{ts}\right)^{m} \qquad (5)$$

where

$m = c\phi$

c = constant = 1.2

K_{ts} = sand thermal conductivity

K_{tf} = fluid thermal conductivity

However, Asaad's formulation was extremely inaccurate when tested against the data which Kunii and Smith (21) obtained for unconsolidated and consolidated systems. Later studies by these researchers presented an expression for effective thermal conductivity in unconsolidated and consolidated porous media (25). The expression used by Kunii and Smith requires knowledge of the system particle mean grain diameter and fluid thermal conductivity. They extended the information to situations in which fluid flow takes place (24). Gopalarathnam, Hoelscher, and Laddha (26) have extended the work of Kunii and Smith on the role of fluid movement in conductive heat transfer in porous systems. They developed an expression for effective thermal conductivity which is equal to the stagnant effective conductivity plus a term involving the system Prandtl and Reynolds numbers and the fluid mass flow rate. Adivarahan, Kunii, and Smith (27) obtained a similar expression for effective thermal conductivity. In addition, they presented an expression relating stagnant conductivity to porosity.

The following representations are employed for the thermal conductivity of the system and the system constituents:

$$K_{tf} = K_{to}K_{tw}\left[(1 + \mu_o/\mu_w) \;/\; (K_{to} + (\mu_o/\mu_w)K_{tw})\right] \tag{6}$$

$$K_{te} = K_{ts}^{(1-\phi)}K_{tf}^{\phi\,(S_o+S_w)} \tag{7}$$

$$K_{ts} = 6.75 - 0.01(T - 80.0), \tag{8}$$

where T is temperature in $^{\circ}F$.

Equation (6) is the relation proposed by Grover and Knudsen (19). Equation (7) is based on Woodside and Messmer's work (28). Equation (8) is based on the data presented by Crichlow (30) for unconsolidated sand. For consolidated sand the form suggested by Adivarahan, Kunii, and Smith is used:

$$K_{ts} = 25\ (1-\phi)\ \exp\ \left[-U\ \frac{\phi}{1-\phi}\right],\ U = 10 \qquad (9)$$

Reservoir system properties are considered in Appendix C.

The dependence of absolute permeability on temperature in the presence of hot fluids is evident from the experimental studies of Somerton, Mehta, and Dean (23), Somerton and Gupta (31), and Waldorf (32). The first study cited revealed that absolute permeability begins to increase rapidly with temperature for temperatures above 500° C. The investigation by Somerton and Gupta indicated that the introduction of salt solutions during reservoir heating influences the extent of permeability alteration by temperature, provided the temperature is above the melting point of the salt used. Waldorf's experiments (32) are more directly pertinent to hot fluid injection studies. He conducted tests to determine whether or not the introduction of steam would cause plugging of the pore space in water-sensitive sandstone having a high montmorillonite content. He demonstrated that the steam actually dehydrates the montmorillonite in the system, leading to an increase in permeability for the sandstone used.

Several investigators (33,34,35,36) have studied the effect of temperature on relative permeability, but so far this phenomenon is not clearly understood. Studies by Housain (33) and Edmundson (36)

have revealed that the relative permeability of water-wet porous media to liquid hydrocarbons increases with temperature. Housain attributed this behavior to a decrease in the interfacial energy existing at the oil-water interface. While Housain's experiments were conducted only with refined oils, Edmundson conducted a number of tests using native crude oils. The relationship between relative permeability and temperature change during these tests was not as consistent as behavior associated with the refined oils. Both investigators, however, reported a decrease in residual oil saturation with increase in temperature. Habowski (35) and Poston (34) found that as the temperature increases, the irreducible water saturation increases and the residual oil saturation decreases. They also found the water-oil relative permeability ratio to be temperature-sensitive, but no general trend was identified.

III. DEVELOPMENT OF THE MATHEMATICAL MODEL

A complete description of reservoir behavior during the electric heating process requires the use of a system of equations which specify the thermal energy and fluid content of the reservoir as functions of position and time. An adequate description of the non-isothermal behavior is obtained from flow equations for the fluid phases, a mass balance for each phase, a flow equation for the electric current, and a thermal energy balance, combined with appropriate equations of state.

In considering the development of the reservoir behavior simulators, it will be convenient to state initially certain assumptions which are common to all of them. This will be followed by the development of the system of equations.

The following assumptions are implicit in the development of the system of equations:

1. Fluid flows only in directions normal to the wellbore.
2. The wellbore is vertical so that all flow is horizontal and two-dimensional.
3. The reservoir is homogeneous with regard to porosity and permeability.
4. The system is of uniform thickness.
5. The reservoir contains no free gas.

The development of the basic system of equations will be considered in the order stated.

A. MASS FLOW EQUATIONS

The most general form of fluid flow is described by the Navier-Stokes equation or the equation of conservation of momentum. For slow

(laminar) flow through porous media, the macroscopic field equation commonly used to describe fluid flow is Darcy's Law, which states that volumetric flux at a point is proportional to the gradient of the flow potential at that point. The suitability of this expression for describing fluid movement associated with thermal recovery processes may be assessed by consideration of the assumptions used in deriving Darcy's Law from the Navier-Stokes equation. The assumptions involved are discussed in two papers by Hubbert (37,38). The crux of Hubbert's argument in deriving Darcy's Law from the Navier-Stokes equation is that the inertial force acting on the fluid become negligible in comparison with the viscous resistance force as the volumetric flux tends to zero. If this tendency holds, the inertial force may be assumed negligible and Darcy's Law obtained by equating the driving force and the viscous resistance force. Only those assumptions presented by Hubbert which might be violated in the system under consideration will be presented here.

1. Assumptions. i. The flow conditions in the system satisfy a modified Reynolds criterion for laminar flow in porous media which Hubbert has postulated. Hubbert's modified Reynolds number must be less than one if this assumption is to be satisfied. This criterion may not be met near the wellbore during steam injection.

ii. The vector field formed by the gradient of the flow potential at every point in the system is conservative, i.e., irrotational. This condition is met in isothermal systems or in systems for which constant temperature surfaces are everywhere parallel to constant flow potential

surfaces. Possible exceptions to these requirements are discussed in Appendix A.

2. Statement of the Equations. The volumetric flux for oil and water can be written by Darcy's Law as follows:

$$V_o = -(K_o/\mu_o) \text{ grad } (P_o) \tag{10}$$

$$V_w = -(K_w/\mu_w) \text{ grad } (P_w) \tag{11}$$

In these expressions V is velocity vector, K is the effective permeability, μ is the fluid viscosity, and P is the pressure acting on the fluid. The subscripts o and w denote the oil and water phases, respectively.

B. CONTINUITY EQUATIONS

In a fixed volume, the increase with time of the amount of any physical quantity may be written as:

$$\begin{bmatrix}\text{net flow of quantity into fixed volume}\end{bmatrix} + \begin{bmatrix}\text{net amount of quantity generated in volume}\end{bmatrix} = \begin{bmatrix}\text{increase of quantity in volume}\end{bmatrix}$$

This is a general expression, and the continuity equations are obtained from it by letting the mass of the fluid component be the physical quantity to which the expression refers (39). The two mass conservation equations for oil and water can be written as:

$$\nabla \cdot (\rho_o V_o) \mp q_o + \frac{\partial}{\partial t} (\rho_o \phi S_o) = 0 \tag{12}$$

$$\nabla \cdot (\rho_w V_w) \mp q_w + \frac{\partial}{\partial t} (\rho_w \phi S_w) = 0 \tag{13}$$

In these expressions q is the mass source term per unit volume. In this development, transport of mass by molecular diffusion is neglected. Relative importance of liquid-liquid diffusion is considered in Appendix B.

Combining Darcy's equations with the corresponding mass conservation equation gives the partial differential equations governing flow of oil and water within a reservoir sand:

$$\nabla \cdot K_o \rho_o / \mu_o \ (\nabla P_o) \pm q_o = \frac{\partial}{\partial t}(\phi \rho_o S_o) \tag{14}$$

$$\nabla \cdot K_w \rho_w / \mu_w \ (\nabla P_w) \pm q_w = \frac{\partial}{\partial t}(\phi \rho_w S_w) \tag{15}$$

These equations differ from the flow equations encountered in the usual reservoir engineering in that fluid viscosities and densities are both temperature and pressure dependent. The oil and water phase pressures at a point in the sand differ by the capillar pressure,

$$\begin{aligned} P_c &= P_o - P_w \\ P_c &= P_c(S_w) \end{aligned} \tag{16}$$

which is defined to depend on the local saturation and on the direction of saturation change (increasing or decreasing). It will be assumed that for a displacement situation the water saturation will everywhere be increasing; thus capillary pressure data taken under imbibition conditions will uniquely describe the relationship between P_c and S_w.

The condition of saturation in a system that contains no gas is:

$$S_o + S_w = 1 \tag{17}$$

The initial conditions are:

$$P(x,y,t=0) = P_{initial}$$

$$S_w(x,y,t=0) = S_{w\ initial}$$

$$S_o(x,y,t=0) = S_{o\ initial}$$

Statements of the boundary conditions are simply $U_{pb} = 0$ for the two fluids, where U_{pb} is the component of the flow vector in the direction perpendicular to the confining boundary.

Reservoir rock and fluid properties are considered in Appendix C.

C. ELECTRIC FLOW EQUATION

When an alternating voltage is applied to a porous medium saturated with oil and water (a conducting dielectric), both conduction and displacement currents are present. Expressing the instantaneous value of the electric field by E, the conduction current is then

$$\tilde{J}_{conduction} = \sigma E \tag{18}$$

and the displacement current is

$$\tilde{J}_{displacement} = \varepsilon \frac{\partial E}{\partial t} \tag{19}$$

Expressing the time variation of the field by:

$$E = E_o\, e^{\tilde{i}\omega t} \tag{20}$$

where: $\omega = 2\pi f$

f = frequency, cycles/second

$$\tilde{J}_{displacement} = \tilde{i}\omega\varepsilon E \tag{21}$$

Referring to the time-phase diagram of Figure 1, the total current density $\tilde{J}_{total}$ can be expressed in terms of its component parts

$$\tilde{J}_{total} = \sigma E + i\omega\epsilon E \tag{22}$$

The operator $\tilde{i}$ in the displacement current term signifies that the displacement current is advanced in phase by 90^{o} with respect to the conduction current.

The relative importance of the displacement current to the conduction current can be determined by considering the ratio $\sigma/(\omega\epsilon)$, which is the ratio of the conduction current to the displacement current. The best approach to determining the dielectric constant of a rock is the experimental investigation. Because of the lack of experimental data, a logarithmic mixing rule is sometimes used to predict the dielectric constant for a mixture of materials:

$$\log\epsilon = v_1\log\epsilon_1 + v_2\log\epsilon_2 + v_3\log_3 \tag{23}$$

where v_1, v_2 and v_3 are the volume fractions of the three materials forming a composite dielectric, and ϵ_1, ϵ_2, ϵ_3 are the dielectric constants for each of the three components. Applying the same rule to predict the permittivity for 30% porosity sand, saturated with 20% sea water and 80% oil, the permittivity is found to be equal to $4.2\text{x}10^{-11}$ farad/meter. The electric conductivity of the same medium is equal to 0.02 mhos/meter at 20^{o} C (applying equation 3). Since the ratio $\sigma/(\omega\epsilon)$ is greater than $1.0\text{x}10^{6}$, the displacement current is negligible and equation (22) reduces Ohm's Law:

$$\tilde{J} = \sigma E$$

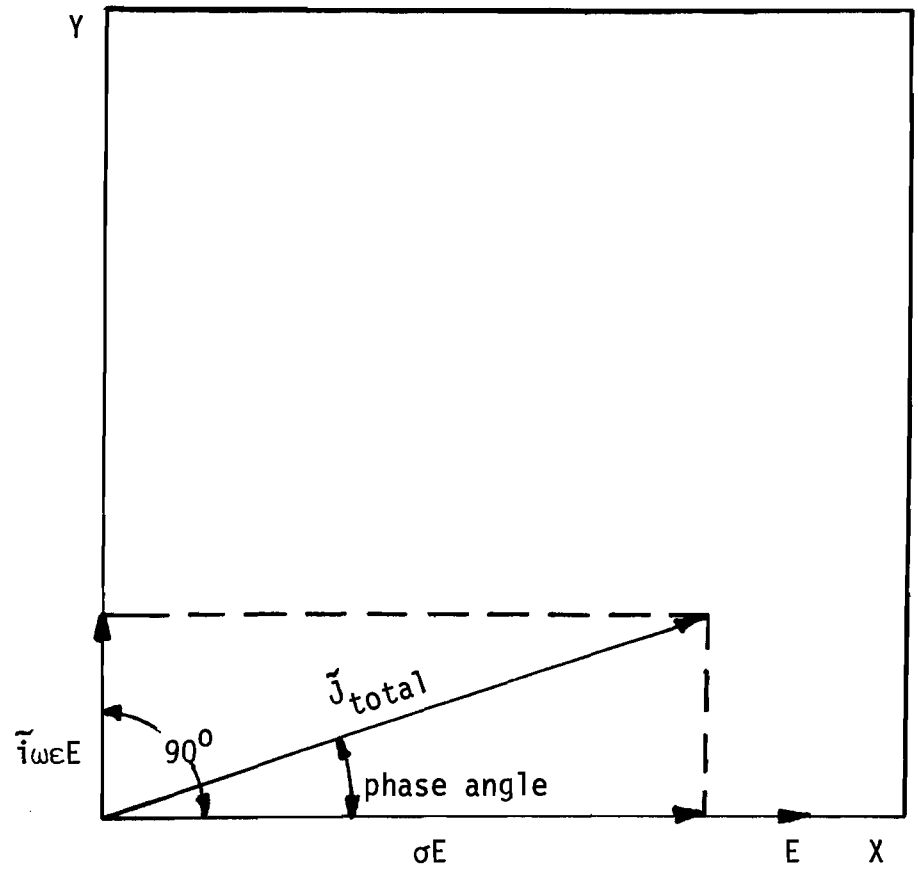

FIGURE 1. TIME-PHASE DIAGRAM FOR A CONDUCTING DIELECTRIC

(SOURCE : REFERENCE 28)

1. Divergence of $\tilde{J}$ and Continuity Relation for Current. Let it be assumed that the small volume element dv shown in Figure 2 is located inside of a porous medium. The current density $\tilde{J}$ is a vector having the direction of the current flow. Considering the situation if the current is not steady, then the difference between the total current flowing out of and into the elemental volume must equal the rate of change of electric charge inside the volume. Specifically, a net flow of current out of the volume (positive current flow) must equal the negative rate of change of charge with time (rate of decrease of charge). Now the total charge in the volume dv of Figure 2 is $\rho_c dv$ where ρ_c is the average charge density.

Therefore

$$\oint_s \tilde{J} \cdot ds = - \iiint_R \frac{\partial \rho_c}{\partial t} dv \tag{25}$$

The product of the current density and the area of a face of the volume element yields the current passing through the face. Current flowing out of the volume is taken as positive and current flowing in as negative. The integral of the normal component of $\tilde{J}$ over the surface s of the volume is equal to the sum of the outward current for the four faces of the volume element, or

$$\oint_s \tilde{J} \cdot ds = \iiint_R \nabla \cdot \tilde{J} \, dv \tag{26}$$

Equating equations (25) and (26) yields:

$$\nabla \cdot \tilde{J} = - \frac{\partial \rho_c}{\partial t} \tag{27}$$

This is the general continuity relation between current density $\tilde{J}$ and the charge density at a point. It is a point relation that applies

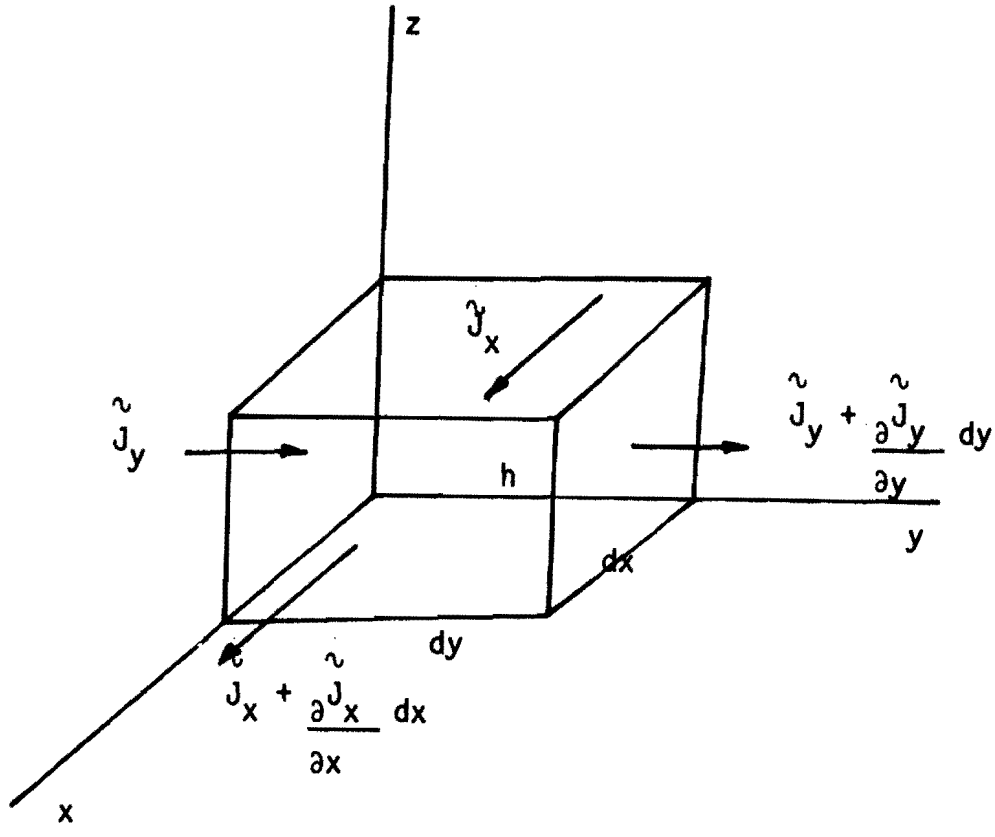

FIGURE 2. CONSTRUCTION USED TO DEVELOP DIFFERENTIAL EXPRESSION FOR DIVERGENCE OF CURRENT

to any point in the medium where current is flowing.

The electric field strength E can be represented by the relation

$$E = - \nabla \Psi \tag{28}$$

where Ψ is the e.m.f.

Combining equation (24) with the continuity equation for current flow (27) and replacing E by the scalar function in equation (28) we obtain the partial differential equation governing current flow in the medium.

$$\frac{\partial}{\partial x} \left(\frac{\sigma \partial \Psi}{\partial x}\right) + \frac{\partial}{\partial y} \left(\frac{\sigma \partial \Psi}{\partial y}\right) = \frac{\partial \rho_c}{\partial t} \tag{29}$$

The four boundary conditions are simply $\frac{\partial \Psi}{\partial n} = 0$, where n is the direction of the perpendicular to the confining boundary.

D. THERMAL ENERGY EQUATION

A precise development of the expression for the thermal energy distribution in a reservoir system would require formulation of separate energy equations for the solid and fluid phases. However, if it is assumed that the transfer of heat between phases is practically instantaneous, then an adequate expression is obtained using only one equation. The single statement may be formulated on a volume element dv located inside the porous medium (Figure 3) as:

The net heat conducted and convected into the element per unit time	+	The energy generated within the element per unit time	=	The change in internal energy of the element per unit time		(30)

The following assumptions are involved in the above statement.

1. Transfer of heat between the solid and liquid phases is instantaneous. Bailey and Larkin (40) demonstrate that this approximation is quite reasonable. It is assumed that heat transfer coefficient is very large so that at any point $T_{rock} \approx T_{fluid}$.

2. Conversion from mechanical to thermal energy because of viscous dissipation may be neglected. An examination of the magnitude of friction effects by Miller (41) partially verifies this assumption.

3. Reversible interchange of energy between thermal and mechanical forms is quite small in the liquid phase.

Expressions for the heat flow terms illustrated by Figure 3 can be written as follows:

$$Q_{1k} = -K_{te}(hdy)\frac{\partial T}{\partial x}$$

$$Q_{1c} = \rho CV_x(hdy)T$$

$$Q_{3k} = -K_{te}(hdx)\frac{\partial T}{\partial y}$$

$$Q_{3c} = \rho CV_y(hdx)T$$

$$Q_{2k} = -K_{te}(hdy)\frac{\partial T}{\partial x} - (hdydx)\frac{\partial}{\partial x}(K_{te}\frac{\partial T}{\partial x})$$

$$Q_{2c} = \rho CV_x(hdy)T + hdydx\frac{\partial}{\partial x}(\rho CV_x T)$$

$$Q_{4k} = -K_{te}(hdx)\frac{\partial T}{\partial y} - (hdydx)\frac{\partial}{\partial y}(K_{te}\frac{\partial T}{\partial y})$$

$$Q_{4c} = \rho CV_y(hdx)T + hdydx\frac{\partial}{\partial y}(\rho CV_y T)$$

$$\rho CV = \rho_o C_o V_o + \rho_w C_w V_w$$

$$\dot{q} = I^2 R_r \quad (3.413)$$

$$\dot{S} = 2K_{ta}(dxdy)\frac{\partial Ta}{\partial z}\Big| \; z = h$$

Substituting into equation (30) we obtain:

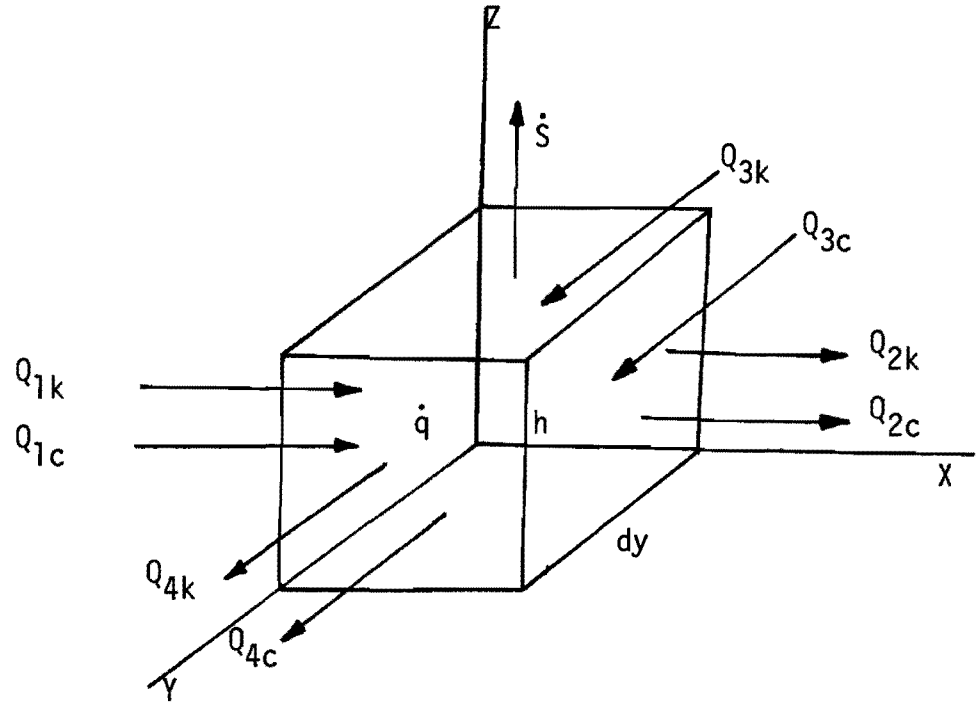

Q_{1k} : Heat conducted into the element, x direction / unit time
Q_{1c} : Heat convected into the element, x direction / unit time
Q_{3k} : Heat conducted into the element, y direction / unit time
Q_{3c} : Heat convected into the element, y direction / unit time
Q_{2k} : Heat conducted out of the element, x direction / unit time
Q_{2c} : Heat convected out of the element, x direction / unit time
Q_{4k} : Heat conducted out of the element, y direction / unit time
Q_{4c} : Heat convected out of the element, y direction / unit time
$\dot{S}$: Heat loss to adjacent stratum / unit time
$\dot{q}$: Heat generated within the element / unit time

FIGURE 3. CONSTRUCTION USED TO DEVELOP DIFFERENTIAL EXPRESSION FOR THE THERMAL ENERGY EQUATION

$$\frac{\partial}{\partial x}(K_{te}\frac{\partial T}{\partial x}) + \frac{\partial}{\partial y}(K_{te}\frac{\partial T}{\partial y}) + \frac{\dot{S}}{dxdyh} + \frac{\dot{q}}{dxdyh} -$$

$$\frac{\partial}{\partial x}((\rho_o V_{ox} C_o + \rho_w V_{wx} C_w)T) - \frac{\partial}{\partial y}((\rho_o V_{oy} C_o + \rho_w V_{wy} C_w)T) =$$

$$\frac{\partial}{\partial t}\{(\phi S_o \rho_o C_o + \phi S_w \rho_w C_w + (1-\phi)\rho_r C_r)T\} \qquad (31)$$

where:

k_{te} = thermal conductivity of porous medium, BTU/Unit Time Ft °F.

K_{ta} = thermal conductivity of adjacent strata, BTU/Unit Time Ft °F.

T = temperature of porous medium, °F.

T_a = temperature of adjacent stratum, °F.

C = specific heat, BTU/Ib °F.

ρ = density, Lb/Ft^3.

V = fluid velocity, Ft/Unit Time.

$\tilde{I}$ = current flowing within the finite element, amps.

R_r = resistance of the element, ohm.

Power factor $\simeq 1$.

Unit time in the above expressions = 1 hour.

Boundary conditions: Statements of the four boundary conditions are simply $\frac{\partial T}{\partial n} = 0$, where n is the direction of the perpendicular to the confining boundary.

Initial condition: $T(x,y,0) = T_{initial}$

The temperature derivative in the heat loss term, $\frac{\partial T_a}{\partial z}\Big|_{z=h}$, is approximated by solving the following equation:

$$\frac{\partial^2 T_a}{\partial z^2} = \frac{\rho_r C_r}{K_{ta}} \frac{\partial T_a}{\partial t} \qquad (32)$$

with

$$T_a(z,0) = T_{initial}$$

$$T_a(z,t) = T_{initial} \text{ as } z \to \infty$$

$$T_a(h,t) = T(t)$$

The thermal energy equation is derived from basic thermodynamic considerations in Appendix D.

IV. NUMERICAL SOLUTION OF THE MATHEMATICAL MODEL

The evident complexity of the reservoir simulation equations makes the task of formulating analytical solutions formidable. While elegant techniques have resulted in such solutions for simpler problems, nothing is available which would be effective with the model presented here. This is clear from the approach which Ames (42) has reviewed. Consequently, even an approximate analytical technique must be ruled out as being presently impossible.

A commonly used technique, when confronted with a system of nonlinear partial differential equations is to solve the finite difference equivalent of the system numerically. This approach has proven to be a powerful one in many instances, and will be followed in this work.

The finite difference scheme is well documented throughout the literature (43,44,45) as a means of solving problems of this type. The methods of solution are varied, and some schemes are applicable only to specific types of problems.

Formulation of the finite difference equations is considered in Appendix E. The system of finite difference equations is an approximation of the differential equations and may converge to a result slightly different from that which would be developed from the original differential equations. An approach to verification of the solution is the comparison of the behavior predicted by the simulation with experimental data. The required data were obtained from a set of experiments conducted for that purpose, and this experimental investigation is considered in Part V.

The experiments with which the calculations are to be compared were conducted in a thin sand pack simulating one-half of a five-spot element with inside dimensions of 30 x 30 x 1.6 inches. A set of computer runs were made, corresponding to the conditions of the experiments conducted in this study, to test the validity of the mathematical model and the numerical solution. Data used with the computer runs throughout the entire calculations are presented in Table II. The functions $P_c(S_w)$, $K_{ro}(S_w)$, and $K_{rw}(S_w)$ were described by tables. Linear interpolation between adjacent values in the tables were used for intermediate values of the arguments. The functions are plotted in Figures 57 and 58 in Appendix C.

In order to achieve what has been termed a stabilized displacement process, in which the flowing pressure gradient should be high compared with the capillary pressure difference between the flowing phases, a high water injection rate and a small time step size were used in the calculations. Results of the calculations are discussed in Part VII.

TABLE II

DATA FOR COMPUTING FIVE-SPOT MODEL

CONSTANTS	
Side of Square, inches	= 30.0
Thickness, inches	= 1.6
Porosity, fraction	= 0.38
Permeability, darcy	= 11.1
Grid Size in X-Direction, inches	= 2.0
Grid Size in Y-Direction, inches	= 2.0
Time Step Size, seconds	= 5.0
Viscosity of Oil @ 60 °F, cp	= 15.0
Alternating Voltage Applied, volts	=110.0
Initial Temperature Distribution, °F	= 80.0

V. DESCRIPTION OF EQUIPMENT

A schematic diagram of the apparatus used to investigate the electrothermic process is shown in Figure 4. The essential components of the system are a flow model, injection equipment, an a.c. voltage recorder, and a temperature recorder. Detailed description of the equipment follows:

A. FLOW MODEL

In order to obtain an areal flow model suitable for the present study, an unconsolidated porous medium was packed in a thin Lucite model representing one-half of a five-spot element. Figure 5 shows a detailed drawing of the model. In as much as the model must be electrically and thermally insulated, it was built of Lucite. The transparent Lucite and the use of colored oil permitted observation of the movement of the oil-water interface. Internal dimensions of the model are: 30 x 30 x 1.6 inches. Because of the thinness of the model, gravity effects were considered negligible. Locations of the four wells are shown in Figure 5. Each well is cased with 3/8-inch perforated stainless steel tubing, wrapped with 100-mesh stainless steel screen. The wellhead includes a pressure gauge and an outlet for fluid injection or production. The wells will be referred to by their numbers as shown in Figure 5.

B. POROUS MEDIUM

The porous medium was prepared by washing granular silica sand (70 - 100 mesh) repeatedly and then drying in an oven for twelve hours. This sand was packed into the Lucite model.

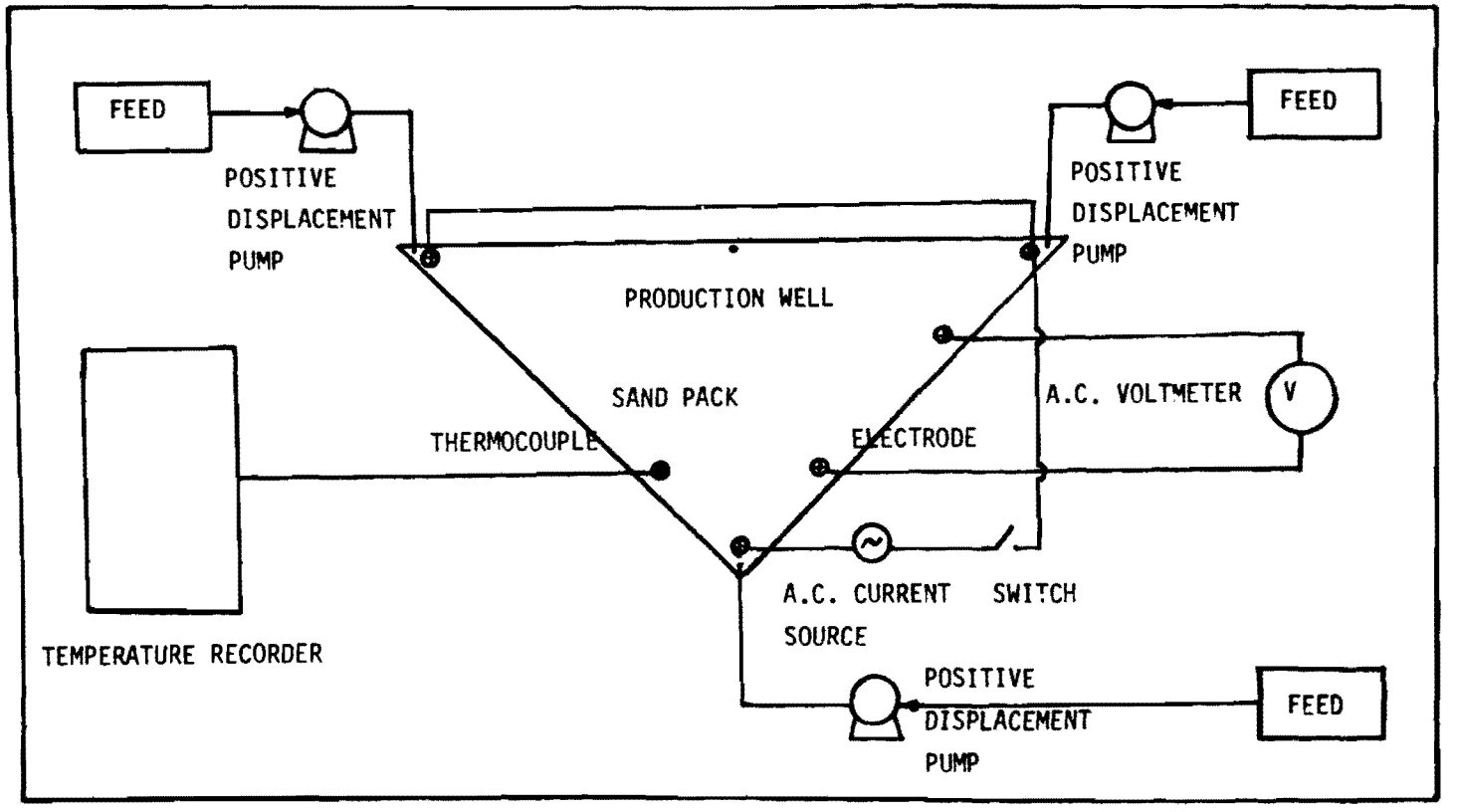

FIGURE 4. SCHEMATIC DIAGRAM OF EQUIPMENT USED FOR LABORATORY RESEARCH ON OIL RECOVERY BY THE ELECTROTHERMIC TECHNIQUE

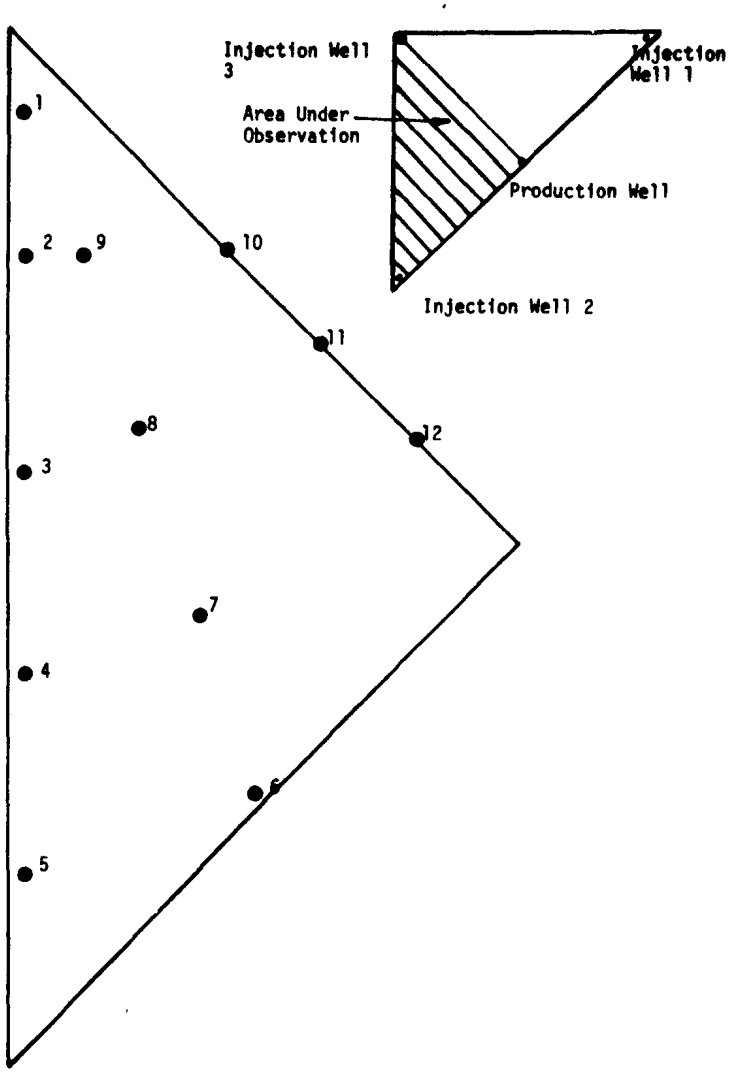

FIGURE 5. THERMOCOUPLE LOCATIONS

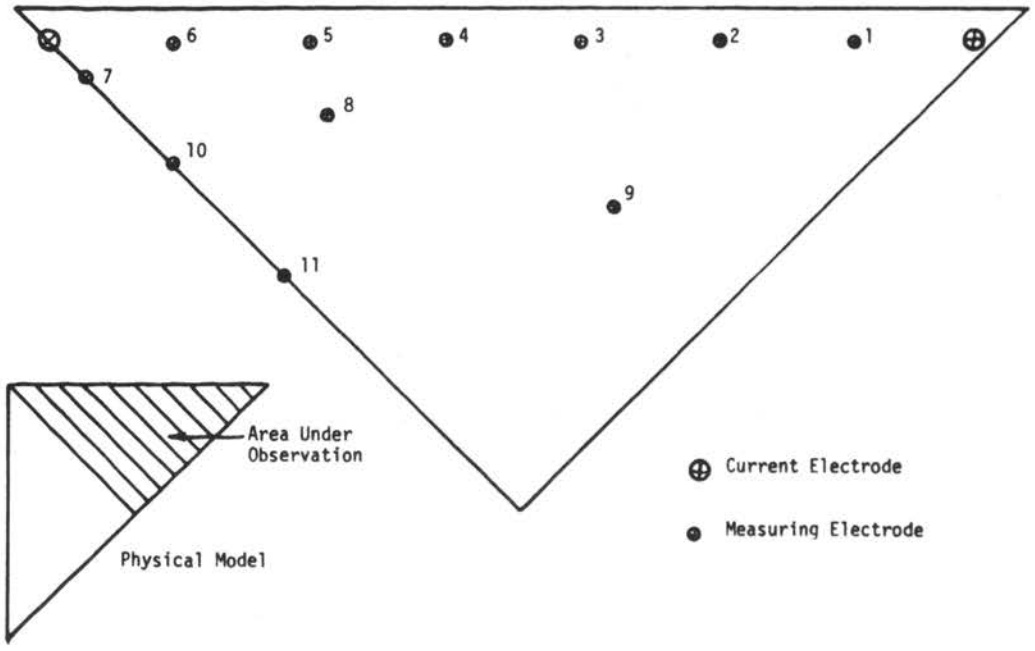

FIGURE 6. ELECTRODE LOCATIONS

The porosity of the pack was determined volumetrically after packing by saturating the evacuated sand pack with water, and checked by calculating the grain volume of the sand (based on grain density of 2.65 gm./c.c.). The porosity obtained was 37.6%. The permeability was determined experimentally by using Darcy's Law for a fluid flowing under a changing potential head in a linear pipe having 0.5 inch diameter and 9.84 inch length:

$$q = \underset{\text{Porous Medium}}{AKH/1030\mu_w L} = \underset{\text{Pipe Flow}}{-A\frac{dH}{dt}} \qquad (33)$$

which, rearranged and integrated between limits H_i at t = 0 to H at time t, gives:

$$\text{Ln } H = -Kt/\mu_w L(1030) + \text{Ln } H_i \qquad (34)$$

The logarithm of the potential head was plotted versus time as shown in Figure 7. This produced a straight line on semilog paper from which the slope could be read. The permeability calculated from this slope was 11.52 darcies.

C. FLUID INJECTION SYSTEM

Three Hills-McCanna positive displacement U pumps were used for liquid injection. In order to reduce surging during the displacement process, a small air chamber was installed on the delivery line of each pump.

D. THERMOCOUPLES AND TEMPERATURE RECORDER

To obtain measurements of temperature, twelve iron-constantan

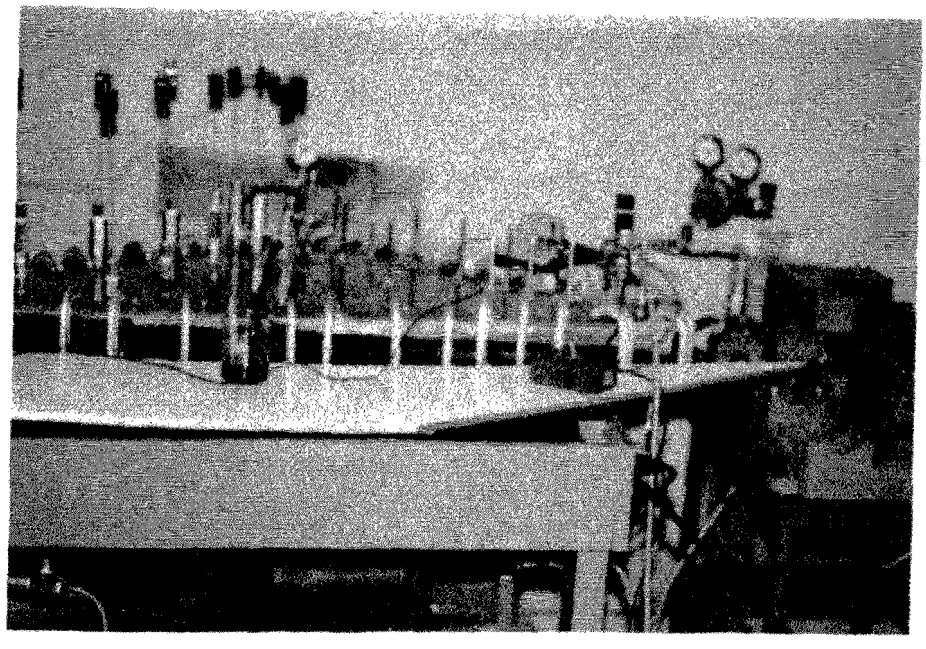

PHOTOGRAPH 1. VIEW OF THE LABORATORY MODEL SHOWING THE THERMOCOUPLES, THE GRAPHITE ELECTRODES, AND THE PUMPS

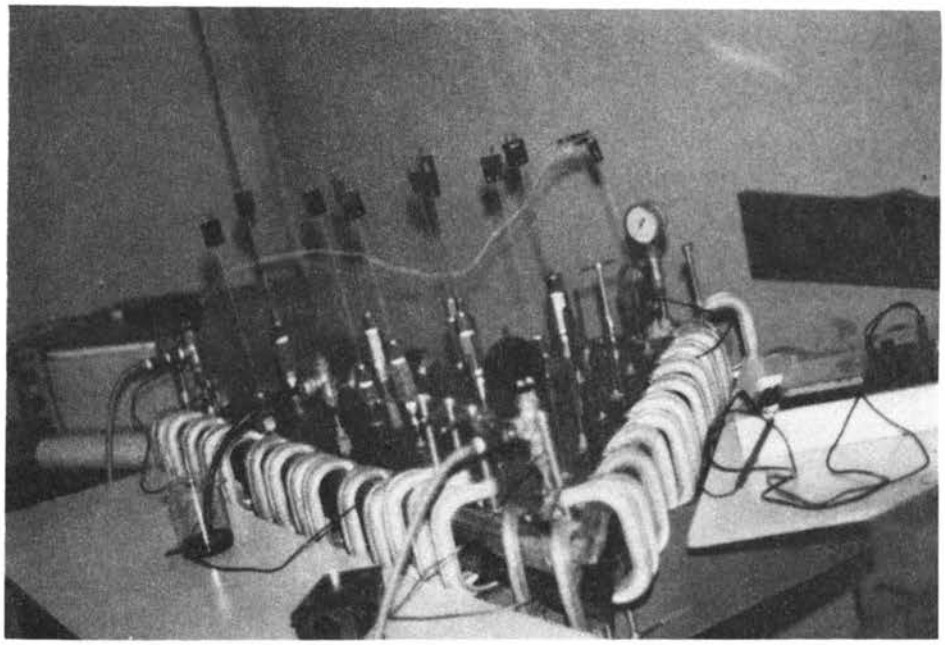

PHOTOGRAPH 2. VIEW OF THE LABORATORY MODEL SHOWING THE TEMPERATURE RECORDER AND A.C. VOLTMETER

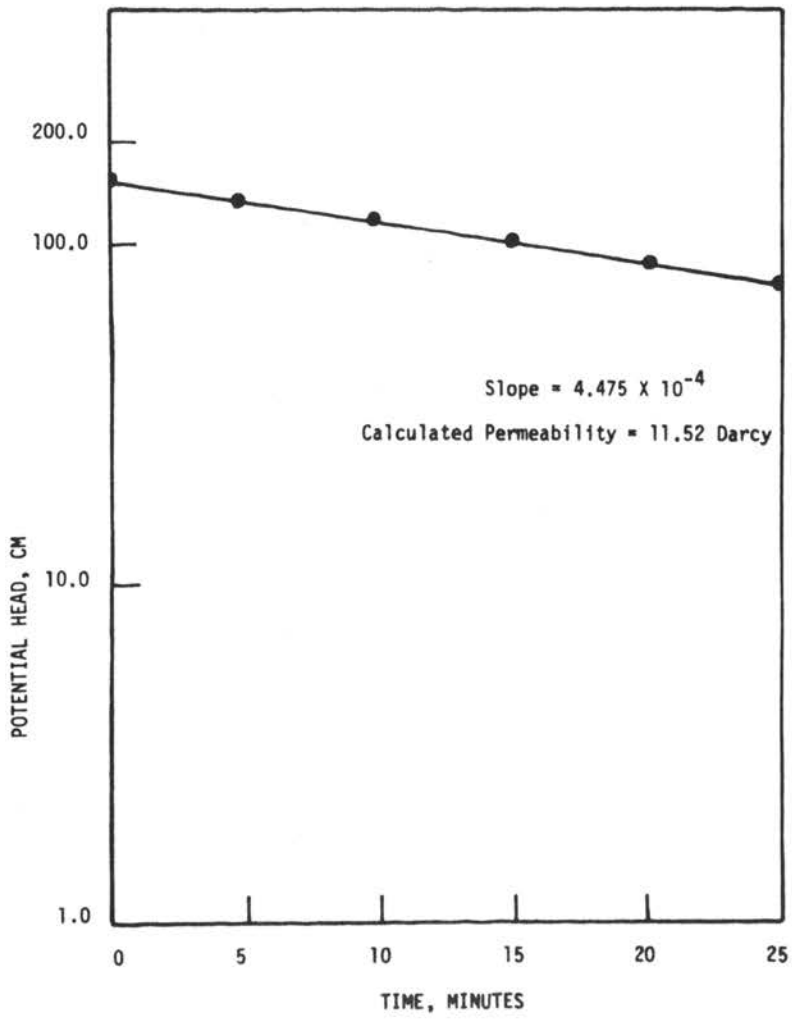

FIGURE 7. POTENTIAL HEAD PLOTTED VS. TIME FOR CALCULATING SAND PERMEABILITY

thermocouples were installed in the laboratory model. Locations of the thermocouples are shown in Figure 5. The thermocouples will be referred to by their numbers as indicated in this Figure. Temperature data from the twelve locations were recorded with a Honeywell recorder. Figure 8 presents the relationship between the temperature recorder millivolt reading and the corresponding temperature for iron- constantan thero-couples.

E. ELECTRODES AND VOLTAGE RECORDER

To obtain measurements of the electric potential, eleven graphite electrodes with 0.25 inch diameter were installed in the laboratory model. Electric current was introduced into the sand pack through three graphite current electrodes located near to the injection wells. An a.c. voltmeter was used to measure the electric potential difference between the eleven measuring electrodes. Locations and numbers of the electrodes are shown in Figure 6.

The stainless steel wells and the thermocouples were coated with graphite spray as a protection against corrosion.

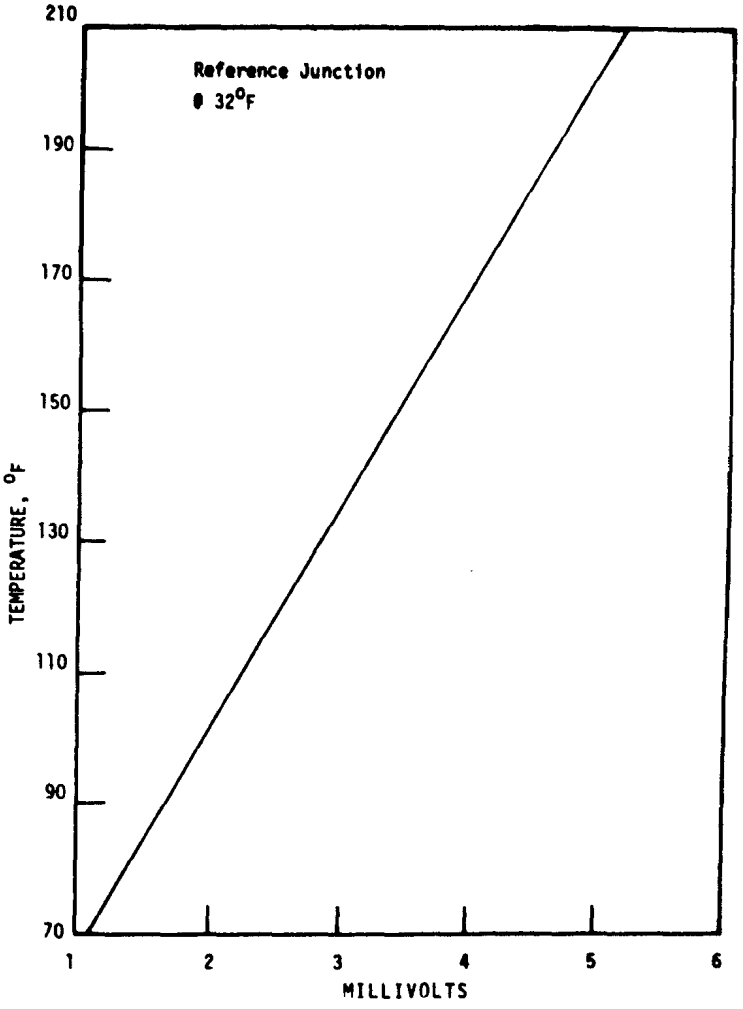

FIGURE 8. TEMPERATURE-MILLIVOLT GRAPH

VI. EXPERIMENTAL PROCEDURE

In order to obtain data with which the numerical calculations of the mathematical model are to be compared, five different experiments were conducted. The purpose of the first three experiments was to investigate the validity of the numerical solution of the electric flow equation, the thermal energy equation, and the expression developed for the salt concentration distribution. The electric potential and the temperature distribution within a porous medium, fully saturated with brine, and subjected to an e.m.f., were recorded.

In experiment 1, heat transfer by convection was zero (brine injection rate = 0). In experiment 2, heat transfer was due to both conduction and convection, but the salt concentration was uniform. In experiment 3, the salt concentration distribution within the system was not uniform (relatively fresh water was introduced into the system). Experiment 4 was a conventional cold waterflood. The purpose of this experiment was to investigate the validity of the numerical solution fo the fluid flow equations by comparing results of the calculations with observed displacements in the physical model. Experiment 5, the actual electrothermic process, was conducted to obtain experimental data with which the numerical calculations of the whole system of equations are to be compared.

Prior to any of the experiments the physical model was filled with 45 lbs. of dry clean sand. The sand was initially saturated with water after being subjected to vacuum. Water was injected into the sand while the vacuum pump was still exhausting air. Two more pore volumes of water were injected to remove any air which might still exist in the

sand. Separate experimental procedures were required for each experiment after saturating the sand with water.

The following outline indicates the steps in making the first three experiments:

1. The sand was saturated with brine of 75,000 p.p.m. sodium chloride concentration.

2. An alternating current supply of 110 volts and 60 cycles per second was connected with the current electrodes as shown in Figure 4.

3. Electric heating was continued for four minutes. After disconnecting the electric current, temperature measurements were recorded in the order of the thermocouples number, i.e. at thermocouples 1,2,3 and so on (thermocouples locations and numbers are shown in Figure 5).

4. The a.c. current source was connected with the current electrodes and the electric potential differences between the measuring electrodes, shown in Figure 6, were recorded in the order of the electrodes numbers, i.e. between electrodes 1 & 2, 2 & 3, 3 & 4 and so on. Measured values of the electric potential and the temperature are given in Tables VI & VII respectively.

5. Two pore volumes of brine of 75,000 p.p.m. dissolved sodium chloride were injected into the sand pack in order to ensure uniform initial temperature distribution as a preparation for the second experiment.

6. The current electrodes were connected with the same a.c. current supply voltage for seven minutes. Brine of 75,000 p.p.m. dissolved sodium chloride was injected into the sand pack at the rate of 20 d.d./min. during this period (injection rate is equivalent to 40 c.c./min. in a five-spot element).

7. The electric potential differences were recorded at the start of the experiment and the temperature measurements were recorded at the end of the experiment. The measured values are given in Tables VIII and IX.

8. Step 5 was repeated as a preparation for experiment 3.

9. Relatively fresh water of 1,000 p.p.m. dissolved sodium chloride was injected into the sand pack at the rate of 20 c.c./min. for 7 minutes.

10. Following the relatively fresh water injection, the current electrodes were connected with the same current supply voltage for 4.5 minutes. Brine of 75,000 p.p.m. dissolved sodium chloride was injected into the sand pack during the heating period. The electric potential differences and the temperature measurements were recorded. Measured values are given in Tables X & XI respectively.

Following this set of experiments, the cold waterflood experiment was conducted. The following outline indicates the steps in making this experiment:

1. The sand was initially saturated with water, then flooded with two pore volumes of synthetic oil (viscosity = 15 cp. at 60^{o}F). One pore volume of oil was injected into well 4 while the three corner-wells served as producers. Influx of oil at the boundaries of the sand pack was achieved by injecting one pore volume of oil into wells 1 & 3 while well 2 served as a producer. Initial oil saturation attained was 0.864. The sand and operating characteristics for this experiment are described in Table XII.

2. Water was then injected into the three corner-wells at the rate of 80 c.c./min. (equivalent to 160 c.c./min. in a five-spot element).

The amount of oil and water produced from well 4 was measured as a function of time. Results are given in Table XIII.

The following outline indicates the steps followed in making the last experiment:

1. The sand pack was initially saturated with brine of 16,500 p.p.m. dissolved sodium chloride, then flooded with the synthetic oil used in the cold waterflood experiment.

2. Relatively fresh water of 1,000 p.p.m. dissolved sodium chloride was injected into the sand pack until water breakthrough (1,500 c.c.).

3. Salt saturated water of 200,000 p.p.m. dissolved sodium chloride was injected into the sand pack for 14 minutes (equivalent to 1,120 c.c.).

4. The a.c. current supply voltage was connected with the current electrodes and electric heating continued for 30 minutes. Electric potential differences between the measuring electrodes and temperature at the thermocouple locations were recorded at different stages of the heating process.

5. Cold water injection was continued until three pore volumes were injected. The amounts of oil and water produced were recorded as a function of time. Results are given in Tables XIV through XIX.

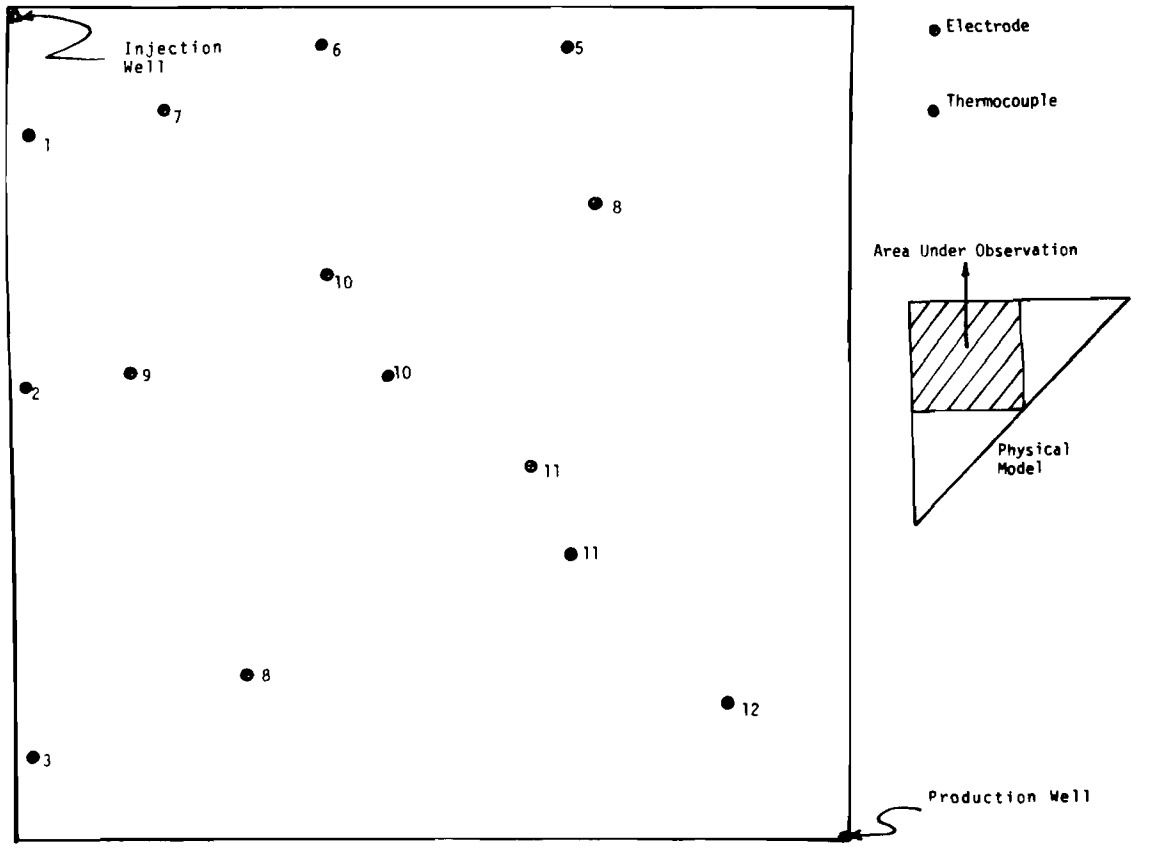

FIGURE 9. A QUADRANT OF THE FIVE-SPOT ELEMENT SHOWING ELECTRODE AND THERMOCOUPLE LOCATIONS

VII. DISCUSSION OF RESULTS

In the present study the response of either the physical model or reservoir is determined from the oil production rate and the distribution of the electrical potential, temperature, water saturation, and salt concentration in the model or reservoir. In the discussion to follow, the data obtained from the experiments described in Part VI have been compared with the calculated response obtained from computer runs simulating these experiments. The experimental and calculated data are presented in Tables VI through XLIV in Appendix F. The experiments and computer runs will be referred to by their numbers mentioned earlier in this study. Finally the mathematical model has been utilized to investigate the response of single layer and double layer oil reservoirs to the electrothermic process. The two hypothetical oil reservoirs are assumed to be overlain and underlain by electrically resistive formations. In the two layer reservoir, cross flows between the two layers (fluid flow, electric flow, and heat flow) has been neglected as a first approximation of the response of this case to the electrothermic technique.

A. COMPARISON OF MATHEMATICAL MODEL NUMERICAL SOLUTION WITH THE EXPERIMENTAL DATA

The experimental and calculated behavior of the physical model will be presented for a square section of the five-spot unit. Figure 9 shows locations of the thermocouples and measuring electrodes in the section under observation.

Accuracy of the calculated numerical solution to the fluid flow equations is tested by comparing oil recoveries at different stages of the cold waterflood (experiment No. 4) with the corresponding calculated values. Figure 10 gives a comparison of the experimental and calculated data. The produced oil, expressed as a fraction of initial oil in place, is plotted vs. cumulative water injected, expressed in pore volumes. Agreement between measured and calculated recoveries is excellent.

Figure 11 details the calculated water saturation contours at water breakthrough. It shows the transition from high to low water saturation and the developed cusp toward the producing well. As reported by other investigators, the water invaded zone in the five-spot model was found to be radial during the initial flooding stages, then stretched into a squared off pattern, and finally developed a cusp toward the producing well (46,47,48). With increasing oil-to-water viscosity ratios this cusp became more pronounced and began to form at an earlier flooding stage, resulting in an overall decrease of oil recovery at the moment of water breakthrough. Figure 12 details the water saturation contours for this run at 1.69 pore volumes of cumulative water injected.

Comparison between the measured and calculated electrical potential and temperature behavior for experiments 1 through 3 is given in Figures 14 through 20. The operating conditions are specified in Table XXIV. The calculated response for these experiments is interpreted as entirely satisfactory. The electrical potential distribution obtained agrees with what has been very early realized concerning the potential distribution

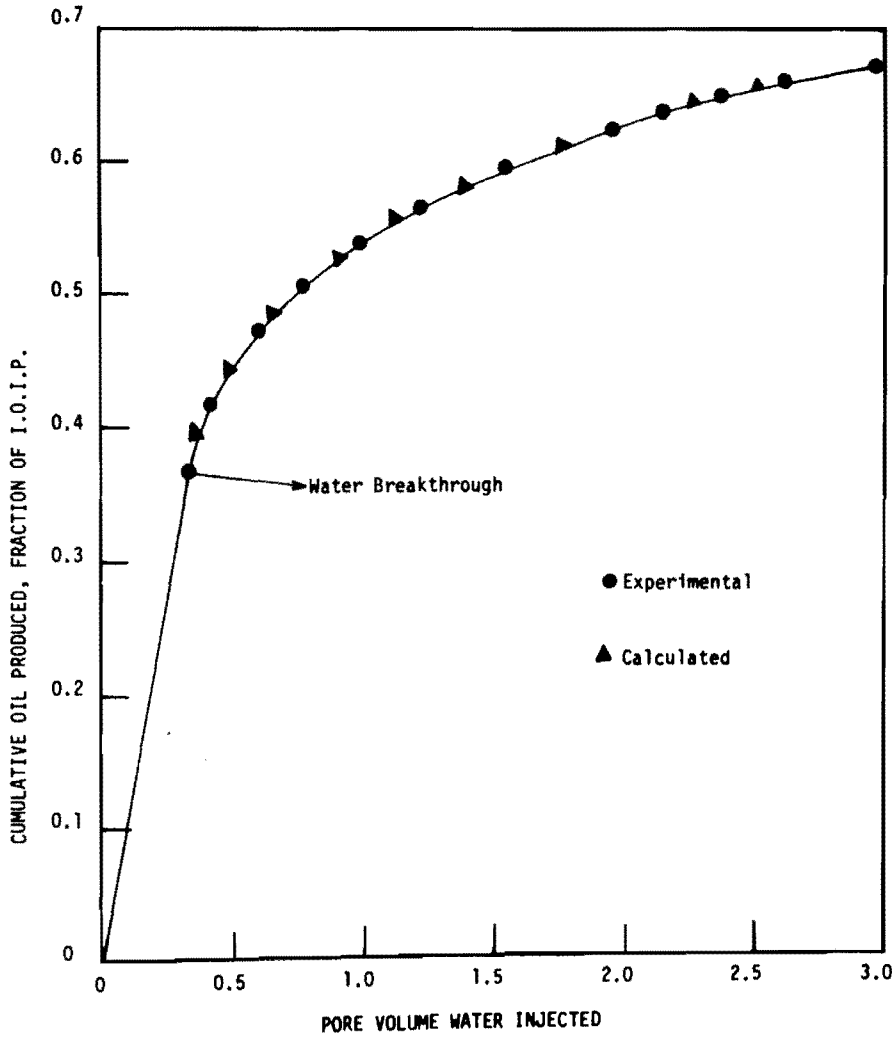

FIGURE 10. OIL RECOVERY BY COLD WATERFLOOD FOR EXPERIMENT AND COMPUTER RUN NO. 4

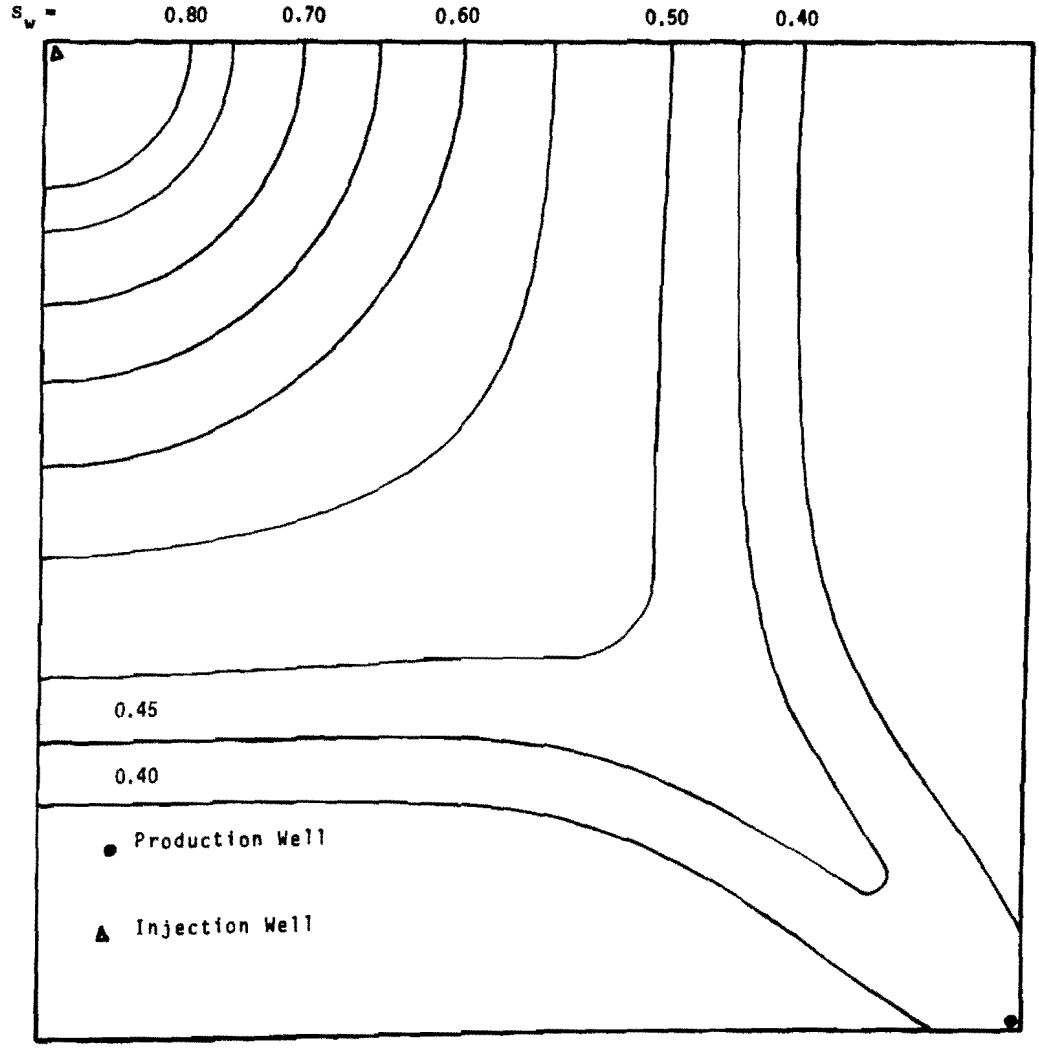

FIGURE 11. CALCULATED WATER SATURATION DISTRIBUTION AT BREAKTHROUGH FOR COLD WATERFLOOD EXPERIMENT

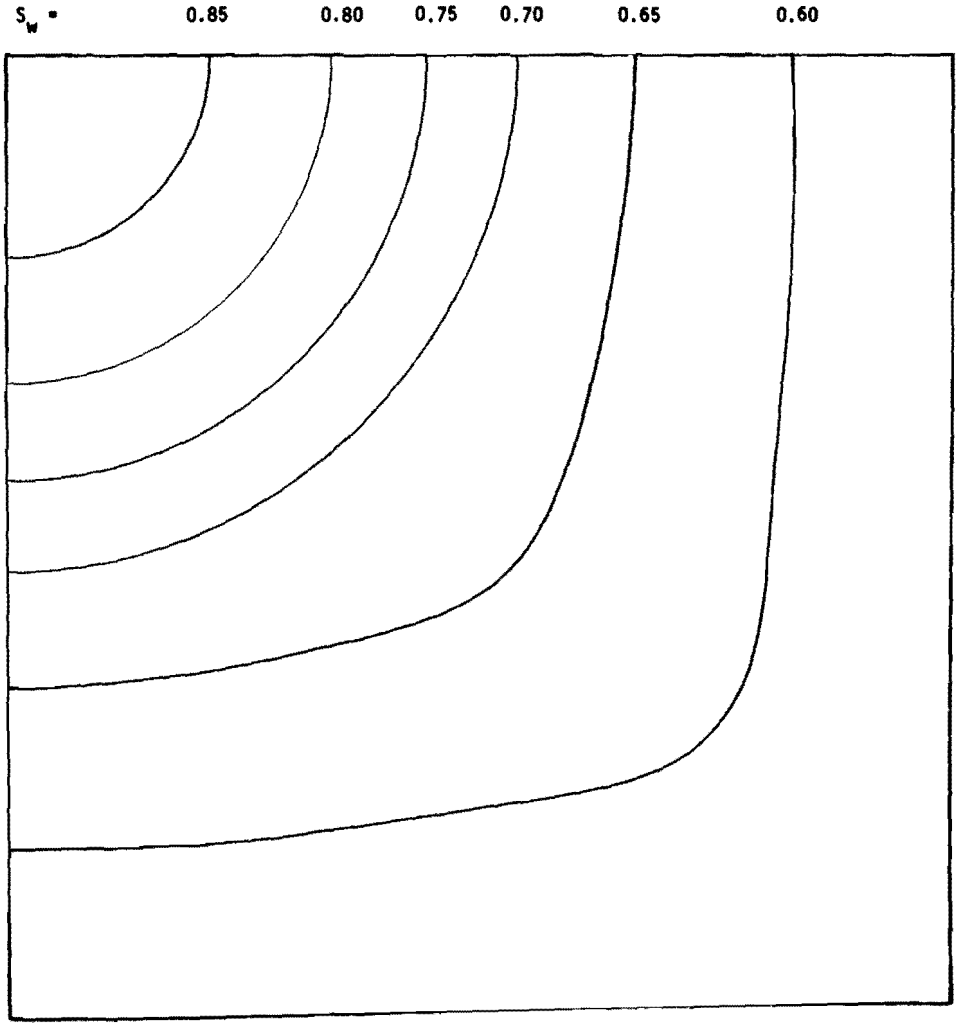

FIGURE 12. CALCULATED WATER SATURATION DISTRIBUTION AT 1.69 PORE VOLUMES CUMULATIVE WATER INJECTED FOR COLD WATERFLOOD EXPERIMENT

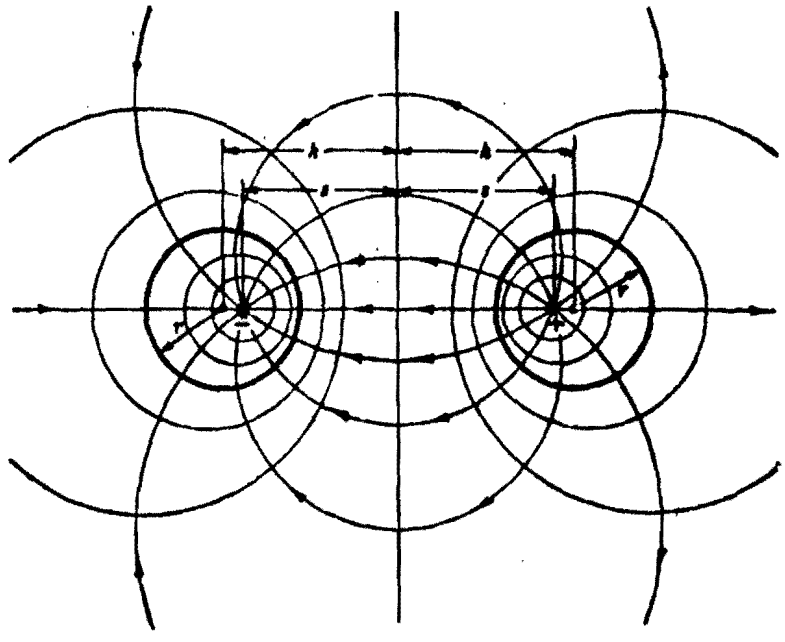

FIGURE 13. ELECTRIC POTENTIAL DISTRIBUTION EXTERNAL TO TWO PARALLEL CYLINDRICAL CONDUCTORS

(SOURCE : REFERENCE 28)

external to two parallel cylindrical conductors under a constant e.m.f. shown in Figure 13.

Figures 24, 26, and 28 give a comparison of the calculated and experimental electric potential distribution at different stages of the electric heating process. Figures 30 and 31 give a comparison of the calculated and experimental temperature distribution at the end of the heating period and at 0.6 pore volume water injected that followed the heating period, for experiment and computer Run No. 5. A comparison between experimental and calculated oil recovery by the electrothermic technique, and a comparison between oil recovery by cold waterflood and that obtained by the electrothermic process, are given by Figure 33. Water saturation distribution for computer Run No. 5 at 2.62 pore volumes cumulative water injected, is given in Figure 34. Calculated water saturation and salt concentration distribution for the electrothermic process are given in Figures 21, 22, 25, 27, and 29.

Calculated response is considered to be entirely satisfactory. Figure 23 presents the variation of the injected electric current and average porous medium temperature with time during electric heating. There is a ten-fold increase in the magnitude of the injected electric current during the heating period. This can be explained as due to the reduction in porous medium electric resistance caused by the salt saturated water injection and increase in temperature. Average porous medium temperature increased by 20 °F during the first 15 minutes of the heating period, and by 54 °F during the last 15 minutes due to the increase in the magnitude of the injected electric current. The variability of the electric potential distribution exhibited by the system with time can be explained as due to both the increase of

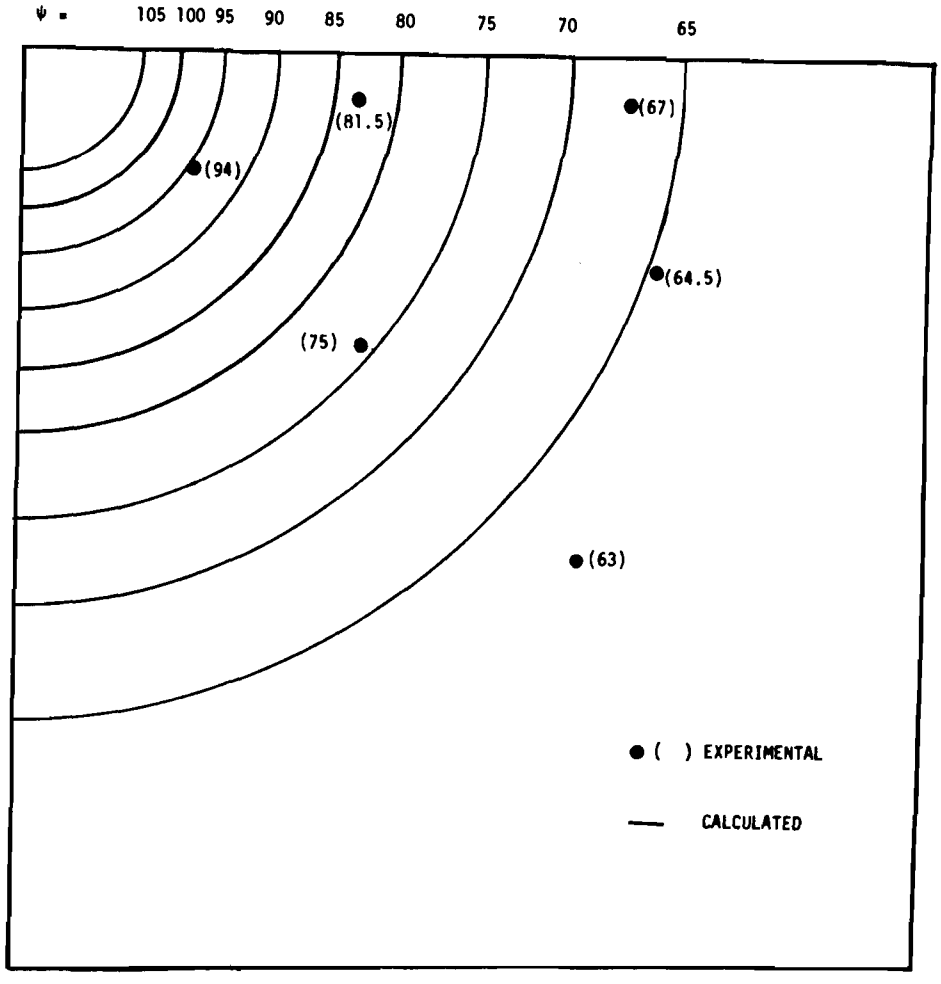

FIGURE 14. MEASURED AND CALCULATED ELECTRIC POTENTIAL DISTRIBUTION FOR EXPERIMENT AND COMPUTER RUN NO. 1

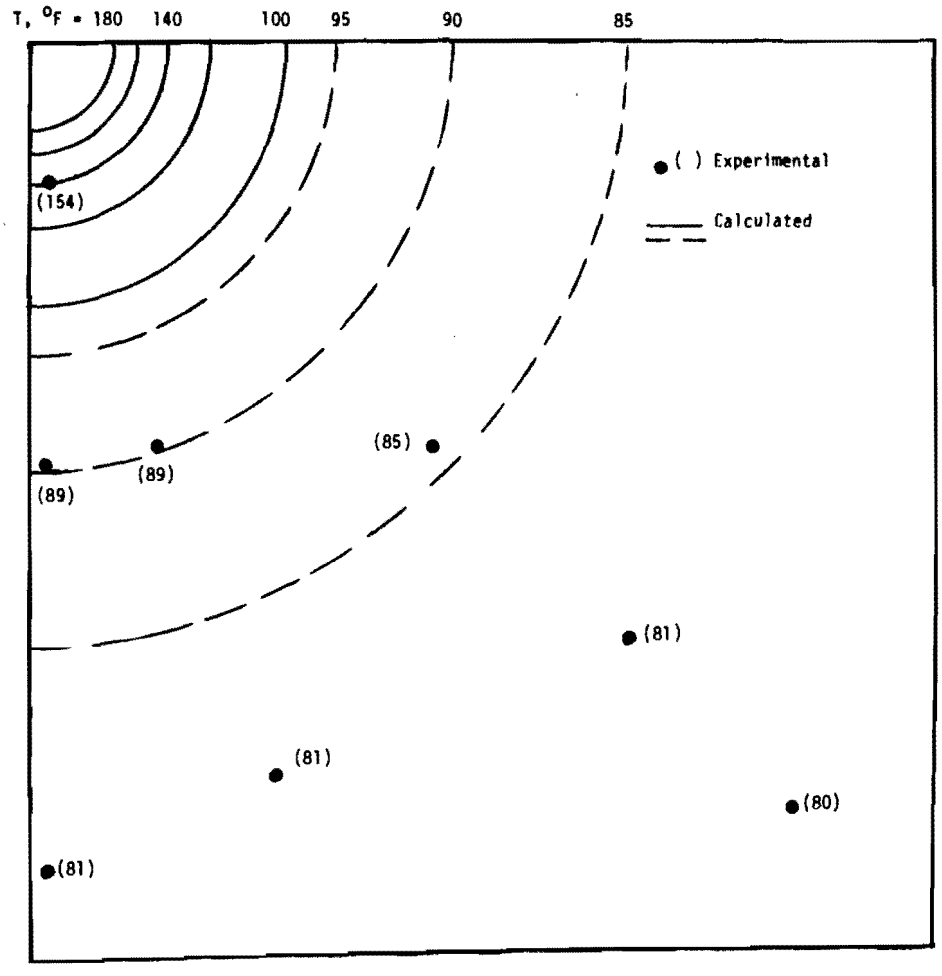

FIGURE 15. MEASURED AND CALCULATED TEMPERATURE DISTRIBUTION FOR EXPERIMENT AND COMPUTER RUN NO. 1

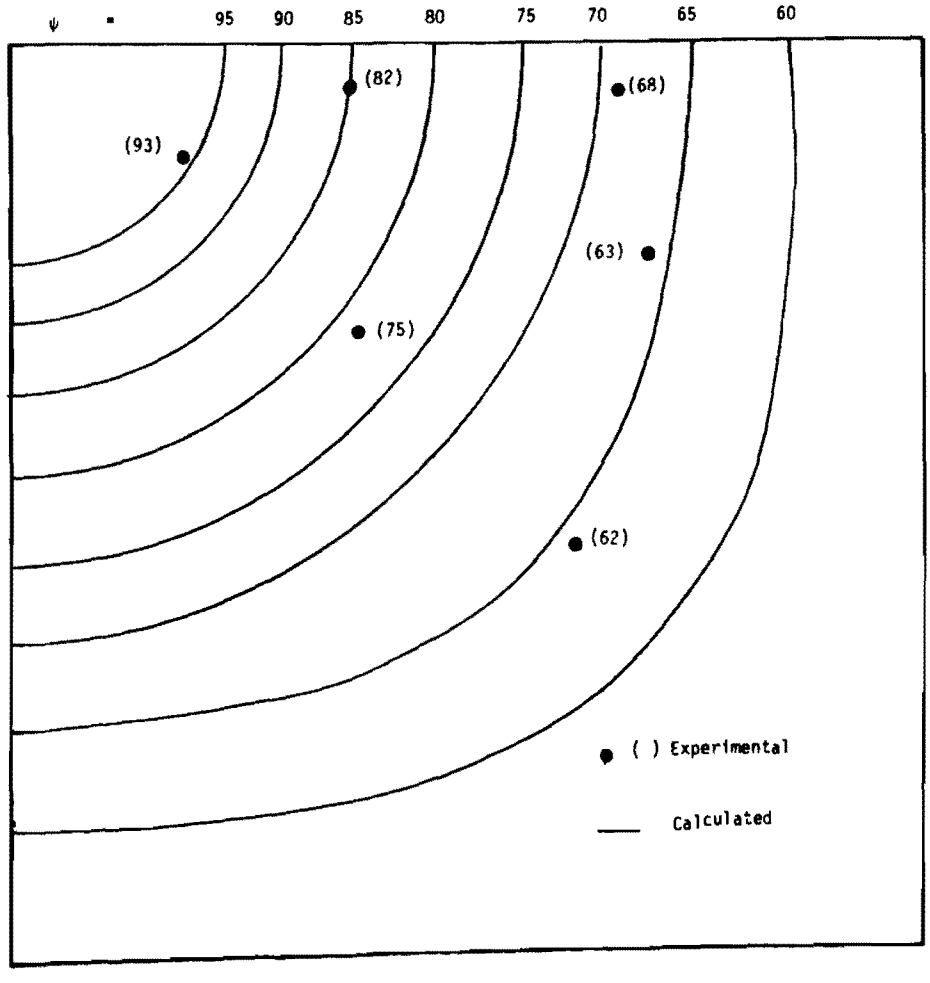

FIGURE 16. MEASURED AND CALCULATED ELECTRIC POTENTIAL DISTRIBUTION FOR EXPERIMENT AND COMPUTER RUN NO. 2

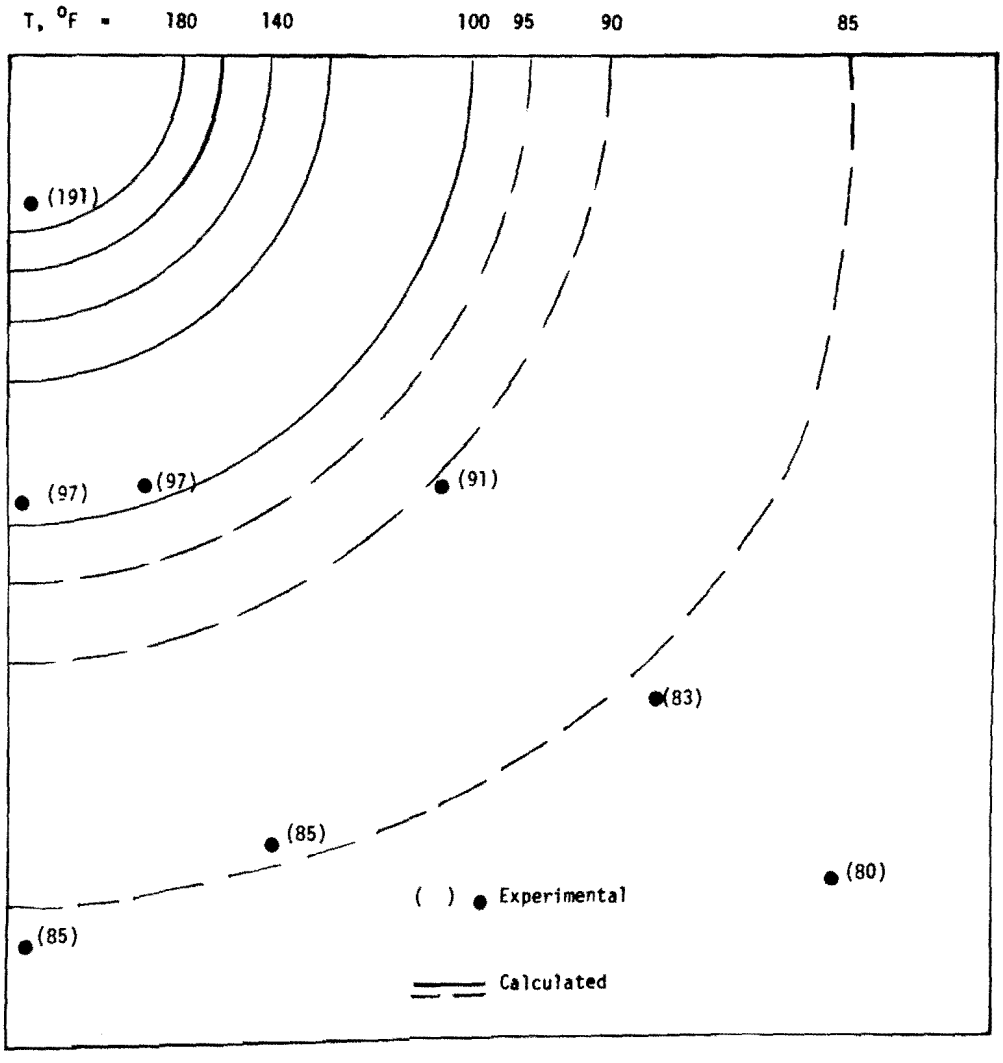

FIGURE 17. MEASURED AND CALCULATED TEMPERATURE DISTRIBUTION FOR EXPERIMENT AND COMPUTER RUN NO. 2

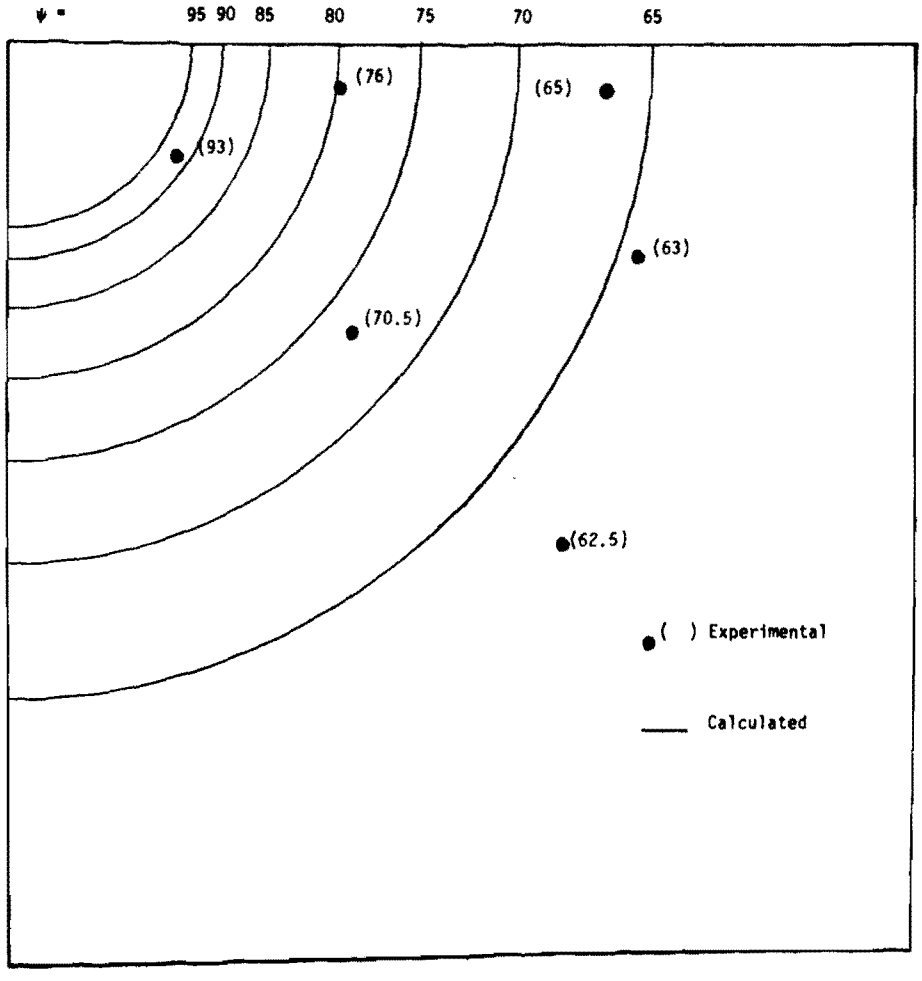

FIGURE 18. MEASURED AND CALCULATED ELECTRIC POTENTIAL DISTRIBUTION FOR EXPERIMENT AND COMPUTER RUN NO. 3

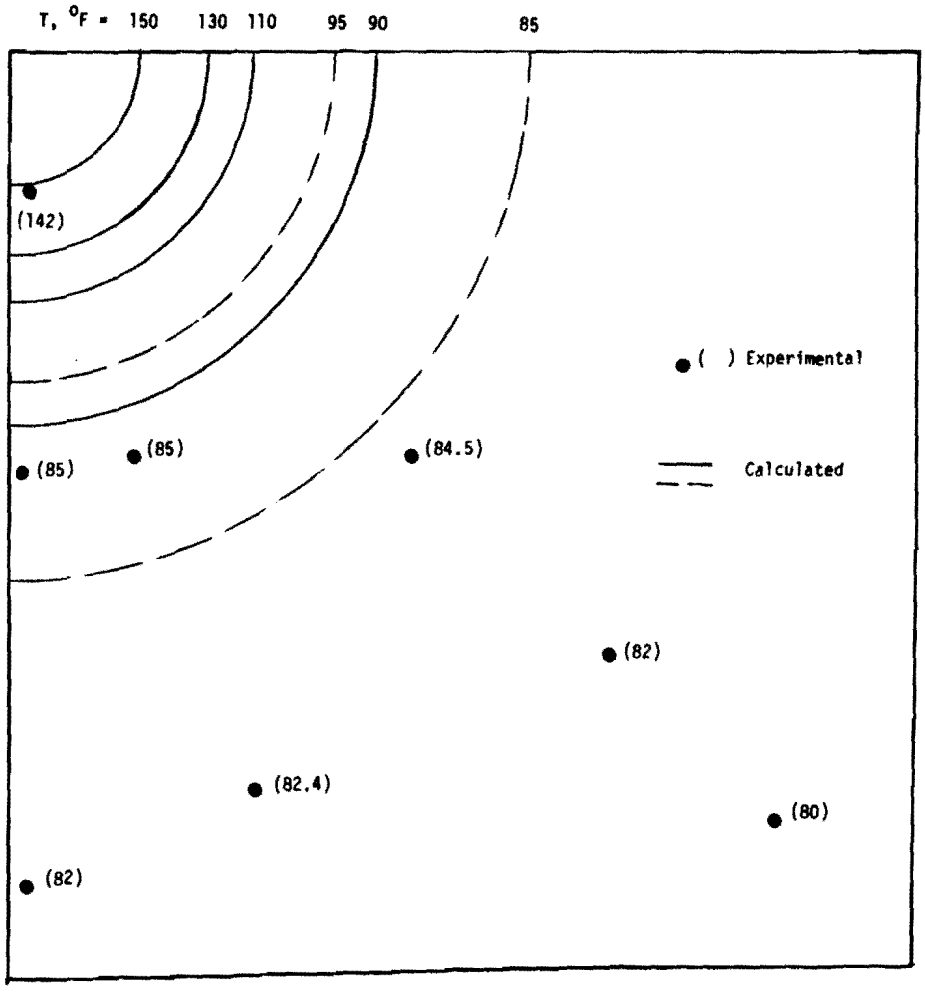

FIGURE 19. MEASURED AND CALCULATED TEMPERATURE DISTRIBUTION FOR EXPERIMENT AND COMPUTER RUN NO. 3

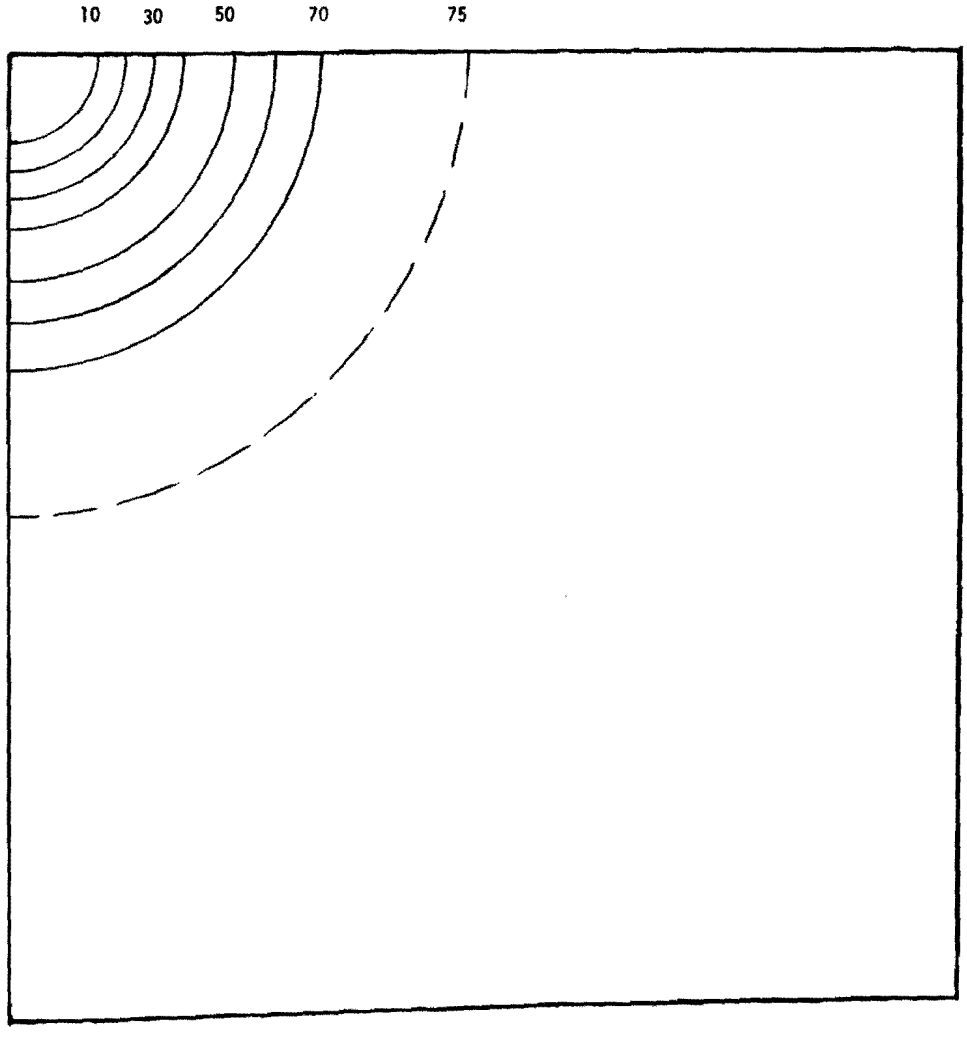

FIGURE 20. CALCULATED SALT CONCENTRATION DISTRIBUTION, THOUSAND P.P.M., AT START OF HEATING FOR COMPUTER RUN NO. 3

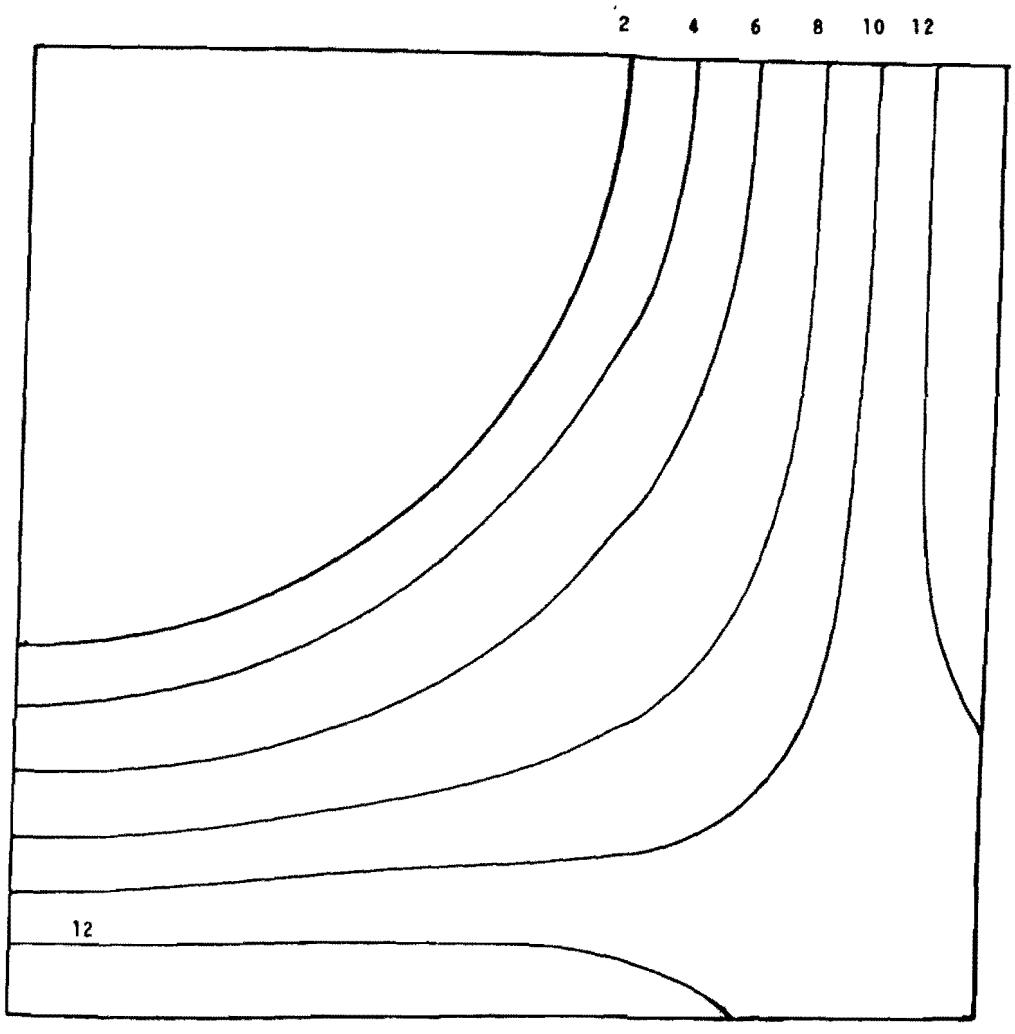

FIGURE 21. CALCULATED SALT CONCENTRATION DISTRIBUTION, THOUSAND P.P.M., FOR COMPUTER RUN NO. 5, DURATION OF FRESH WATER INJECTION EQUALS 18.5 MINUTES (0.31 PORE VOLUME)

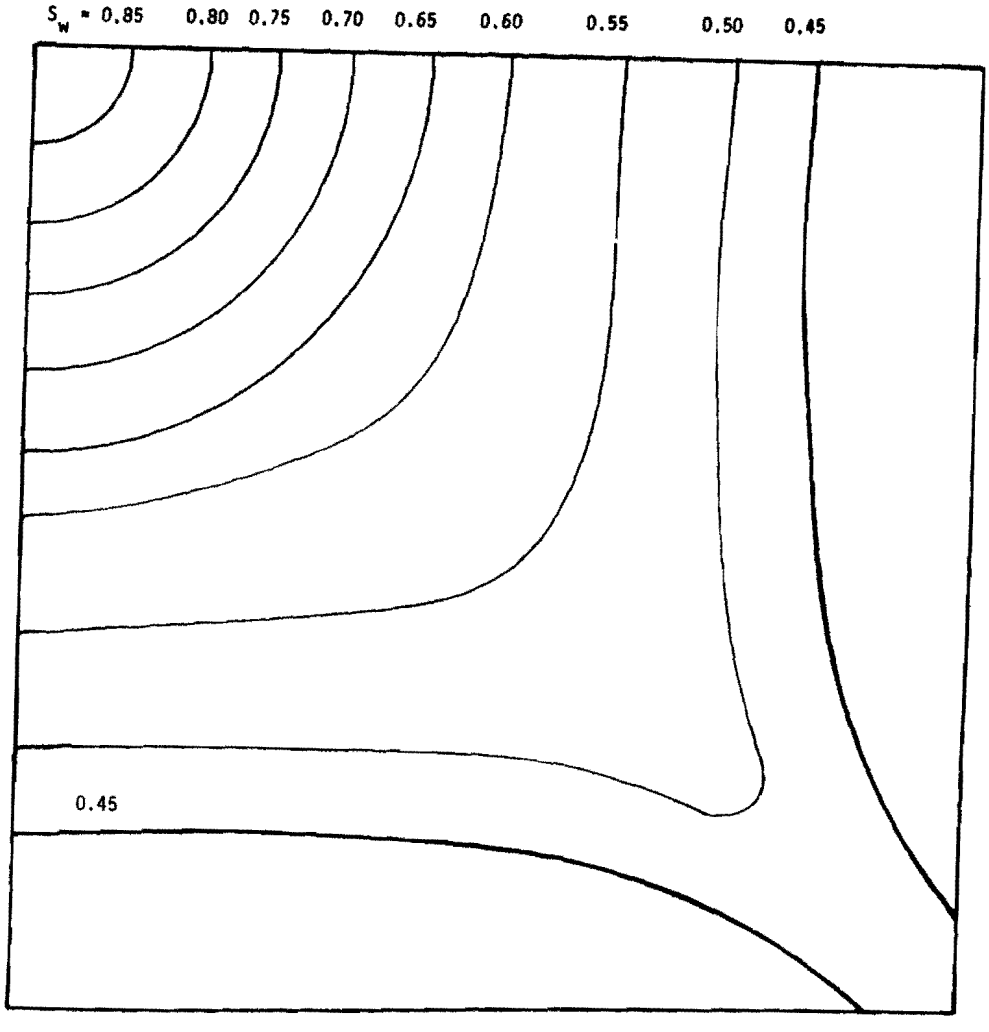

FIGURE 22. CALCULATED WATER SATURATION DISTRIBUTION FOR RUN NO. 5, DURATION OF SALT SATURATED WATER INJECTION EQUALS 14 MINUTES (0.24 PORE VOLUME)

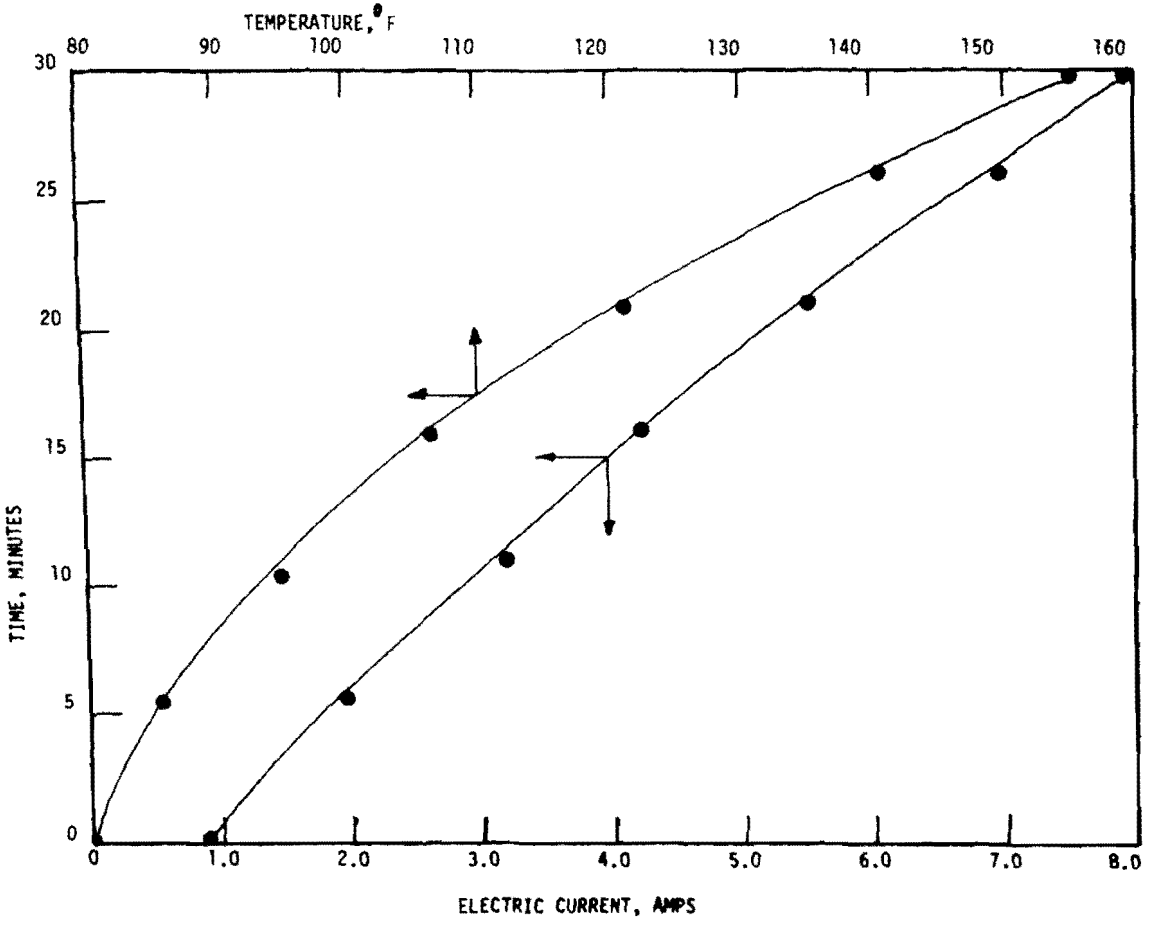

FIGURE 23. ELECTRIC CURRENT AND POROUS MEDIUM AVERAGE TEMPERATURE VS. TIME, RUN NO. 5

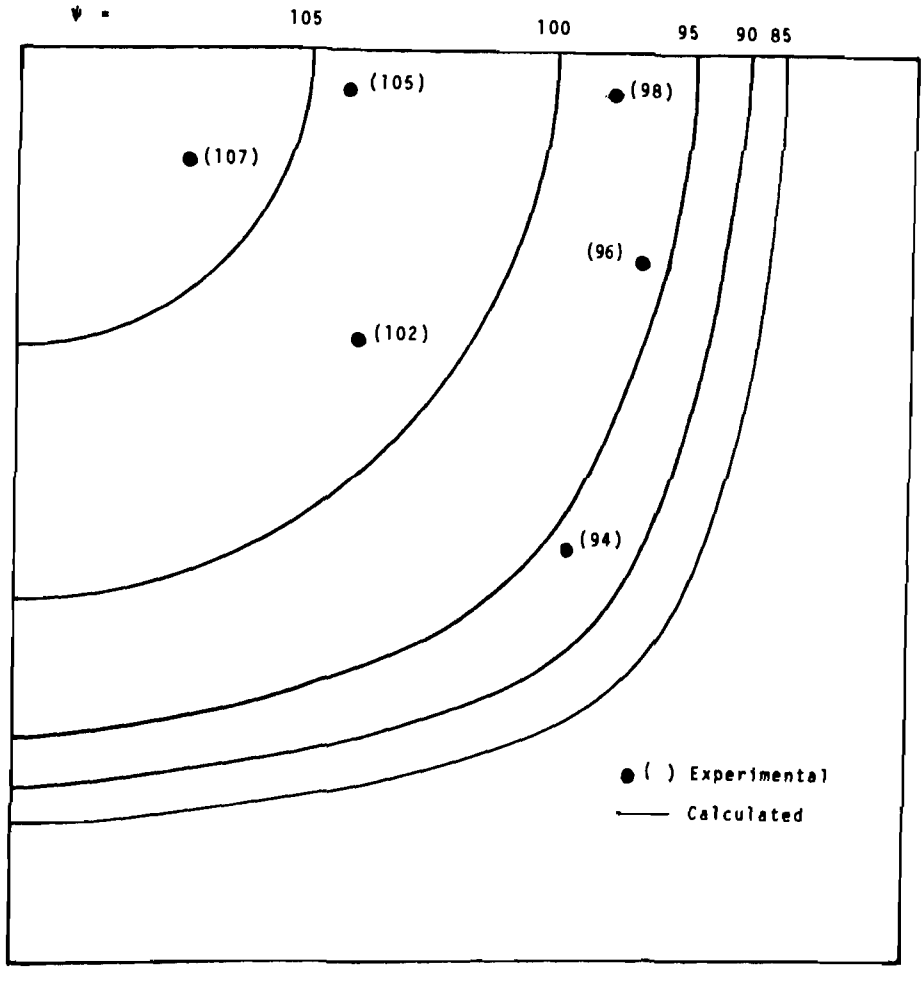

FIGURE 24. MEASURED AND CALCULATED ELECTRIC POTENTIAL DISTRIBUTION FOR EXPERIMENT AND COMPUTER RUN NO. 5, DURATION OF HEATING EQUALS 0.17 MINUTES

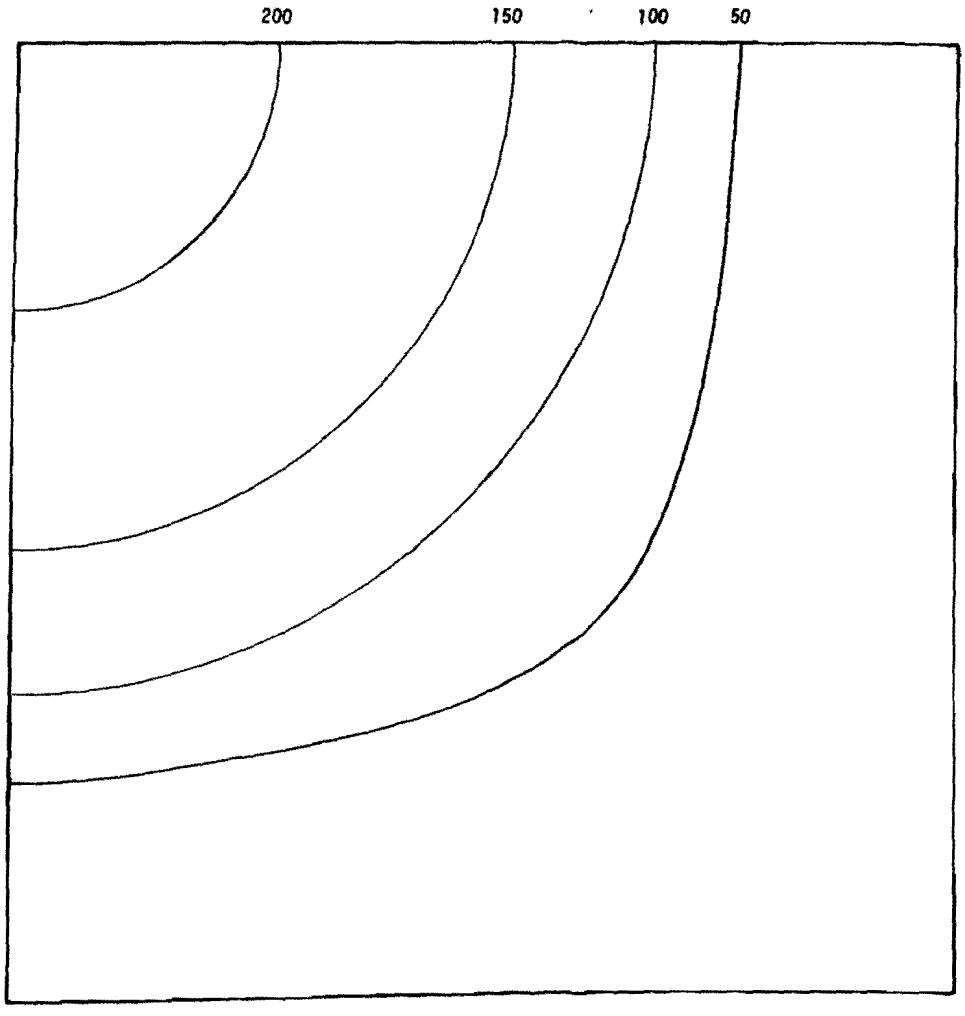

FIGURE 25. CALCULATED SALT CONCENTRATION DISTRIBUTION, THOUSAND P.P.M., FOR COMPUTER RUN NO. 5, DURATION OF SALT SATURATED WATER INJECTION EQUALS 14.17 MINUTES (0.24 PORE VOLUME)

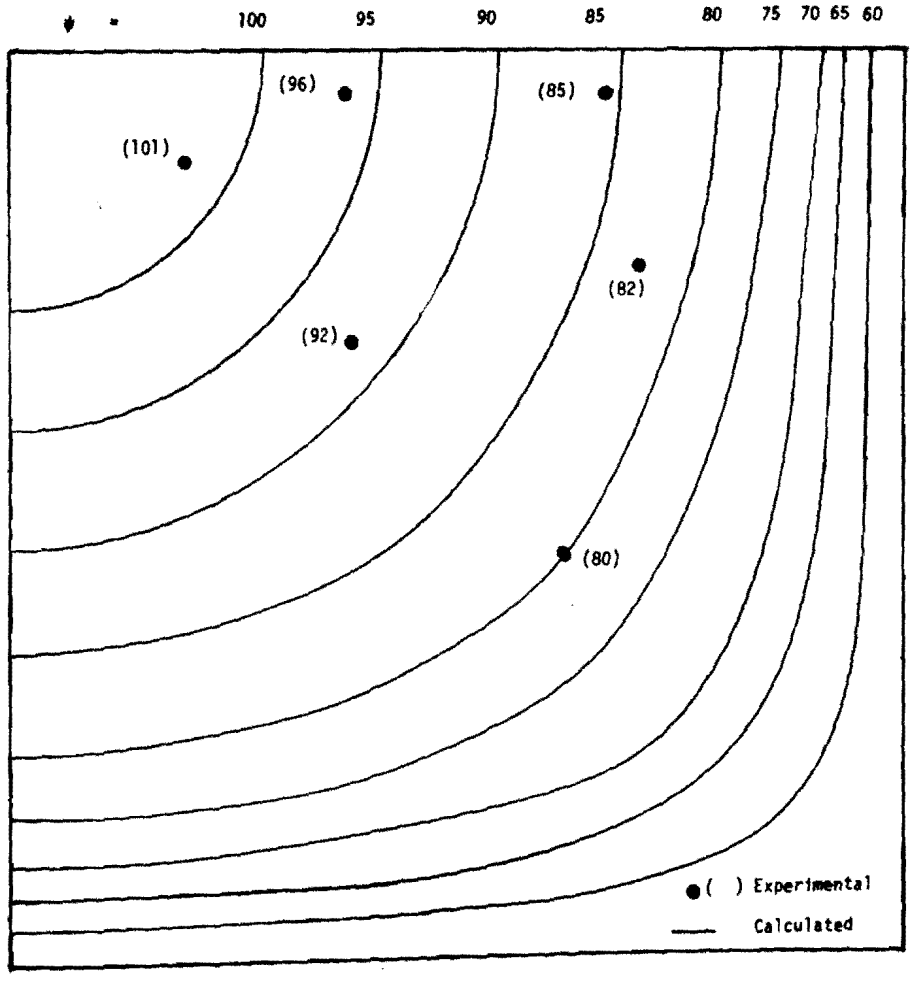

FIGURE 26. MEASURED AND CALCULATED ELECTRIC POTENTIAL DISTRIBUTION FOR EXPERIMENT AND COMPUTER RUN NO. 5, DURATION OF HEATING EQUALS 9.33 MINUTES

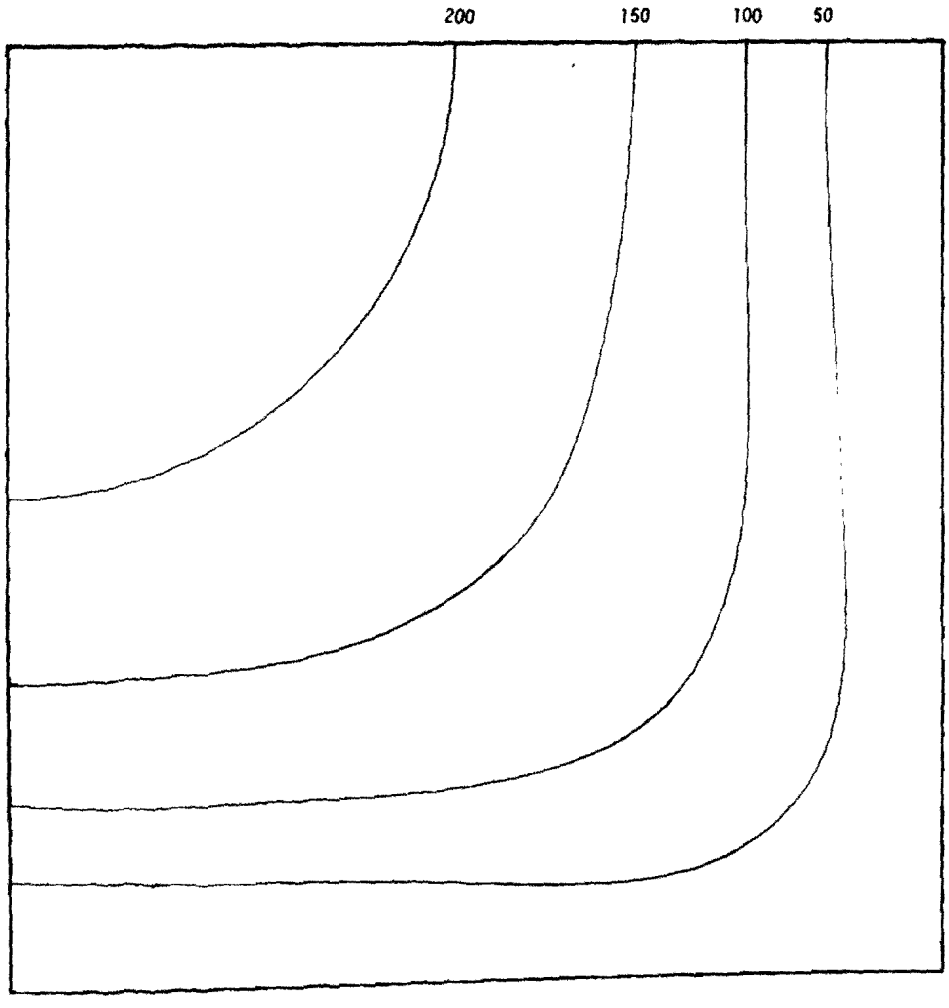

FIGURE 27. CALCULATED SALT CONCENTRATION DISTRIBUTION FOR COMPUTER RUN NO. 5, THOUSAND P.P.M., DURATION OF SALT SATURATED WATER INJECTION EQUALS 23.33 MINUTES (0.4 PORE VOLUME)

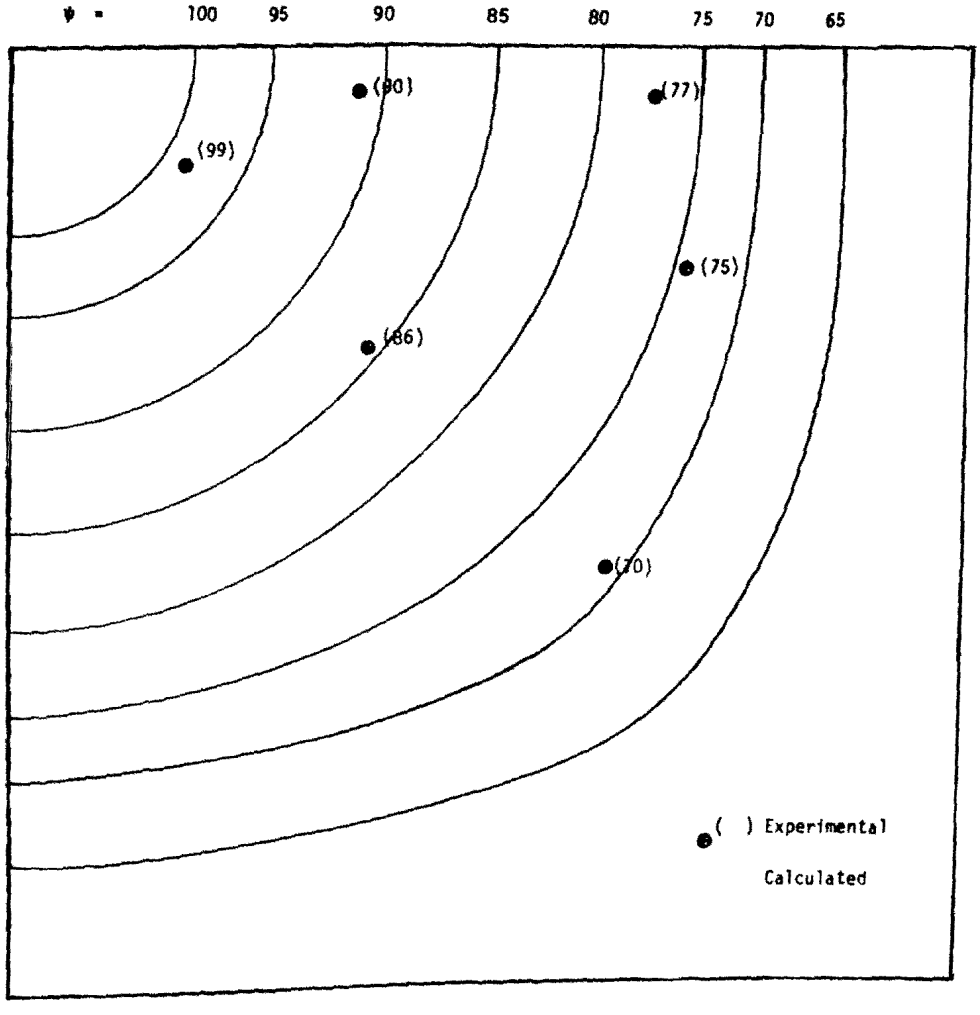

FIGURE 28. MEASURED AND CALCULATED ELECTRIC POTENTIAL DISTRIBUTION FOR EXPERIMENT AND COMPUTER RUN NO. 5, DURATION OF HEATING EQUALS 29.5 MINUTES

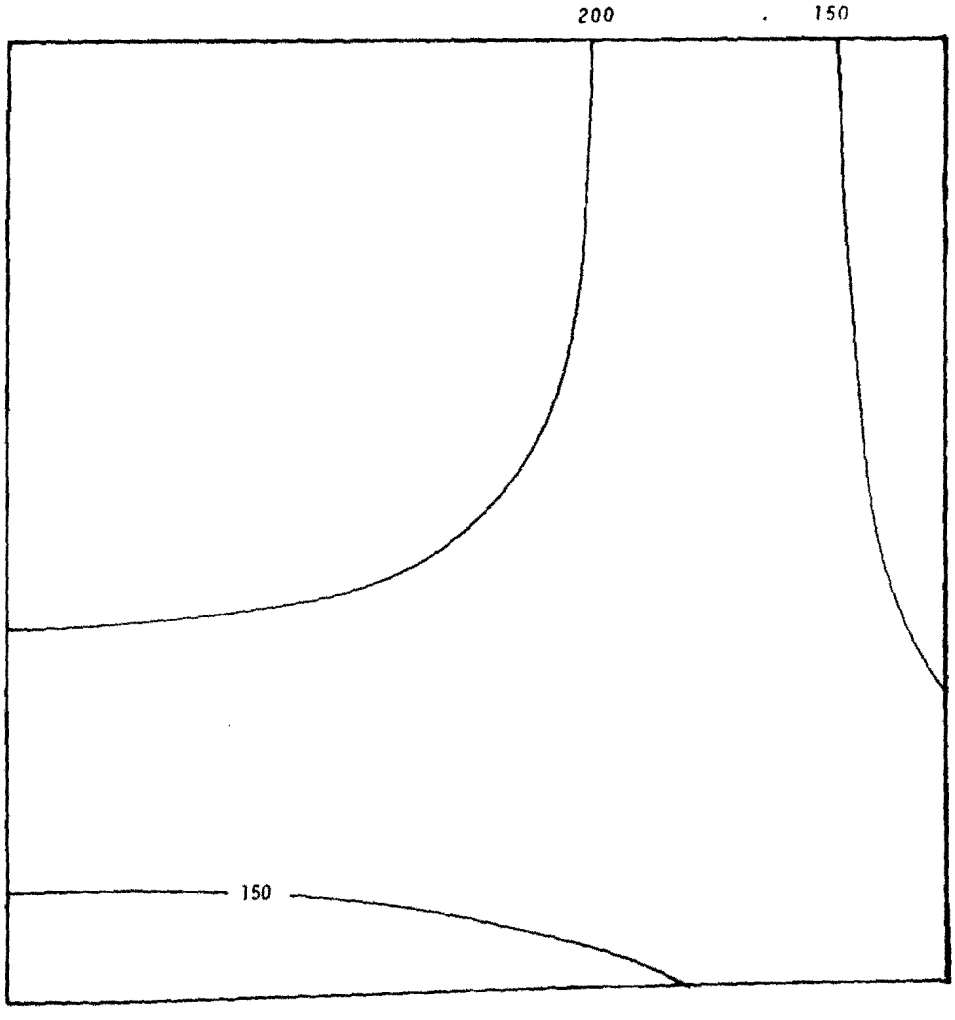

FIGURE 29. CALCULATED SALT CONCENTRATION DISTRIBUTION, THOUSAND P.P.M., FOR COMPUTER RUN NO. 5, DURATION OF SALT SATURATED WATER INJECTION EQUALS 43.5 MINUTES (0.74 PORE VOLUME)

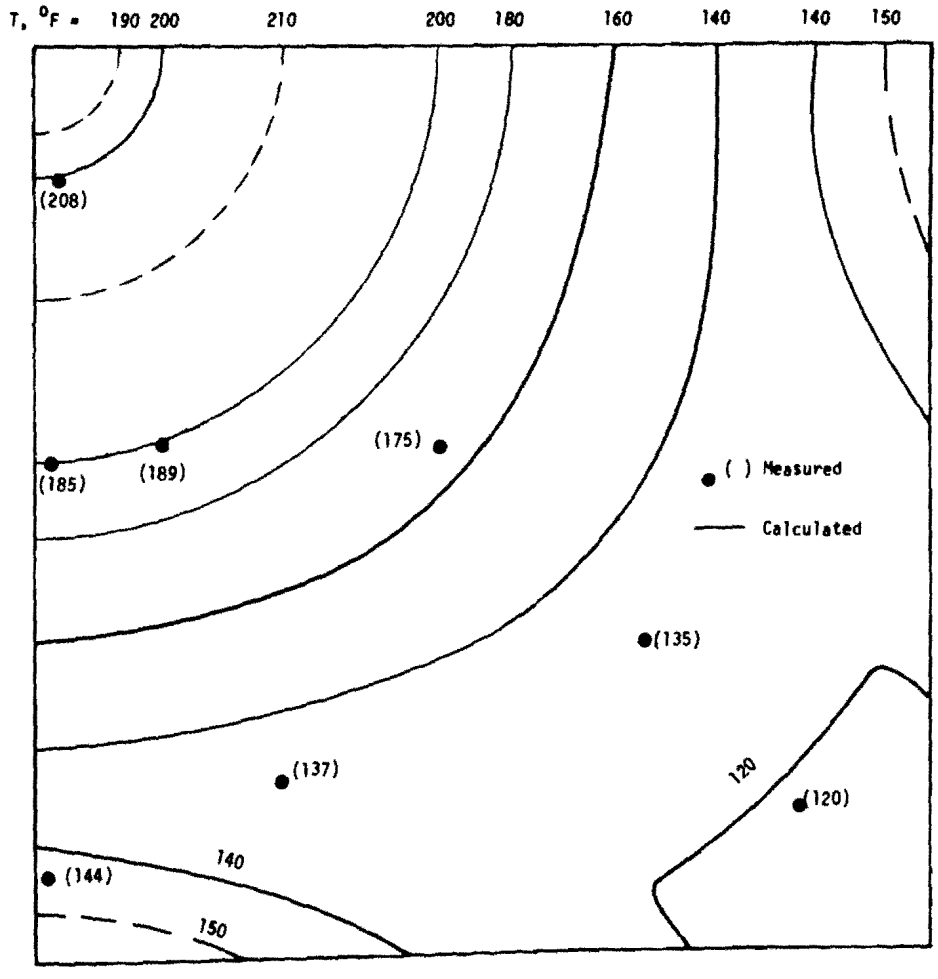

FIGURE 30. MEASURED AND CALCULATED TEMPERATURE DISTRIBUTION FOR EXPERIMENT AND COMPUTER RUN NO. 5, DURATION OF HEATING EQUALS 29.5 MINUTES

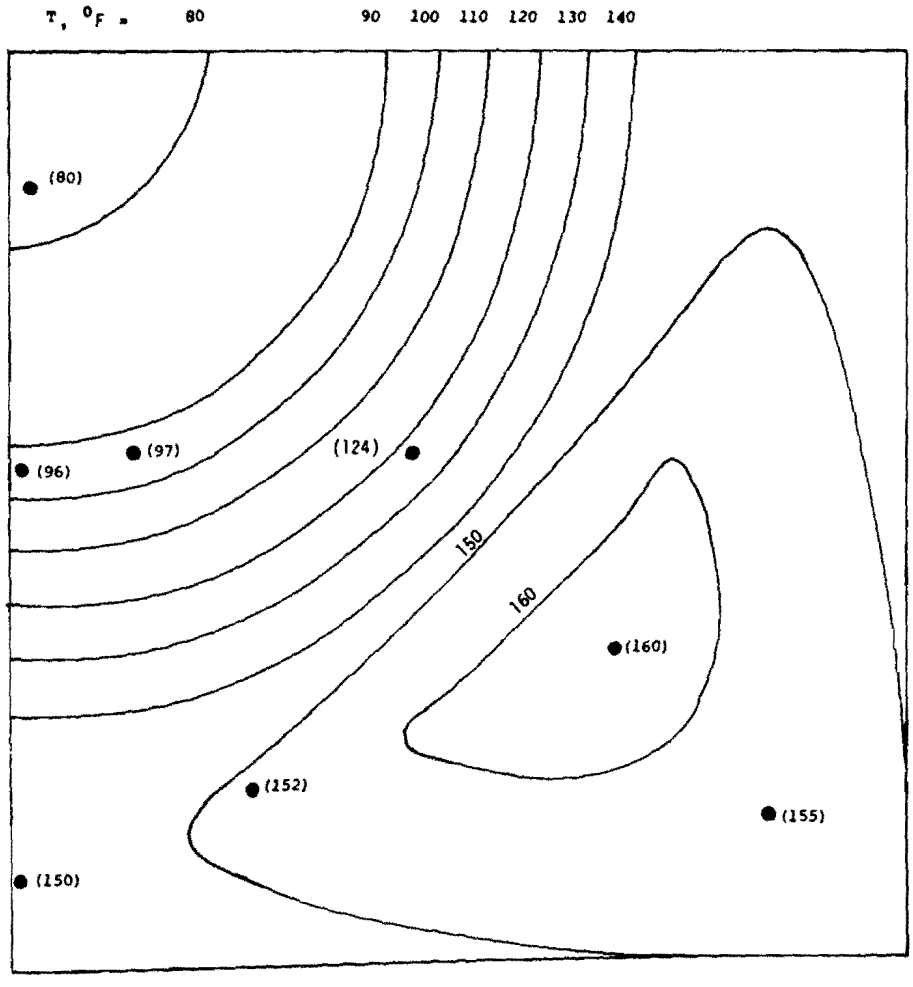

FIGURE 31. MEASURED AND CALCULATED TEMPERATURE DISTRIBUTION FOR EXPERIMENT AND COMPUTER RUN NO. 5, DURATION OF COLD WATER INJECTION EQUALS 34.33 MINUTES (0.58 PORE VOLUME)

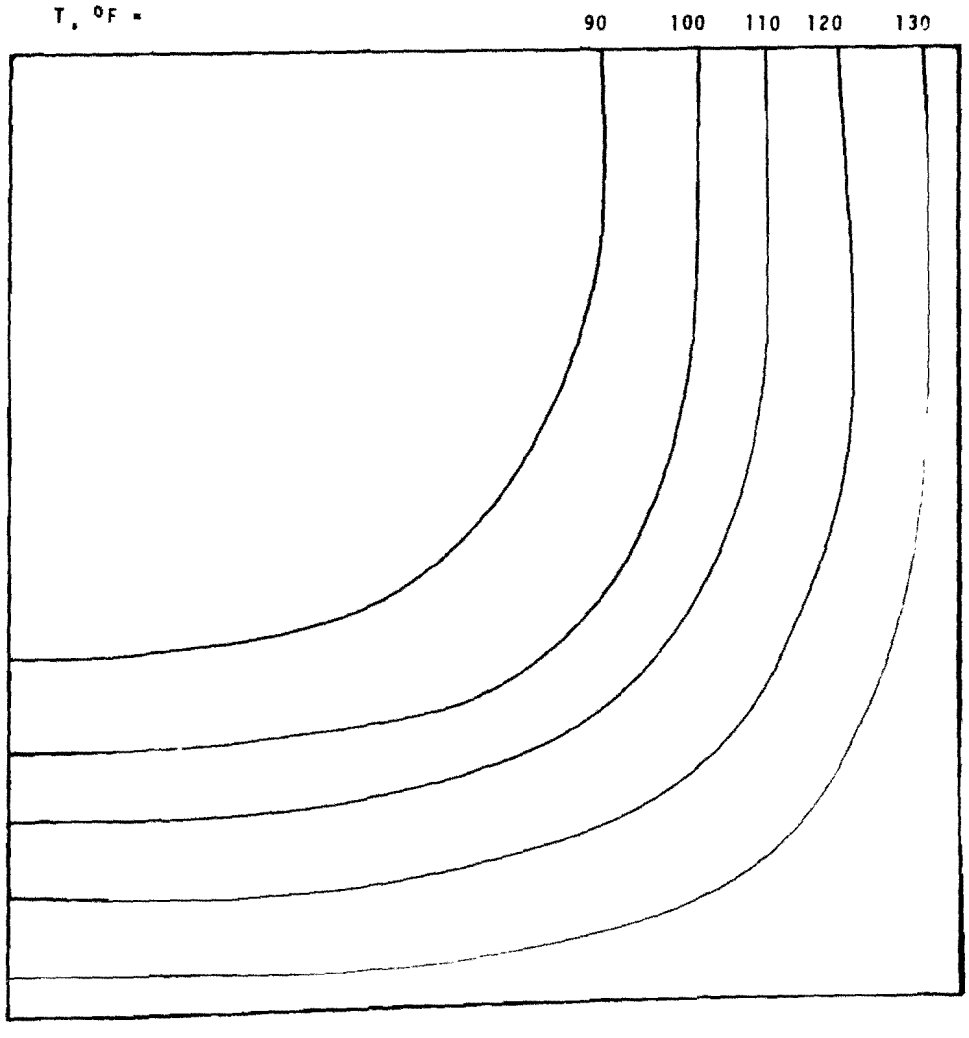

FIGURE 32. CALCULATED TEMPERATURE DISTRIBUTION FOR COMPUTER RUN NO. 5, DURATION OF COLD WATER INJECTION EQUALS 68.66 MINUTES (1.17 PORE VOLUME)

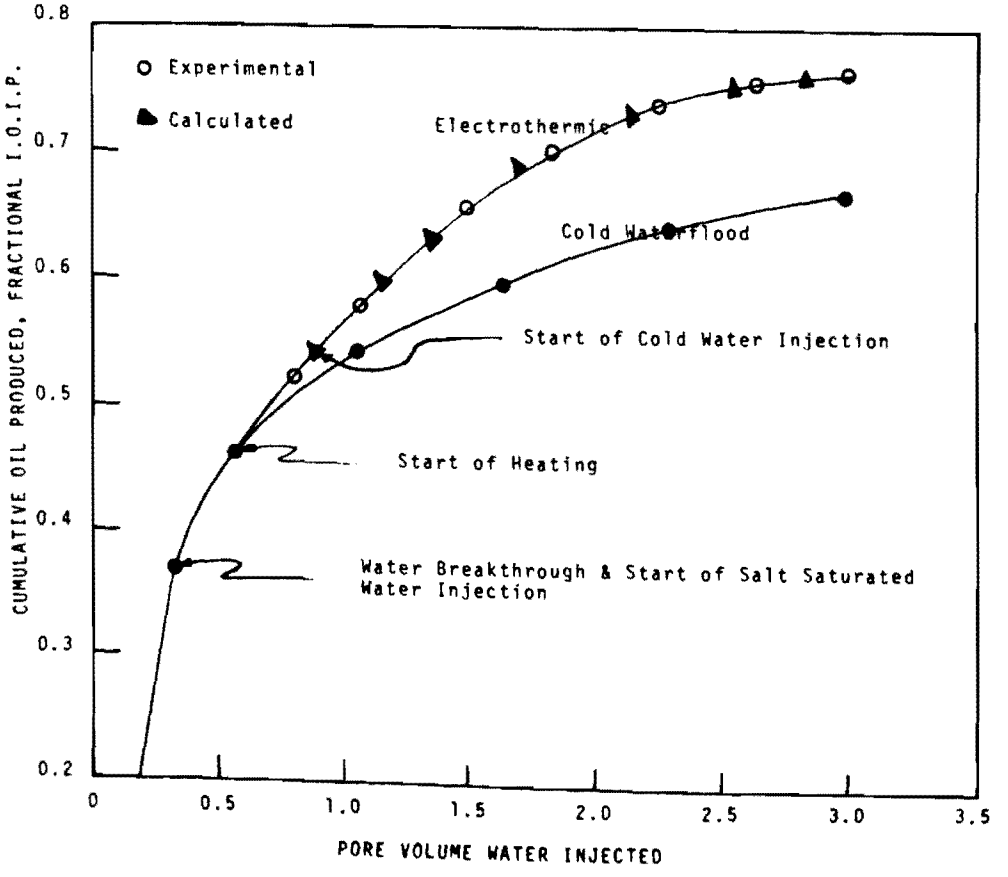

FIGURE 33. EXPERIMENTAL AND CALCULATED OIL RECOVERY BY THE ELECTROTHERMIC TECHNIQUE

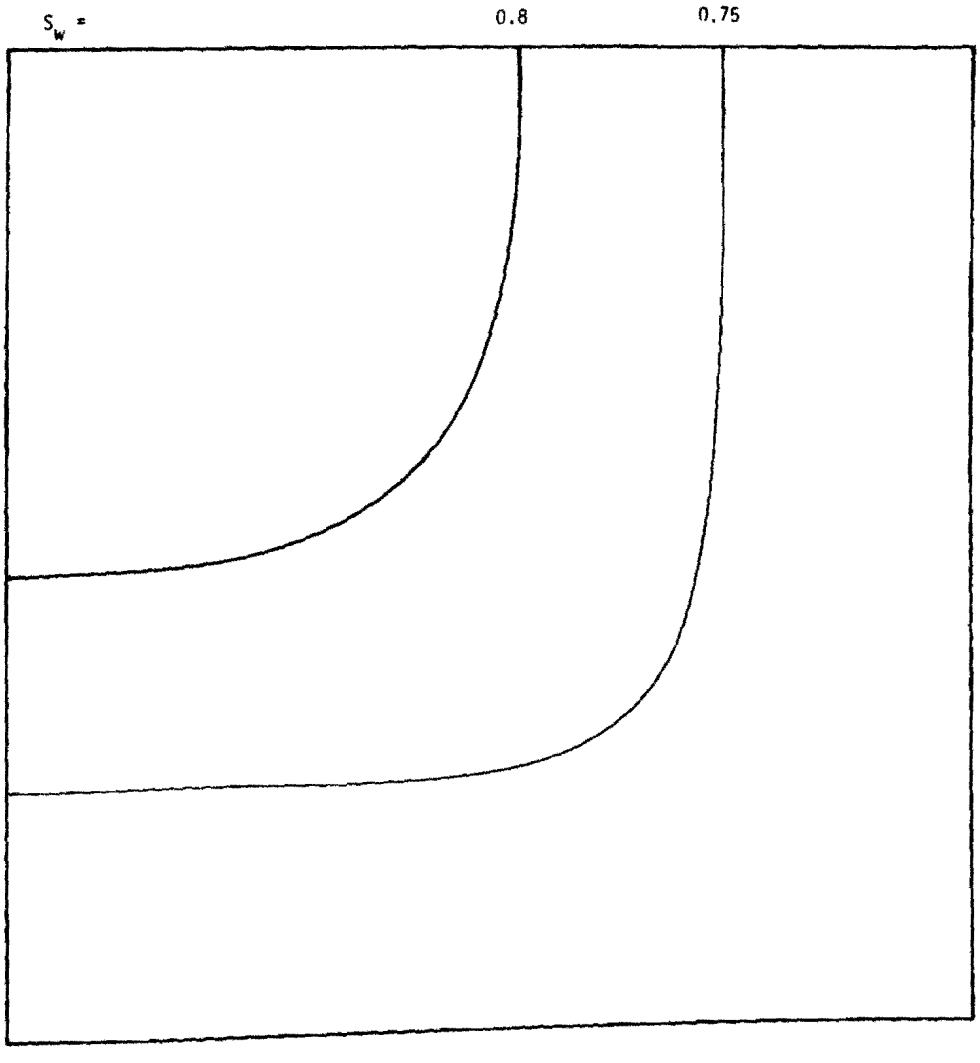

FIGURE 34. CALCULATED WATER SATURATION DISTRIBUTION AT 2.62 PORE VOLUMES WATER INJECTED FOR COMPUTER RUN NO. 5

electric conductivity and the injected current. The relatively high temperature at the edges of the area under observation can be explained by the relatively high resistance in these areas caused by relatively high oil saturation that is coupled with low salt concentration. The high oil saturation and low salt concentration in these areas are produced by the developed cusp toward the producing well as has been mentioned in the discussion of the flow pattern.

Comparison between oil recovery by the electrothermic technique and that obtained by cold waterflood shown in Figure 33 indicates 13% increase in oil recovery by the electrothermic technique over that obtained by cold waterflood.

B. FIELD APPLICATION OF THE ELECTROTHERMIC TECHNIQUE

In the discussion to follow, the computer simulation scheme has been utilized to analyze the behavior of a five-spot pattern within two hypothetical oil reservoirs during conventional waterflooding and electric heating. The two reservoirs will be designated as Field Case I and Field Case II. In Field Case I, the oil reservoir is assumed to be made up of a single oil-bearing formation overlain and underlain by electrically resistive formations. Table III summarizes the reservoir and operating characteristics of Field Case I. In Field Case II, the oil reservoir is assumed to be made up of two oil-bearing formations overlain and underlain by electrically resistive formations. The two oil-bearing formations are distinguished from one another mainly by the absolute permeability. Table IV summarizes the reservoir and operating characteristics of Field Case II. The analysis of each case will begin with a brief outline of the steps of the simulated

electrothermic process used with it, followed by a discussion of the calculated response. Field Case I and Field Case II will be considered in the order stated.

1. Field Case I

The following outline indicates the steps of the simulated electrothermic process used with Field Case I:

i. Brine of high salinity (200,000 p.p.m.) was injected into the oil reservoir until water breakthough.

ii. An alternating current supply of 1,000 volts was connected with current electrodes placed in injection wells, and electric heating was continued for 42 days. Brine of the same salinity, (200,000 p.p.m.) was injected into the oil reservoir during the heating period.

iii. Conventional waterflooding followed the electric heating and continued until 0.7 pore volume of cumulative water was injected.

Figure 35 details the calculated water saturation distribution before heating. The salt concentration distribution before heating is shown in Figure 36. Figure 37 presents the increase in reservoir average temperature and the amount of the electric current injected during the electric heating process. An increase in average reservoir temperature of 121.5 ^{o}F in a period of 42 days was achieved. The electric energy consumed amounts to 7.2336×10^{6} KWH. The calculated temperature distribution after heating is shown in Figure 38. Comparison of cumulative oil produced by the electrothermic process and that by conventional waterflood is shown in Figure 39. An increase of 55,581 STB of cumulative oil produced is achieved. Consequently, the electric energy utilized per additional STB of oil amounts to 130.15 KWH/ additional STB of oil.

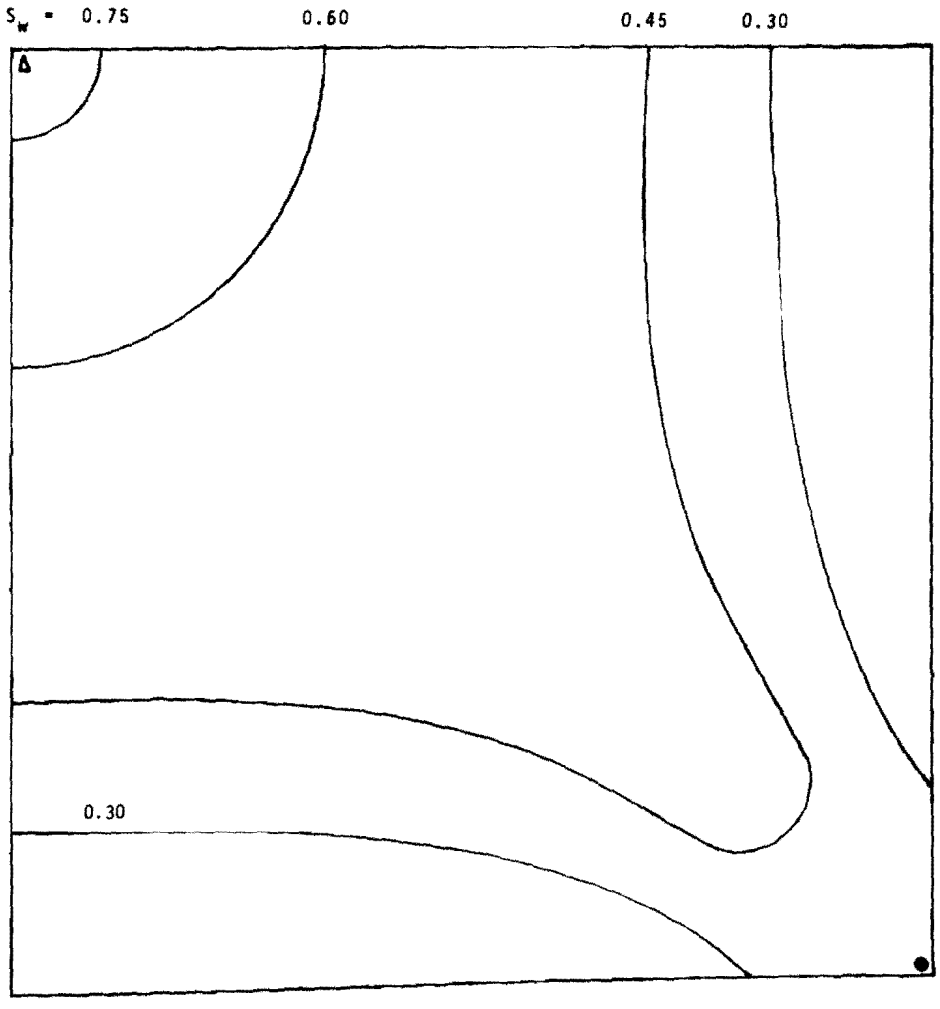

FIGURE 35. CALCULATED WATER SATURATION DISTRIBUTION BEFORE ELECTRIC HEATING FOR FIELD CASE I

△ INJECTION WELL

● PRODUCTION WELL

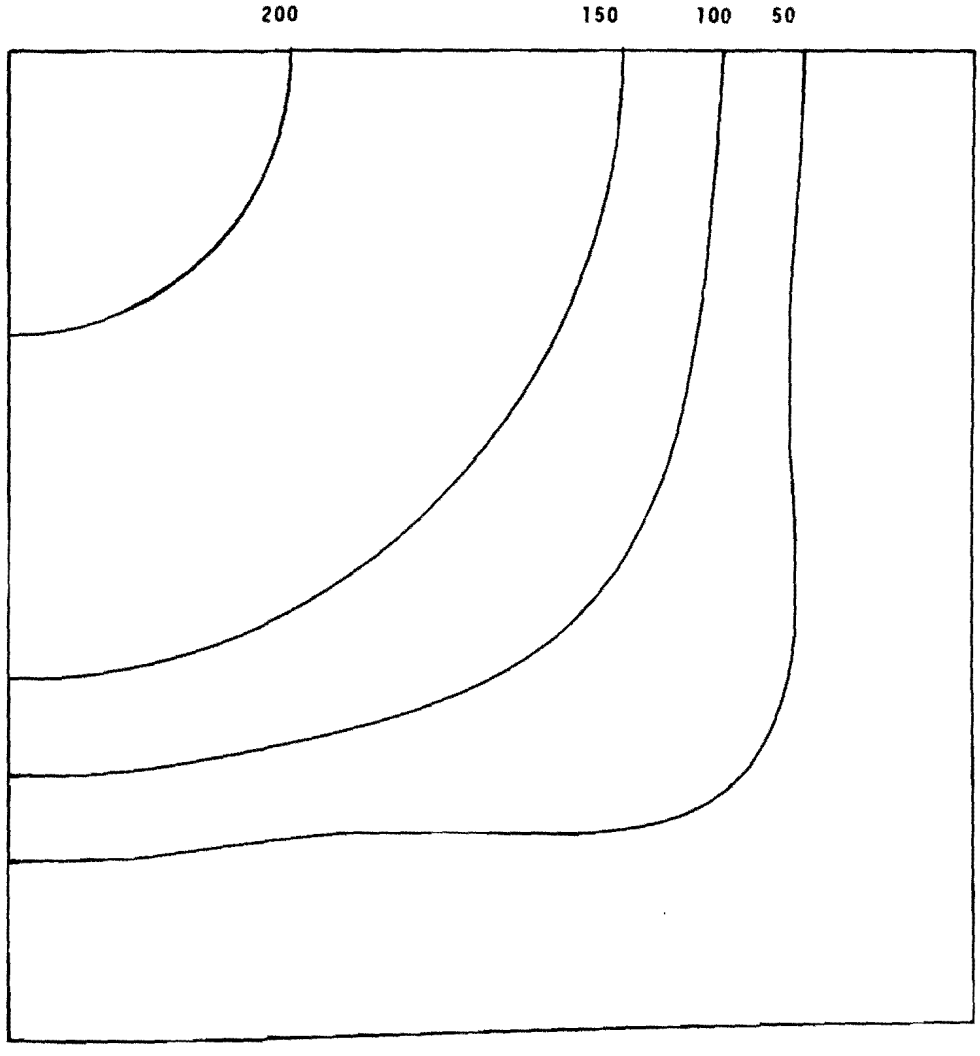

FIGURE 36. CALCULATED SALT CONCENTRATION DISTRIBUTION, THOUSAND P.P.M., BEFORE HEATING FOR FIELD CASE I

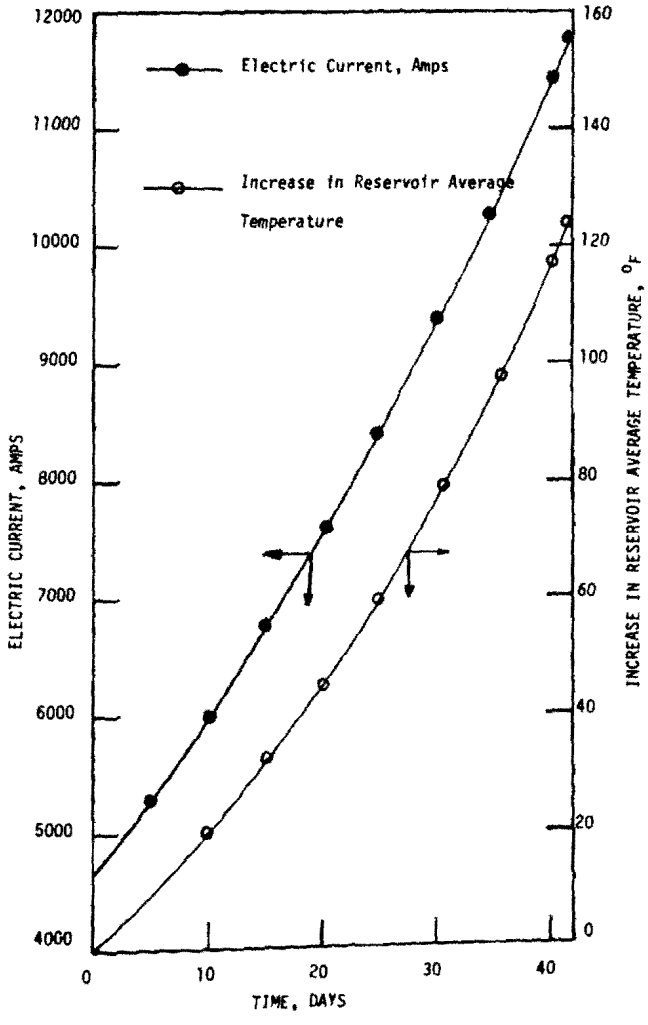

FIGURE 37. ELECTRIC CURRENT AND INCREASE IN AVERAGE RESERVOIR TEMPERATURE VS. TIME FOR FIELD CASE I

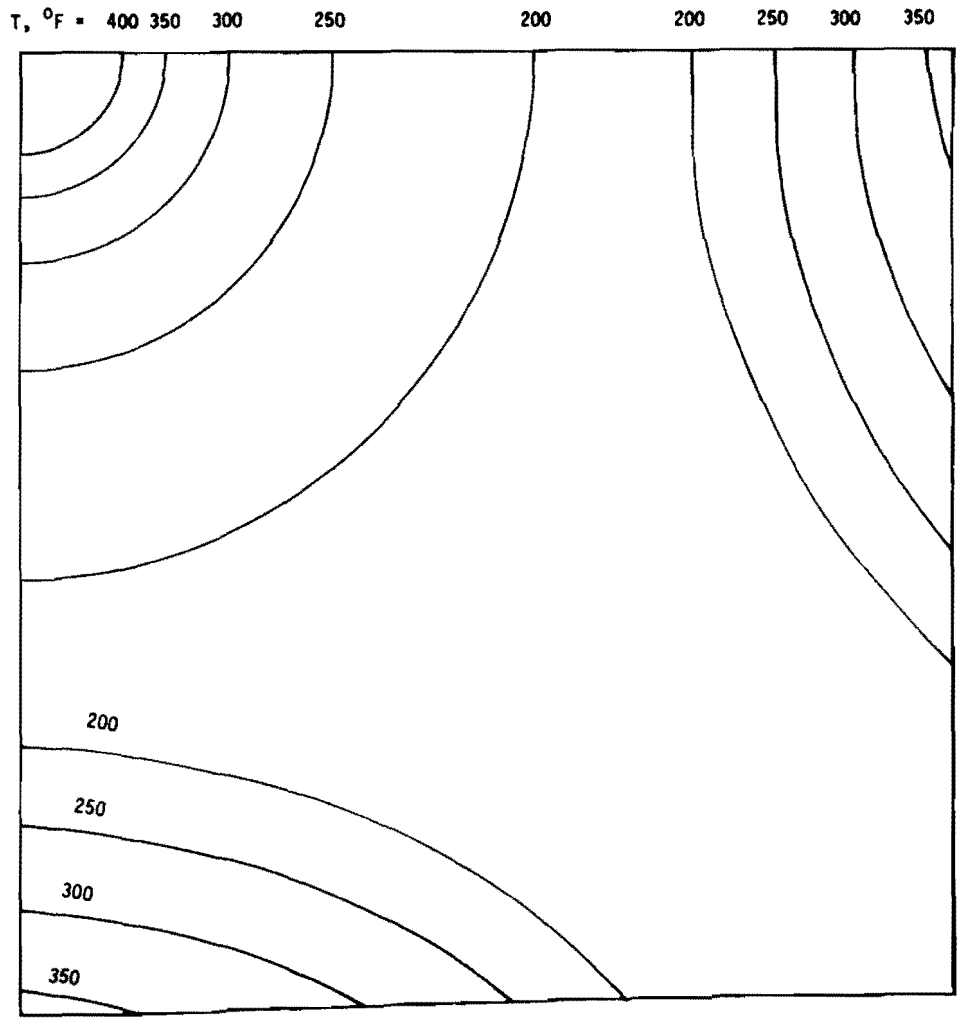

FIGURE 38. CALCULATED TEMPERATURE DISTRIBUTION AFTER HEATING FOR FIELD CASE I

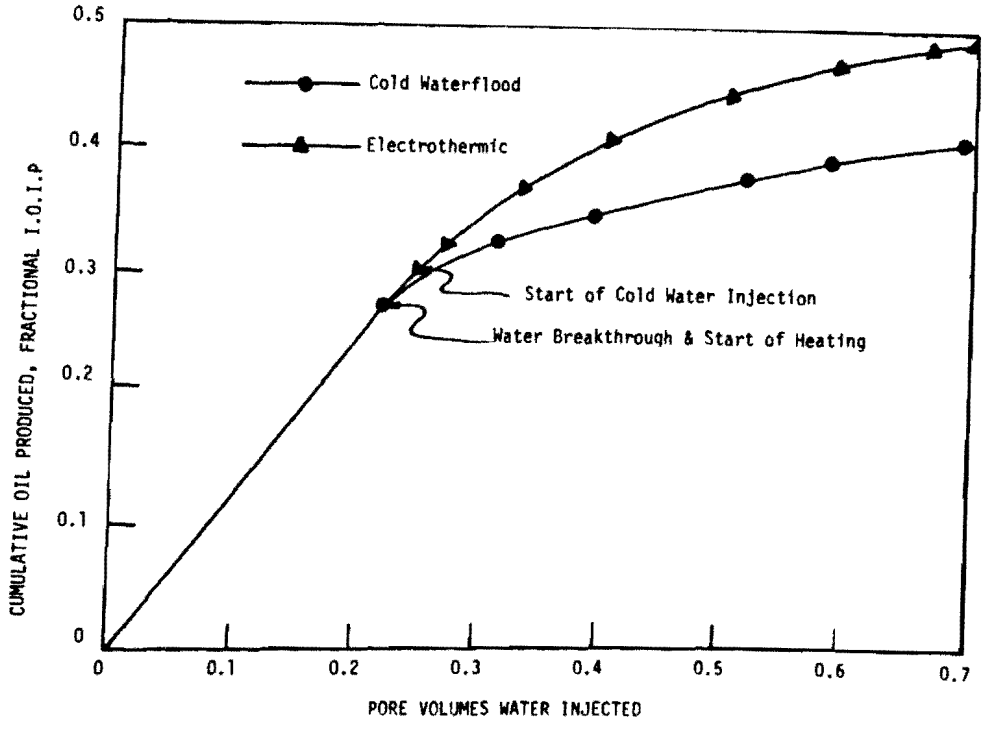

FIGURE 39. OIL RECOVERY BY THE ELECTROTHERMIC TECHNIQUE FOR FIELD CASE I

TABLE III

RESERVOIR AND OPERATING CHARACTERISTICS

USED WITH FIELD CASE I

Reservoir Characteristics:	
Well Spacing, Ft.	450
Thickness, Ft.	100
Porosity, Fraction	0.3
Absolute Permeability, Darcy	0.6
Initial Oil Saturation, Fractional Pore Volume	0.8
Initial Water Saturation, Fractional Pore Volume	0.2
Initial Reservoir Pressure, psi	3,000
Initial Reservoir Temperature, °F	130
Oil Viscosity @ 130 °F, cp	50
Initial Salt Concentration of Connate Water, p.p.m	16,500
Operating Characteristics:	
Water Injection Rate, STB/Day	800
Salt Concentration of Water Injected Before and During Electric Heating, p.p.m	200,000
E.M.F. Applied, Volts	1,000
Duration of Electric Heating, Days	42
Thermal Conductivity of Adjacent Strata, BTU/hr-ft-°F (Reference 39)	0.45

TABLE IV

RESERVOIR AND OPERATING CHARACTERISTICS

USED WITH FIELD CASE II

Reservoir Characteristics:	
Well Spacing, Ft.	500
Thickness, Ft:	
Less Permeable Layer	100
More Permeable Layer	100
Porosity, Fraction:	
Less Permeable Layer	0.30
More Permeable Layer	0.32
Absolute Permeability, Darcy:	
Less Permeable Layer	0.40
More Permeable Layer	1.20
Initial Oil Saturation, Fractional Pore Volume:	
Less Permeable Layer	0.75
More Permeable Layer	0.80
Initial Water Saturation, Fractional Pore Volume:	
Less Permeable Layer	0.25
More Permeable Layer	0.20
Initial Reservoir Pressure, psi	3,000
Initial Reservoir Temperature, °F	110
Oil Viscosity @110 °F, cp	50
Initial Salt Concentration of Connate Water, p.p.m	200,000

TABLE IV

RESERVOIR AND OPERATING CHARACTERISTICS

USED WITH FIELD CASE II

(Continued)

Operating Characteristics:
Water Injection Rate, STB/Day:
Less Permeable Layer.....400
More Permeable Layer: Presented in Figure 40
Salt Concentration of Water Injected Before Heating, p.p.m.....1,000
Salt Concentration of Injected Water During Heating, p.p.m.....200,000
E.M.F. Applied, Volts: Presented in Figure 47
Duration of Electric Heating, Days.....28
Thermal Conductivity of Adjacent Strata, BTU/hr-ft-$^{\circ}$F (Reference 30).....0.45

2. Field Case II

The following outline indicates the steps of the simulated electrothermic process used with Field Case II:

i. Water of low salinity (1,000 p.p.m.) was injected into the oil reservoir. Injection rate for the less permeable layer was maintained at 400 STB/D. The calculated pressure drop between the injection block and the production block of the less permeable layer during the flooding process was utilized to calculate the water injection rate in the more permeable layer. Low salinity water injection continued until the more permeable layer was flooded with 0.8 pore volume cumulative water injected.

ii. An alternating current supply of 2,000 volts was connected with the current electrodes placed in the injection wells for 11 days. The applied e.m.f. was then reduced to 1,250 volt and electric heating continued for another 17 days. Brine of high salinity (200,000 p.p.m.) was injected into the oil reservoir during the heating period.

iii. Conventional waterflooding followed the electric heating and continued until the water/oil ratio of the combined layers increased to 27.8, which was assumed to be the economic limit of the flood.

Figures 41 and 42 detail the calculated water saturation distribution before heating for the more and less permeable layers respectively. The salt concentration distribution before heating for the two layers is given in Figures 43 and 44. The temperature distribution at the end of the heating period for the two layers is given in Figures 45 and 46. Figure 47 presents the electric current injected into each layer vs. time. Figure 48 shows the increase in the average temperature of the

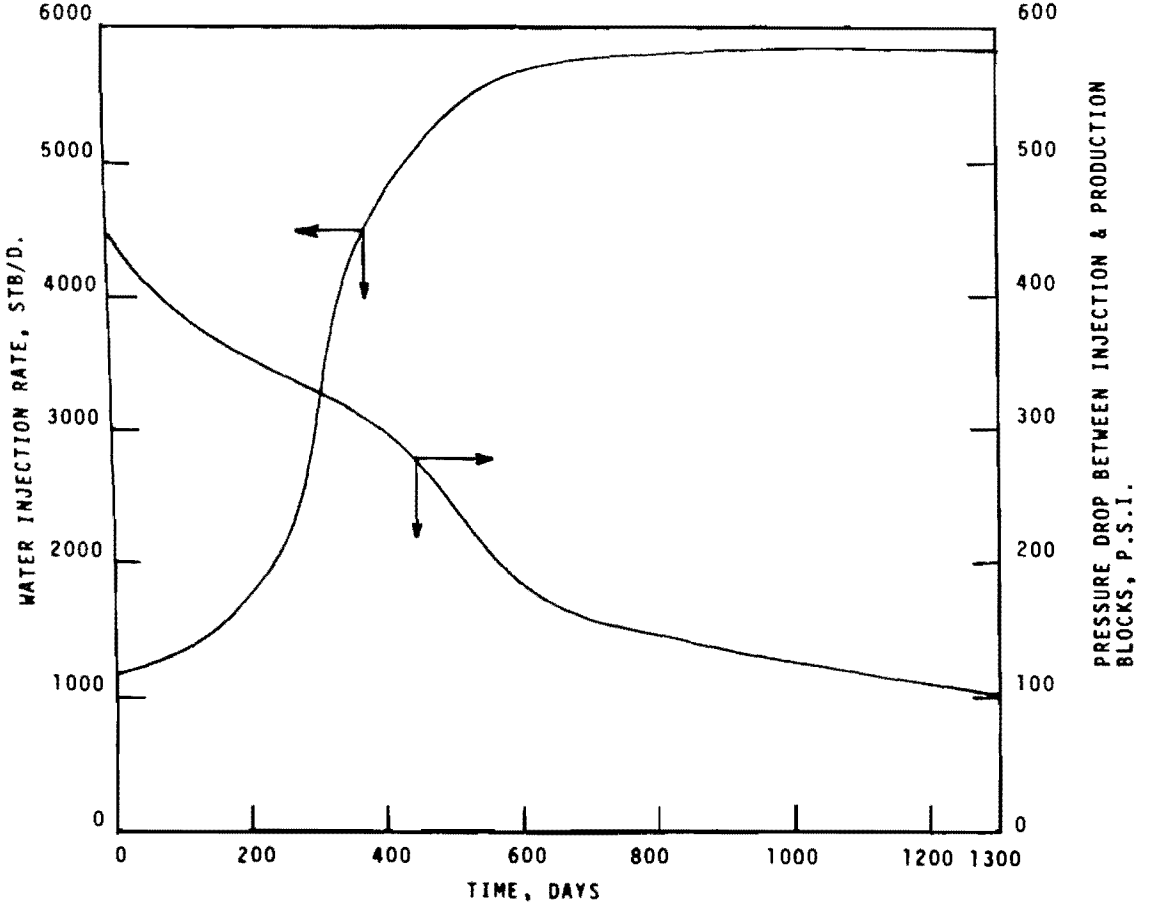

FIGURE 40. WATER INJECTION RATE & PRESSURE DROP VS. TIME FOR THE MORE PERMEABLE LAYER, FIELD CASE II

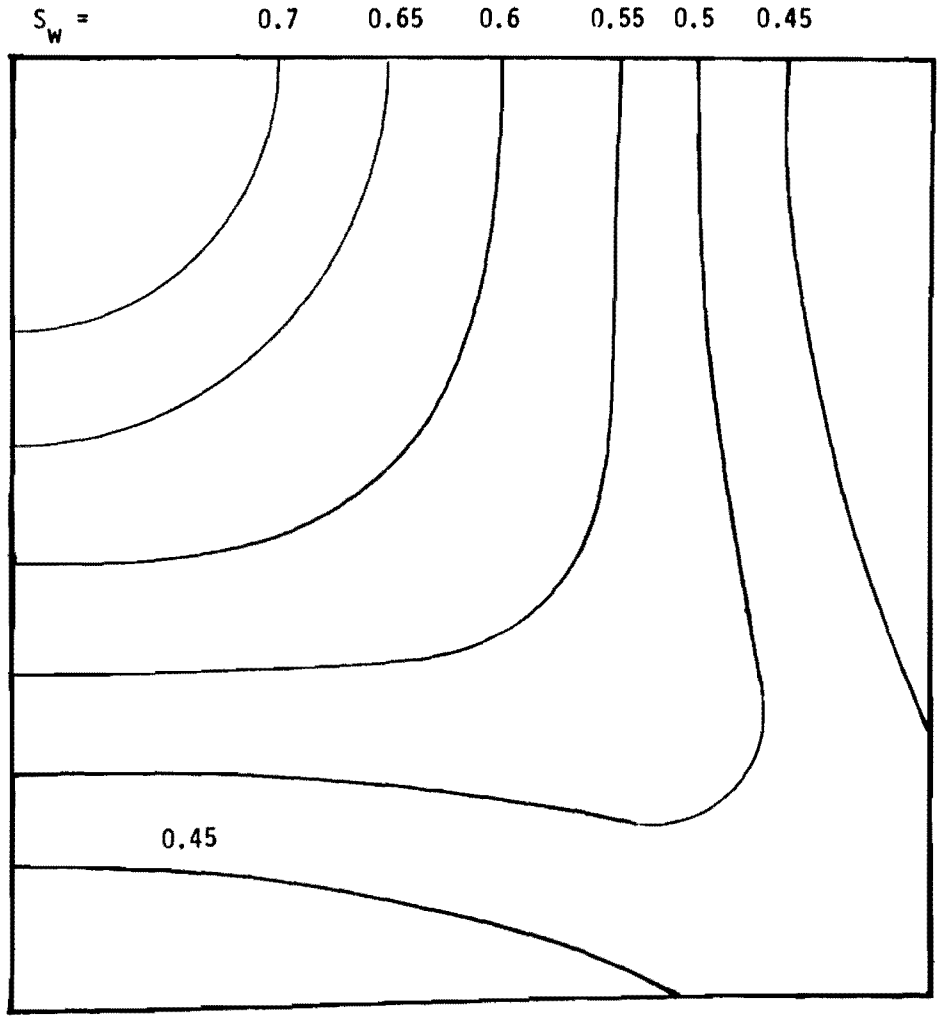

FIGURE 41. CALCULATED WATER SATURATION DISTRIBUTION BEFORE HEATING FOR THE MORE PERMEABLE LAYER, FIELD CASE II

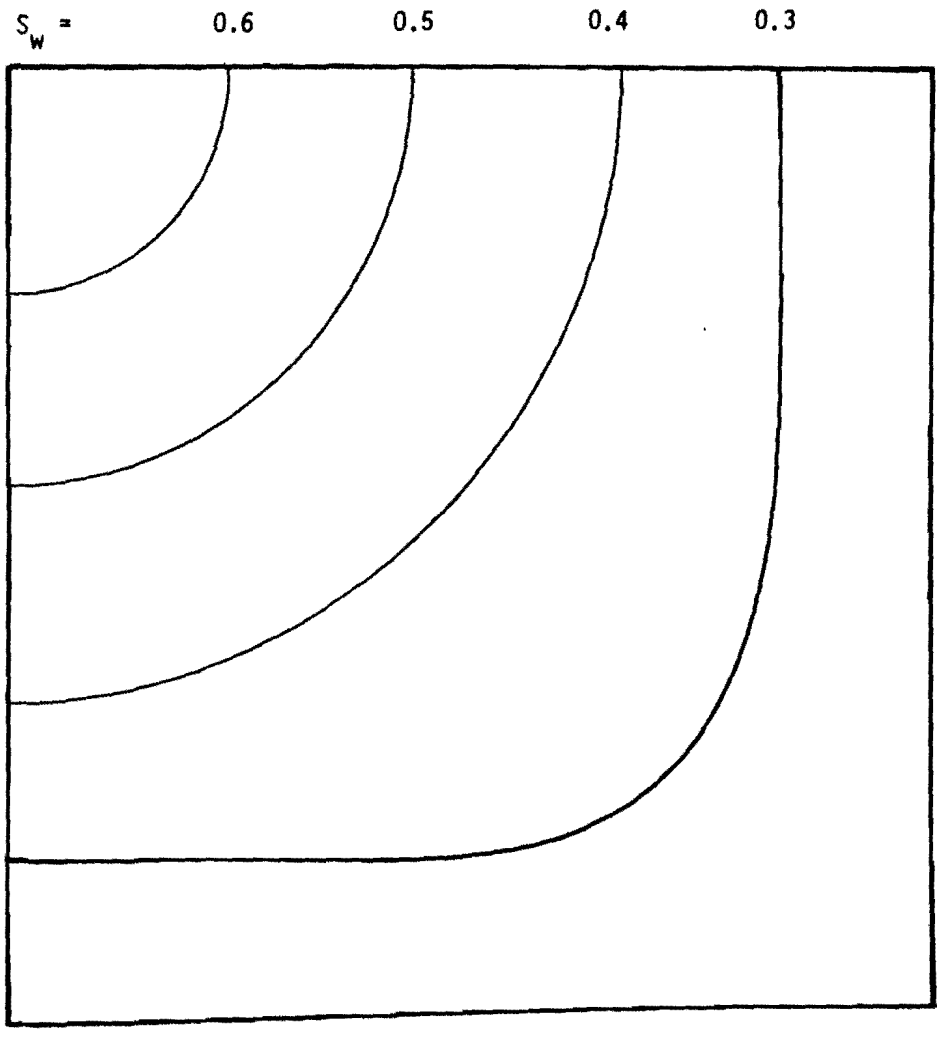

FIGURE 42. WATER SATURATION DISTRIBUTION BEFORE HEATING FOR THE LESS PERMEABLE LAYER, FIELD CASE II

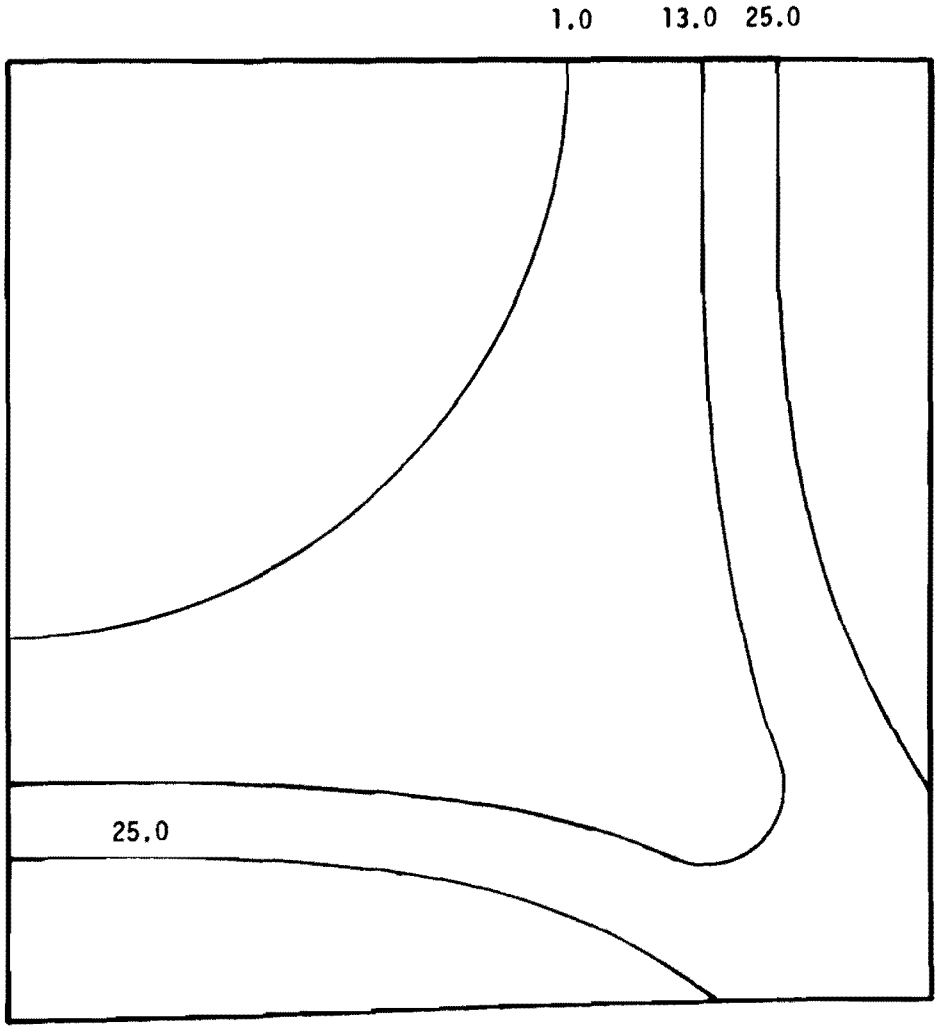

FIGURE 43. SALT CONCENTRATION DISTRIBUTION BEFORE HEATING, THOUSAND P.P.M., FOR THE MORE PERMEABLE LAYER, FIELD CASE II

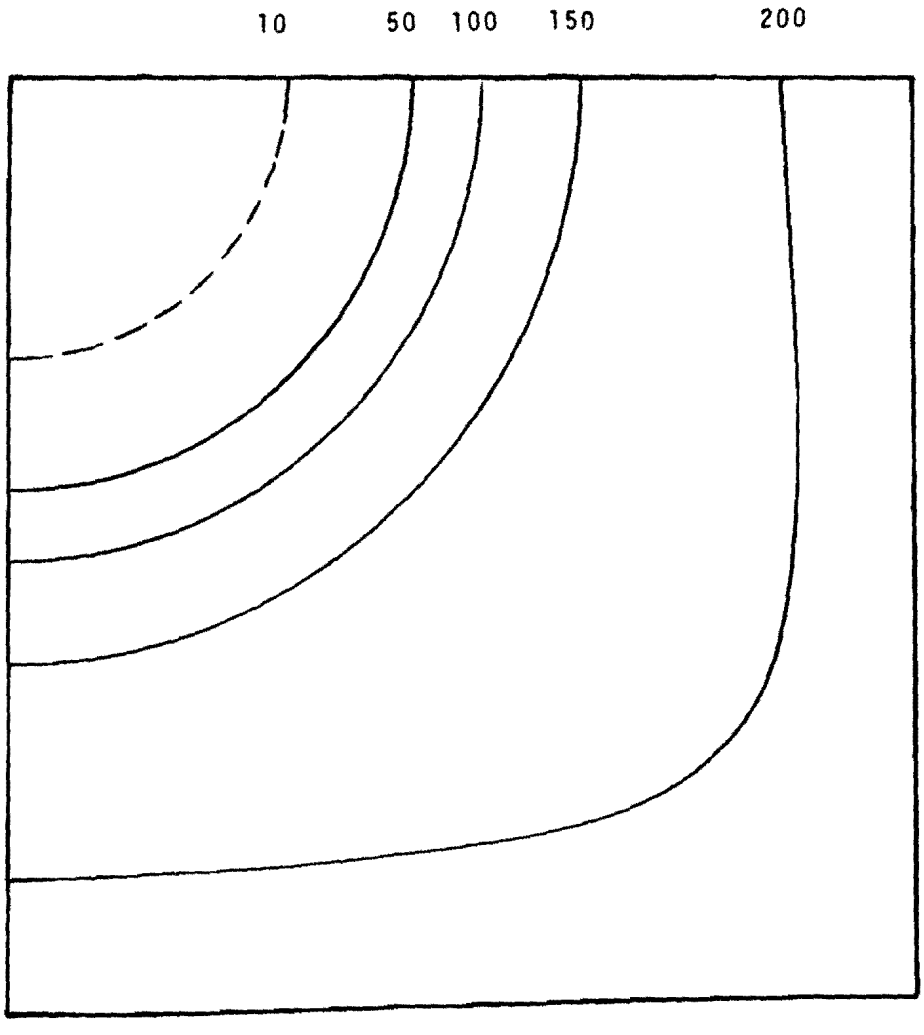

FIGURE 44. SALT CONCENTRATION DISTRIBUTIO BEFORE HEATING, THOUSAND P.P.M., FOR THE LESS PERMEABLE LAYER, FIELD CASE II

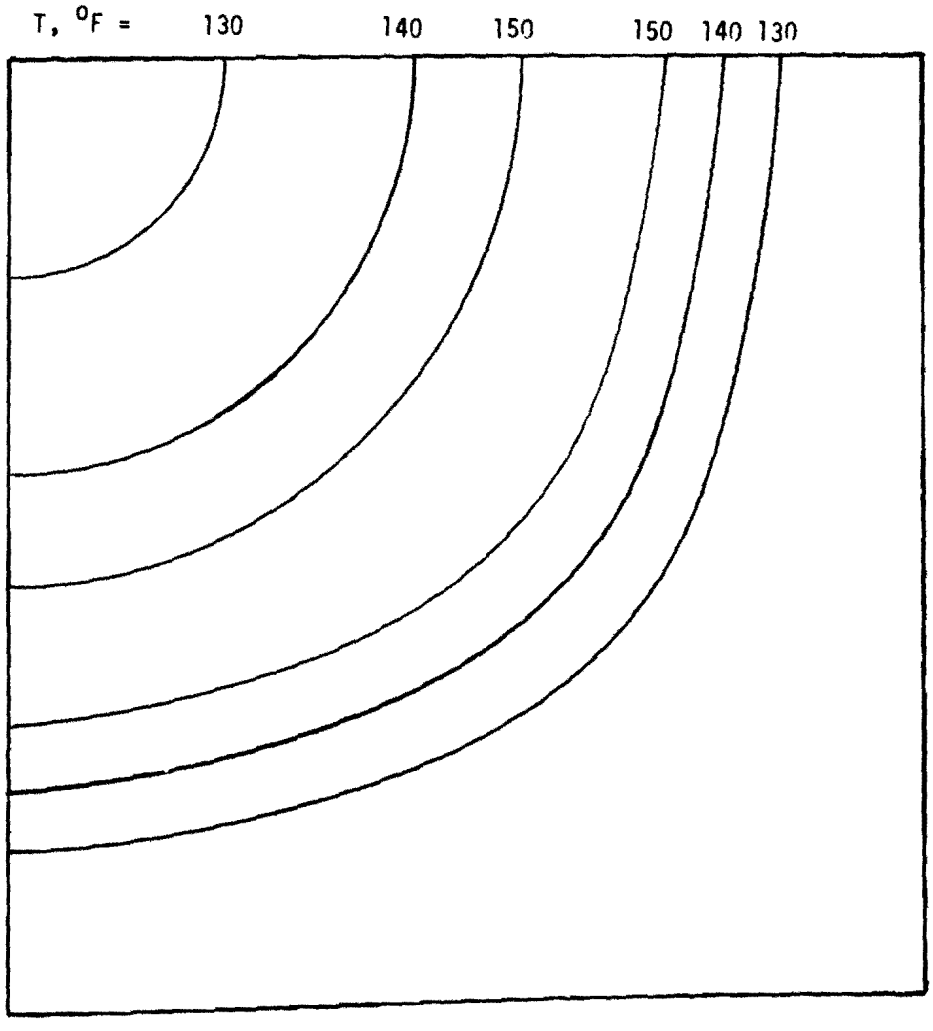

FIGURE 45. TEMPERATURE DISTRIBUTION AT THE END OF ELECTRIC HEATING FOR THE MORE PERMEABLE LAYER, FIELD CASE II

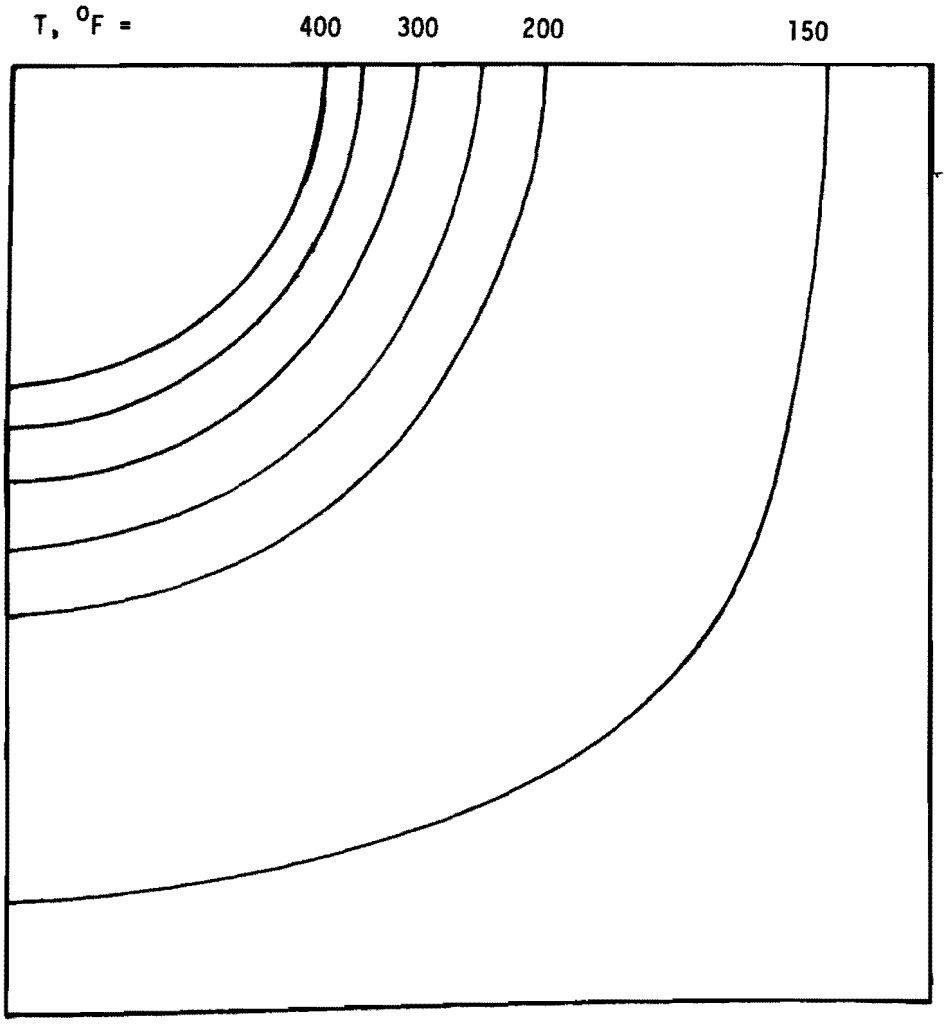

FIGURE 46. TEMPERATURE DISTRIBUTION AT THE END OF ELECTRIC HEATING FOR THE LESS PERMEABLE LAYER, FIELD CASE II

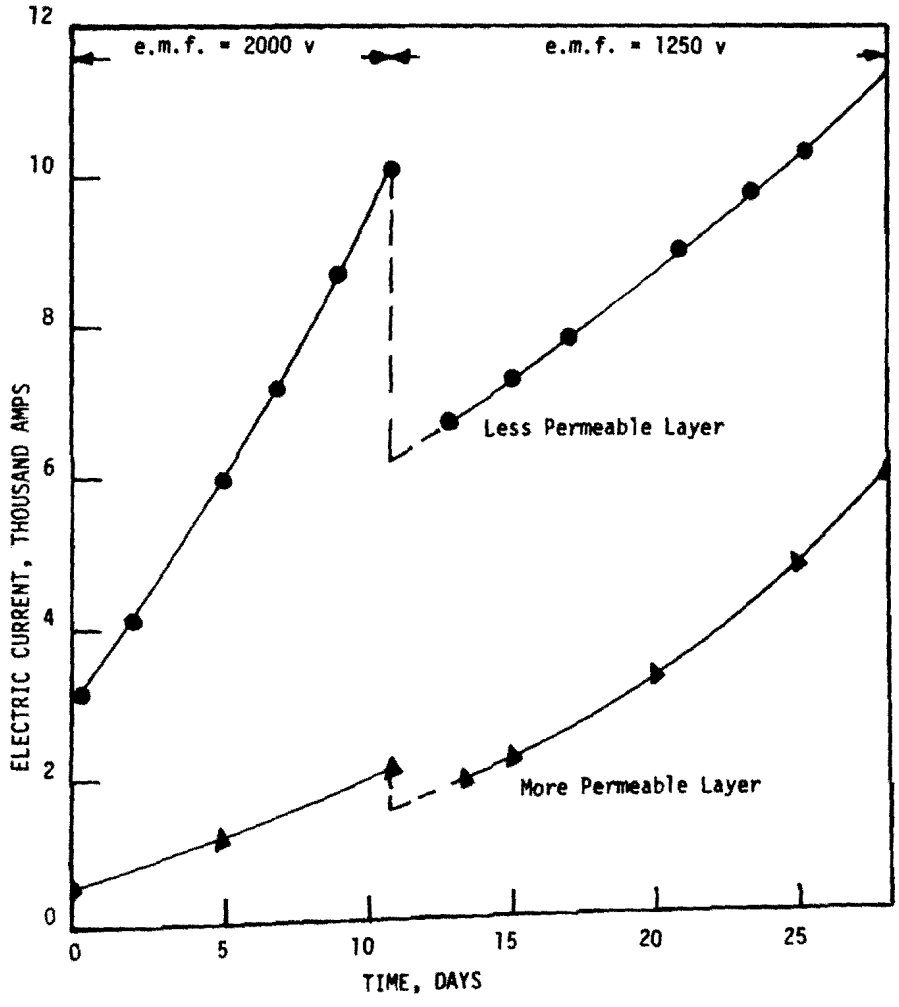

FIGURE 47. ELECTRIC CURRENT VS. TIME FOR FIELD CASE II

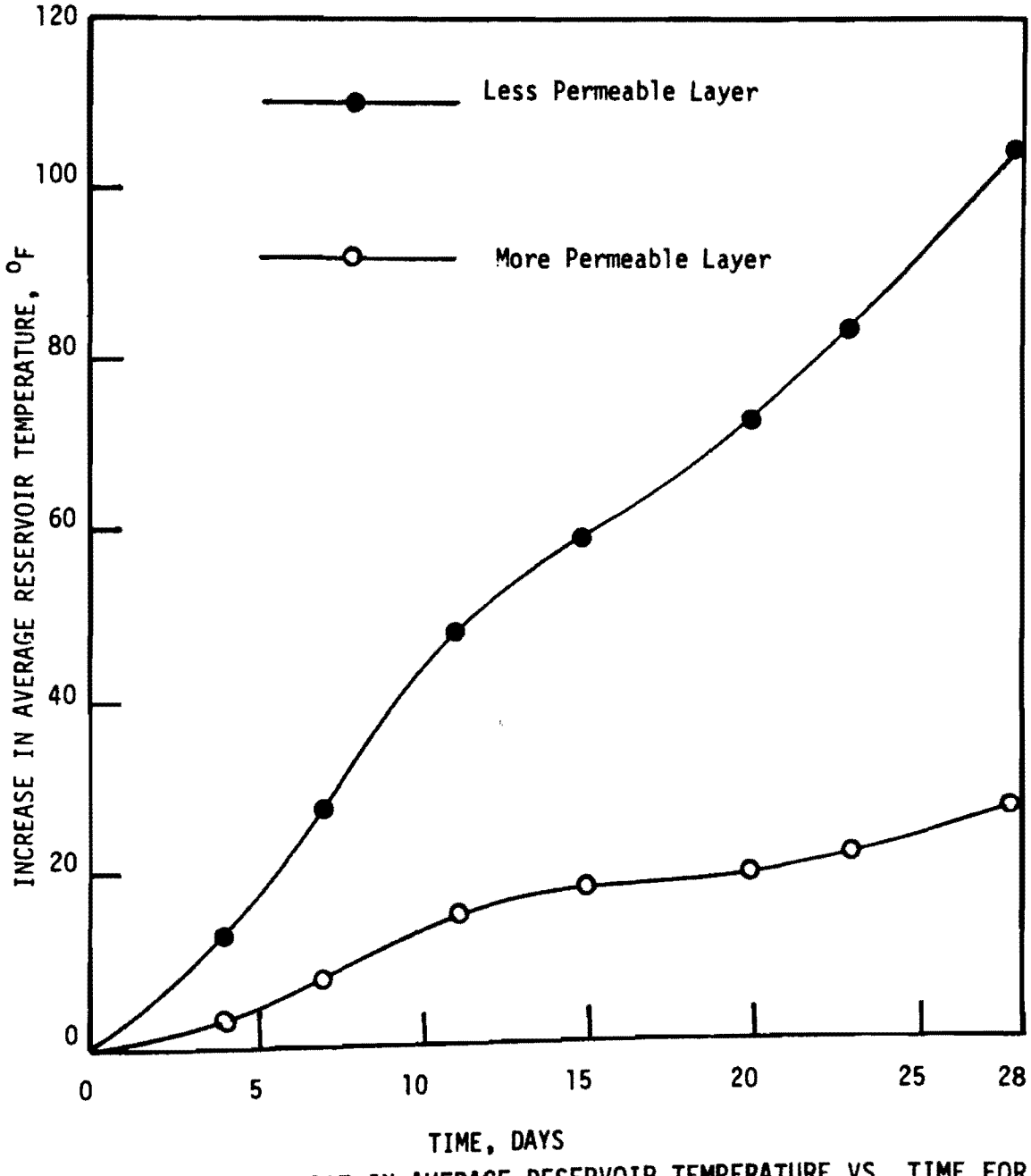

FIGURE 48. INCREASE IN AVERAGE RESERVOIR TEMPERATURE VS. TIME FOR FIELD CASE II

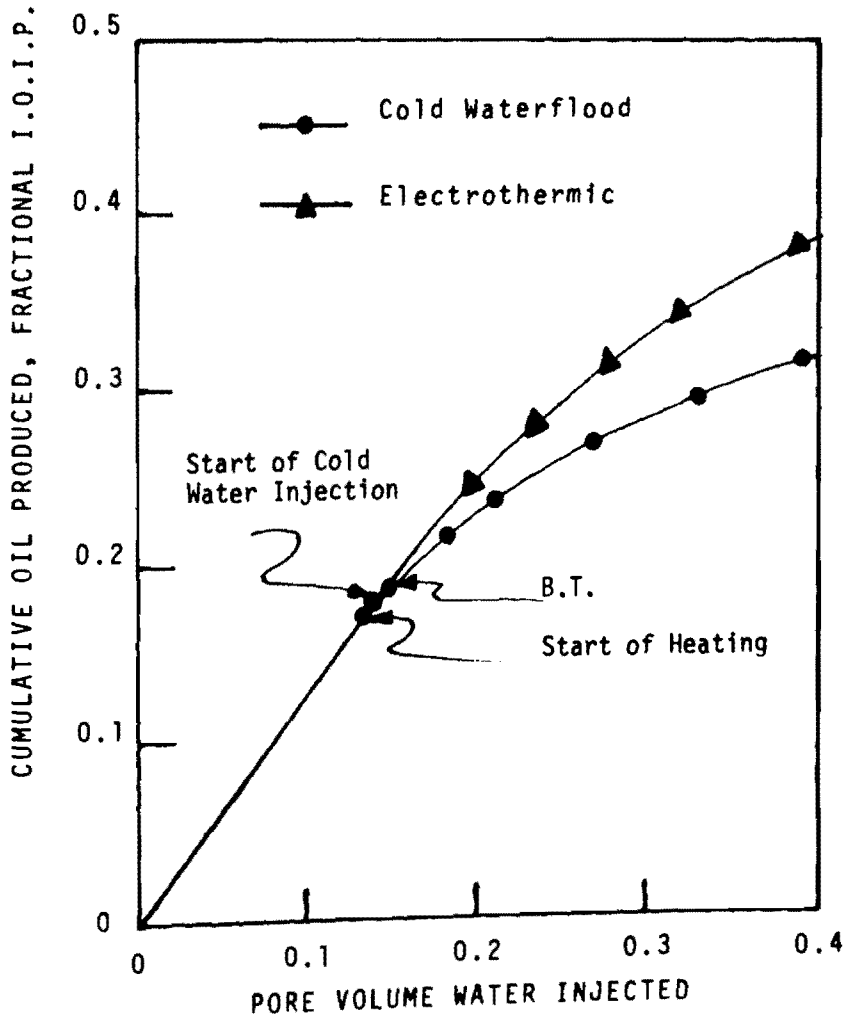

FIGURE 49. OIL RECOVERY BY THE ELECTROTHERMIC TECHNIQUE FOR THE LESS PERMEABLE LAYER, FIELD CASE II

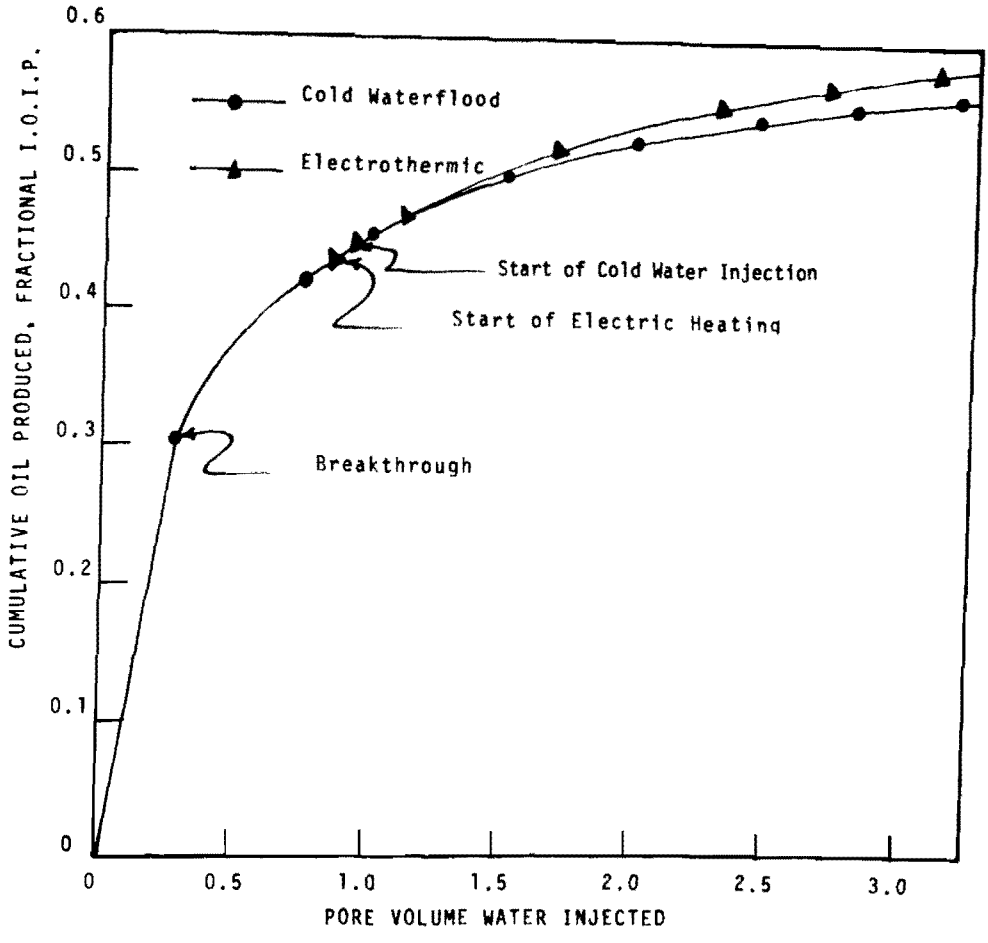

FIGURE 50. OIL RECOVERY BY THE ELECTROTHERMIC TECHNIQUE FOR THE MORE PERMEABLE LAYER, FIELD CASE II

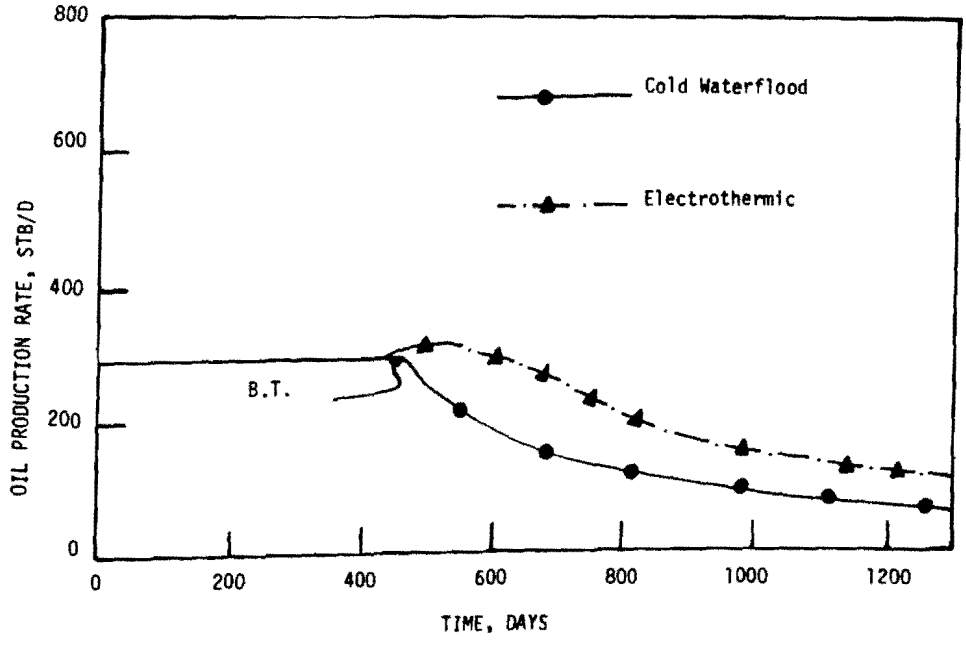

FIGURE 51. OIL PRODUCTION RATE VS. TIME FOR THE LESS PERMEABLE LAYER, FIELD CASE II

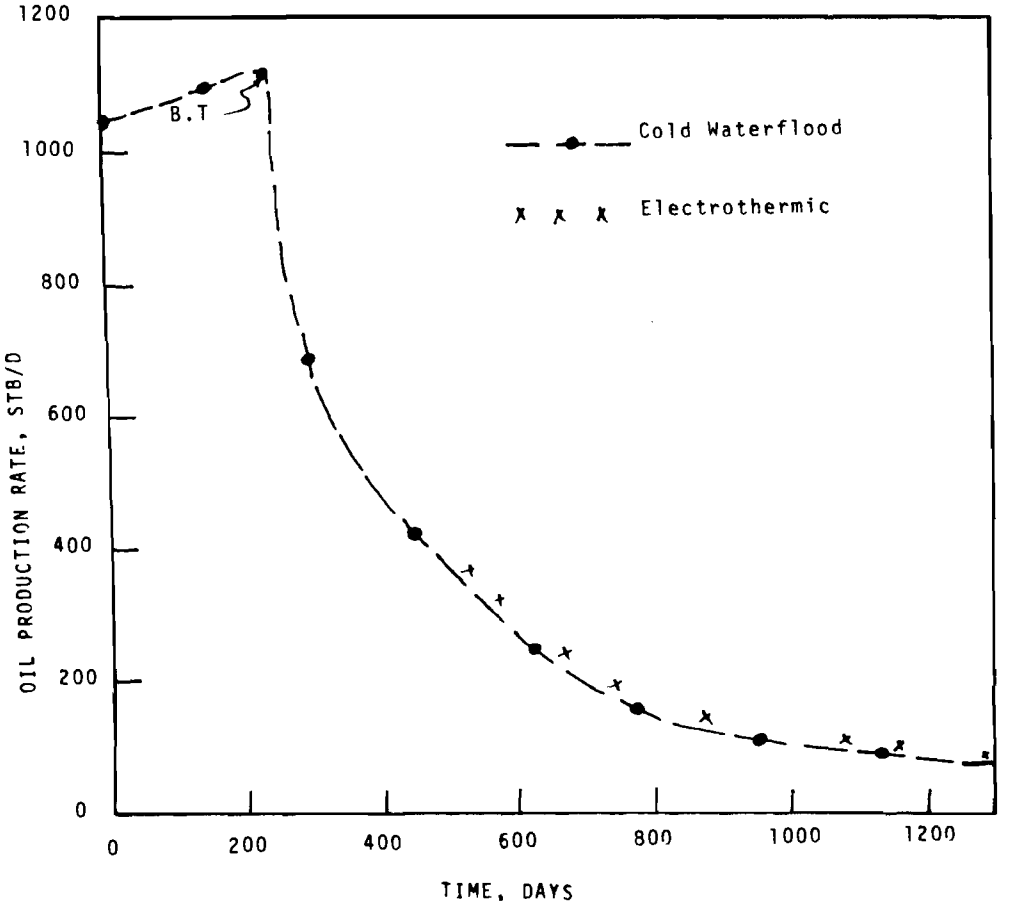

FIGURE 52. OIL PRODUCTION RATE VS. TIME FOR THE MORE PERMEABLE LAYER, FIELD CASE II

two layers during the heating process. The increase in the less permeable layer average temperature was 105^{o}F while that of the more permeable layer was 29^{o}F. Comparison of cumulative oil produced by the electrothermic technique and that by conventional waterflood for each layer is given in Figures 49 and 50. Table V summarizes the additional oil produced and the electric energy utilized in Field Case II.

TABLE V

THE ADDITIONAL OIL PRODUCED AND ELECTRIC ENERGY UTILIZED

FOR FIELD CASE II

Less Permeable Layer	
Additional Oil Produced, STB	53,538
Electric Energy Utilized, KWH	8.0152×10^6
KWH/STB	149.71
More Permeable Layer	
Additional Oil Produced, STB	7,864
Electric Energy Utilized, KWH	3.43×10^6
KWH/STB	436.16
KWH/STB for Field Case II	186.4
KWH Utilized in the More Permeable Layer/KWH Utilized in the LessPermeable Layer	0.428

Comparison between oil production rate by cold waterflood and that by electrothermic technique for each layer is shown in Figures 51 and 52.

VIII. CONCLUSIONS

The following conclusions may be drawn from the experimental and theoretical investigation of oil recovery by the electrothermic technique:

1. The agreement that was obtained between calculated and measured performance of the process in a laboratory model supports the assumptions and mathematical technique employed in this study.

2. The electric energy consumed per additional STB of oil produced from the hypothetical oil reservoirs studied, is low enough to suggest the possibility of commercial application of the process.

3. The high wattage applied during electric heating will require the design of specialized equipment for field use of the process.

4. Under the reservoir conditions that were considered, the approach described in U.M.R. Patent Disclosure No. 75-P-UMR-003 might be used to accomplish the selective heating of relatively undepleted portions of the reservoir.

NOMENCLATURE

Dimensions of the variables are specified by letting M = mass, L = length, Q = charge, t - time, and T = temperature.

Variables

A = area, L^2.

C = heat capacity, L^2/t^2T.

c = constant, dimensionless.

D = flux density, Q/L^2.

E = electric field intensity, ML/t^2Q.

f = frequency, $1/t$.

g = gravitational acceleration, L/t^2.

H = potential head, L.

h = thickness, L.

I = number of grid blocks in x direction, dimensionless.

J = number of grid blocks in y direction, dimensionless.

$\tilde{I}$ = current, Q/t.

i = i'th location in calculation grid, dimensionless.

$\tilde{i}$ = $\sqrt{-1}$, dimensionless.

j = j'th location in calculation grid, dimensionless.

$\tilde{J}$ = current density, Q/L^2t.

K = effective permeability, L^2.

K_r = relative permeability, dimensionless.

K_t = thermal conductivity, ML/t^3T.

N = number of grid blocks, dimensionless.

n = direction of the perpendicular to the confining boundary, dimensionless.

p = pressure, M/Lt^2.

q_o = oil mass rate (injected or produced) per unit reservoir volume, M/L^3t.

q_w = water mass rate (injected or produced) per unit reservoir volume, M/L^3t.

q_{ov} = volumetric oil rate (injected or produced) per unit reservoir volume at reservoir temperature and pressure, $1/t$.

q_{wv} = volumetric water rate (injected or produced) per unit reservoir volume at reservoir temperature and pressure, $1/t$.

q_{ovstp} = volumetric oil rate (injected or produced) per unit reservoir volume at standard temperature and pressure, $1/t$.

q_{wvstp} = volumetric water rate (injected or produced) per unit reservoir volume at standard temperature and pressure, $1/t$.

q_v = volumetric flux, L/t.

R = resistivity, ML^3/tQ^2.

s = surface area, L^2.

t = time, t.

T = temperature, T.

v = volume, L^3.

x = space coordinate, L.

y = space coordinate, L.

z = vertical coordinate, L.

ε = permittivity (dielectric constant), t^2Q^2/ML^3.

ρ = fluid density, M/L^3.

ρ_c = charge density, Q/L^3.

$\tilde{\sigma}$ = fluid conductivity of porous medium, tL^3/M.

σ = electric conductivity, tQ^2/ML^3.

μ = viscosity, M/Lt.

Φ = fluid flow potential, M/Lt^2.

ϕ = porosity, dimensionless, fraction.

β = formation volume factor, dimensionless.

Ψ = electric potential, ML^2/t^2Q.

Subscripts

a = adjacent strata

c = capillary

e = effective

f = fluid

i,j,k = indices of spatial location

o = oil

ow = oil-water

r = rock

s = sand

w = water

BIBLIOGRAPHY

1. Bleakley, W.B.: "Unique Electrothermic Recovery Method Gets Rocky Mountain Test," Oil and Gas Journal (December, 1969) 162.

2. Editors of World Oil: "AC Current Heats Heavy Oil for Extra Recovery," World Oil (May, 1970) 83.

3. Crowson, F. L., and Gill, G.W.: "Method and Apparatus for Secondary Recovery of Oil," U.S. Patent No. 3,605,888.

4. Parker, H.W.: "Hydro-Electrolysis of Oil Shale in Situ," U.S. Patent No. 3,428,125.

5. Harvey, A.H. and Govier, J.P.: U.M.R. Patent Disclosure No. 75-P-UMR-003, unpublished.

6. Poisson, S.D.: "Theorie Mathematique de la Chaleur," Bachelier, Parie (1835).

7. Lauwerier, H.A.: "The Transport of Heat in an Oil Layer Caused by Injection of Hot Fluid," Applied Scientific Research (1955) A-5, 145.

8. Marx, J.W., and Langenheim, R.H.: "Reservoir Heating by Hot Fluid Injection," Transactions, AIME (1959) 216, 312.

9. Ramey, H.J.: "Reservoir Heating by Hot Fluid Injection," Transactions, AIME (1959) 216, 364.

10. Spillette, A.G.: "Heat Transfer During Hot Fluid Injection into an Oil Reservoir," Journal of Canadian Petroleum Technology (October - December, 1965) 213.

11. Klinkenberg, A.: "Numerical Evaluation of Equations Describing Transient Heat and Mass Transfer in Packed Solids," Ind. Eng. Chem. (1948) 40, 1992.

12. Preston, F.W., and Hazen, R.D.: "Further Studies on Heat Transfer in Unconsolidated Sands During Hot Water Injection," Producers Monthly (February, 1954) 24.

13. Lynch, J.E.: Formation Evaluation. New York: Harper & Row, Inc., 1964.

14. Buckley, S.E., and Leverett, M.C.: "Mechanism of Fluid Displacement in Sands," Transactions, AIME (1942) 164, 1.

15. Hodgman, C.D.: Handbook of Chemistry and Physics. Cleveland, Ohio: Chem. Rubber Publishing Company, Inc., 1965.

16. Beal, C.: "The Viscosity of Air, Water, Natural Gas, Crude Oil and Associated Gases at Oil Field Temperatures and Pressures," Transactions, AIME (1946) 165, 94.

17. Schild, A.: "A Theory of Heating Oil-Producing Wells," Transactions, AIME (1957) 210, 1.

18. Hougen, O.A., Watson, K.M., and Ragatz, R.A.: Chemical Process Principles. New York: Wiley, 1954.

19. Grover, S.S., and Knudsen, J.G.: "Heat Transfer Between Immiscible Liquids," AICHE Chem. Eng. Progress Symposium Series (1955) 51, 71.

20. Somerton, W.H.: "Some Thermal Characteristics of Porous Rocks," Transactions, AIME (1958) 213, 375.

21. Kunii, D., and Smith, J.M.: "Heat Transfer Characteristics of Porous Rocks," AICHE Journal (1960) 6, 71.

22. Somerton, W.H., and Boozer, G.D.: "Thermal Characteristics of Porous Rocks at Elevated Temperatures," Transactions, AIME (1960) 219, 418.

23. Somerton, W.H., Mehta, M.M., and Dean, G.W.: "Thermal Alteration of Sandstones," Journal of Petroleum Technology (May, 1965) 589.

24. Asaad, Y.: A Study of the Thermal Conductivity of Fluid-Bearing Porous Rocks, Ph.D. dissertation, University of California, 1965.

25. Kunii, D., and Smith, J.M.: "Thermal Conductivities of Porous Rocks Filled with Stagnant Fluid," Transactions AIME (1961) 222, 37.

26. Copalarathnam, D.D., Hoelscher, H.E., and Laddha, G.S.: "Effective Thermal Conductivity in Packed Beds," AICHE Journal (1961) 7, 249.

27. Adivarahan, P., Kunii, D., and Smith, J.M.: "Heat Transfer in Porous Rocks Through which Single-Phase Fluids are Flowing," Transactions, AIME (1962) 222, 290.

28. Kraus, J.D.: Electromagnetics. New York: McGraw-Hill Book Company, Inc., 1953.

29. Woodside, W., and Messmer, J.H.: "Thermal Conductivity of Porous Media," Journal of Applied Physics (1961) 32, 1688.

30. Crichlow, H.B.: Heat Transfer in Hot Fluid Injection in Porous Media, Ph.D. dissertation, Stanford University, 1972.

31. Somerton, W.H., and Gupta, V.S.: "Role of Fluxing Agents in Thermal Alteration of Sandstones," Journal of Petroleum Technology (November, 1965) 585.

32. Waldorf, D.M.: "Effect of Steam on Permeability of Water Sensitive Formations," Journal of Petroleum Technology (October, 1965) 1219.

33. Hossain, A.K.M.: "The Displacement of Oil from Unconsolidated Sands by High Temperature Fluid Injection, M.S. thesis, Texas A&M University, 1965.

34. Poston, S.W., Ysrael, S., Hossain, A.K., Montgomery, E.F., and Ramey, H.J.: "The Effect of Temperature on Relative Permeability of Unconsolidated Sands," Paper SPE 1897, presented at 42nd annual Fall Meeting of SPE of AIME, Houston, Texas (October, 1967).

35. Habowski, E.: The Effect of Large Temperature Changes on Relative Permeability Ratios, M.S. thesis, The Pennsylvania State University, 1966.

36. Edmondson, T.A.: "Effect of Temperature on Waterflooding," Journal of Canadian Petroleum Technology (December, 1965).

37. Hubbert, M.K.: "Darcy's Law and the Field Equations of Flow of Underground Fluids," Transactions, AIME (1956) 207, 222.

38. Hubbert, M.K.: "The Theory of Groundwater Motion," Journal of Geology (1940) 48, 785.

39. Davidson, L.B.: A Theoretical Analysis of Reservoir Behavior during the Intermittent Injection of Steam, Ph.D. dissertation, Stanford University, 1966.

40. Bailey, H.R., and Larkin, B.K.: "Conduction-Convection in Underground Combustion," Transactions, AIME (1960) 219, 320.

41. Miller, F.G.: "Multi-Phase Flow Theory and the Problem of Spacing Oil Wells," U.S. Bureau of Mines Bulletin (1954) 529, 1.

42. Ames, W.F.: Nonlinear Partial Differential Equations in Engineering. New York: Academic Press, Inc., 1965.

43. Smith, G.D.: Numerical Solution of Partial Differential Equations. Oxford: University Press, Inc., 1965.

44. Varga, R.S.: Matrix Iterative Analysis. New Jersey: Prentice Hall, Inc., 1962.

45. Dusinberre, G.M.: Numerical Analysis of Heat Flow. New York: McGraw-Hill Book Company, Inc., 1949.

46. Rapoport, L.A., Carpenter, C.W., and Leas, W.J.: "Laboratory Studies of Five-Spot Waterflood Performance," Transactions, AIME (1958) 213, 113.

47. Dyes, A.B., Caudle, B.H., and Erickson, R.A.: "Production After Breakthrough--as Influenced by Mobility Ratio," Transactions, AIME (1954) 201, 81.

48. Craig, F.F., Geffen, T.M., and Morse, R.A.: "Oil Recovery Performance of Pattern Gas or Water Injection Operations from Model Tests," Transactions, AIME (1955) 204, 7.

49. Spiegel, M.R.: Theory and Problems of Vector Analysis. New York: Schaum Publishing Company, 1959.

50. Miller, F.G., and Seban, R.A.: "The Conduction of Heat Incident to theFlow of Vaporizing Fluids in Porous Media," Transactions, AIME (1955) 204, 282.

51. Hirschfelder, J.O., Curtiss, C.F., and Bird, R.B.: Molecular Theory of Gases and Liquids. New York: Wiley, Inc., 1954.

52. Johnson, P.A., and Babb, A.L.: "Liquid Diffusion in Non-Electrolytes," Chem. Revs. (1956) 56, 387.

53. Douglas, J.P., Peaceman, D.W., and Rachford, H.H.: "A Method for Calculating Multi-Dimensional Immiscible Displacement," Transactions, AIME (1959) 216, 297.

54. Bird, R.B., Stewart, W.E., and Lightfoot, E.N.: Transport Phenomena. New York: Wiley, 1960.

55. Chapman, A.J.: Heat Transfer. New York: Macmillan Publishing Company, Inc., 1967.

56. Arnold, M.D.: Personal Communication.

57. Maxwell, J.C.: A Treatise on Electricity and Magnetism. Stanford, California: Academic Reprints, 1953.

58. Stone, H.L.: "Iterative Solution of Implicit Approximations of Multi-Dimensional Partial Differential Equations," SIAM Journal (1968) 5, 530.

59. Spillette, A.G., and Nielson, R.L.: "Two-Dimensional Method for Predicting Hot Waterflood Recovery Behavior," Transactions, AIME (1968) 243, 627.

60. Fayers, F.J.: "Some Theoretical Results Concerning the Distribution of a Viscous Oil by a Hot Fluid in a Porous Medium," Journal of Fluid Mechanics (1962) 13, 65.

61. Ralston, A., and Wilf, H.S.: Mathematical Methods for Digital Computers. New York: Wiley, 1960.

62. Forsythe, G.E., and Richtmeyer, R.D.: Finite Difference Methods for Partial Differential Equations. New York: Wiley, 1960.

63. Kunii, D., and Smith, J.M.: "Heat Transfer Characteristics of Porous Rocks," AICHE Journal (1961) 7, 29.

64. Keller, G.V., and Frischknecht, F.C.: Electrical Methods in Geophysical Prospecting. New York: Pergamon Press, Inc., 1966.

VITA

Samy Abdel-Hakeem El-Feky was born on June 16, 1941, in El-Menoufiah, Egypt. He received his primary and secondary education in Maadi, Egypt, graduating in June, 1960. The author attended Faculty of Engineering, Cairo University, Egypt, for five years, where he obtained a B.S. degree in Petroleum Engineering in June, 1965.

Mr. El-Feky worked for The General Petroleum Company as a Petroleum Engineer in the Eastern Desert, Egypt, from June, 1965, to June, 1971.

The author attended Faculty of Engineering, Al-Azhar University, Egypt, for three years, where he worked as a demonstrator in the Petroleum Engineering Department and obtained an M.S. degree in Petroleum Engineering in October, 1973.

The author has attended the graduate school of the University of Missouri-Rolla since August, 1974.

He is married to Asha A. El-Telb and their first child, Gina, was born in April, 1976.

APPENDICES

APPENDIX A

LIMITATIONS ON THE APPLICABILITY OF DARCY'S LAW

A number of limitations on the generality of Darcy's Law are well known. Some of these are discussed in Part III. Hubbert (37,38) gives a thorough treatment of the principal restrictions. Assumptions about the nature of the fluids in the system are discussed by Davidson (39) who concluded that if the fluid obeys a model other than a Newtonian or a Bingham plastic model, Darcy's Law must be appropriately modified. Assumptions about the potential field in which the fluid moves deserve attention.

The Vector Field of the Volumetric Flux

Darcy's Law may be written in the form

$$\bar{q}_v = -\tilde{\sigma}\nabla\Phi \qquad \text{(A-1)}$$

where Φ is the scalar flow potential and $\tilde{\sigma}$ the conductivity of the syster with respect to the fluid whose movement is given by equation (A-1). This relation states that the flux vector, $\bar{q}_v$, is proportional to the gradient of a scalar. If this is true, an elementary theorem of vector calculus (49) requires that the vector field of q_v be conservative, or equivalently, irrotational. To say that a vector field is conservative implies that the integral

$$\int_{P_1}^{P_2} \bar{q}_v \cdot d\bar{s}$$

where P_1 and P_2 are two points in the space in which the field exists, is independent of the path specified by ds. In particular, the vector

field must satisfy

$$\oint \bar{q}_v \cdot d\bar{s} = 0 \qquad \text{(A-2)}$$

In reservoir systems, equation (A-2) is satisfied when the reservoir is at a uniform temperature or when surfaces of constant temperature are parallel to surfaces of constant potential. Otherwise equation (A-2) is not satisfied (56). A simple example will demonstrate this. The terms in equation (A-1) are assumed to be

$$\tilde{\sigma} = K/\mu \qquad \text{(A-3)}$$

K = permeability

μ = viscosity

$$\frac{\partial \Phi}{\partial x} = \frac{\partial P}{\partial x} - \rho g \frac{\partial z}{\partial x} \qquad \text{(A-4)}$$

g = gravitational acceleration

P = pressure

ρ = density

z = vertical coordinate, positive downward

The integration specified by (A-2) will be carried out for the path ABCD shown in Figure 53. Hence,

$$\oint \bar{q}_v \cdot d\bar{s} = \int_{AB} q_{vx} dx + 0 + \int_{CD} q_{vx} dx + 0 \qquad \text{(A-5)}$$

For a homogeneous rock, $K_2 = K_1 = K$, and

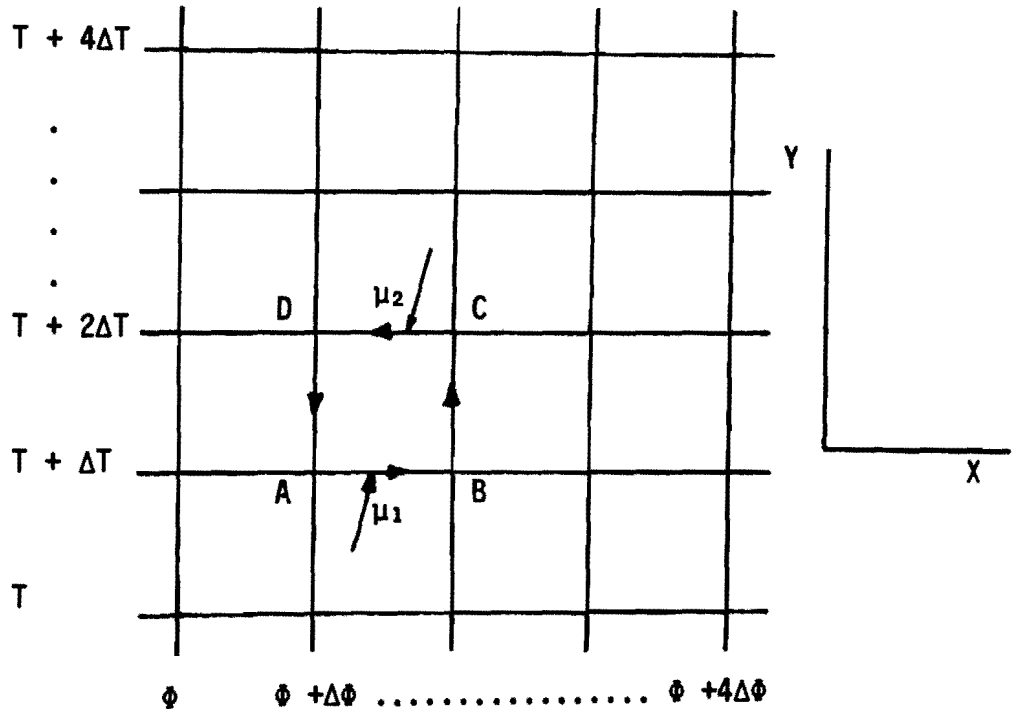

FIGURE 53. HYPOTHETICAL TEMPERATURE AND FLOW POTENTIAL DISTRIBUTION IN A POROUS SYSTEM

$$\int_{AB} q_{vx} dx = \left(\frac{K}{\mu_1}\right)\Delta\Phi$$

$$\int_{CD} q_{vx} dx = -\left(\frac{K}{\mu_2}\right)\Delta\Phi$$

and equation (A-5) is

$$\oint \bar{q}_v \cdot d\bar{s} = \left(\frac{1}{\mu_1} - \frac{1}{\mu_2}\right) K\Delta\Phi \neq 0 \qquad \text{(A-6)}$$

It seems likely, therefore, that rotational flow fields develop in reservoirs subjected to thermal oil recovery processes. This conclusion is not unreasonable, as one would expect some convective effects to take place where fluids are heated. The important question is whether or not these effects are of sufficient magnitude to cause the flow behavior to deviate appreciably from that specified by equation (A-1). Only experimental work on nonisothermal flow in porous media can answer this question completely. From analysis of the experimental and calculated data obtained in this investigation, Darcy's Law appears to be a satisfactory approximation of the non-isothermal flow situations encountered in this study.

APPENDIX B

RELATIVE IMPORTANCE OF LIQUID-LIQUID DIFFUSION

The importance of molecular diffusion as a mass transport mechanism in the liquid phase has not been determined precisely. Lack of experimental data on the diffusion coefficient for liquid-liquid mixtures complicates the difficulty already created by the absence of an adequate theory for liquid diffusion (50). However, certain qualitative conclusions may be drawn regarding the order of magnitude of this effect in a porous system. The limited solubility of oil in water suggests that molecular diffusion of these two phases would be severely limited. Tabulated values of diffusion coefficients for such mixtures support this idea (51,52). For example, the diffusion coefficient of water-n-butanol mixture ranges from 0.267×10^{-5} to 1.24×10^{-5} cm^2/second, while in contrast, the coefficient for an H_2-CH_4 gas mixture is approximately 0.7 cm^2/second. Obviously the effect is much less important for liquids than it is for gases.

Diffusion from regions of high chemical potential to regions of low chemical potential, as, for example, in the diffusion of liquid from warm regions to cold regions or the diffusion of water from regions of high salt concentration to regions of low salt concentration, would also be severly limited. The diffusion coefficient for aqueous solutions of sodium chloride at 25 °C is 1.9×10^{-5} cm^2/second (51). The available data indicate that molecular diffusion can be neglected in the situations encountered in this study.

APPENDIX C

REPRESENTATIONS OF RESERVOIR SYSTEM PROPERTIES

Energy Transport Properties

Data used with laboratory study:

Figures 54, 55, and 56 present the thermal conductivity and heat capacity vs. temperature for synthetic oil, water, and unconsolidated sand.

Data used with field study:

Expressions for the thermal conductivity are given in Part II of the dissertation. The following representations are employed for the heat capacity:

$$C_o = 0.91(0.38 + (0.52 \times 10^{-3} T)) \quad \text{(C-1)}$$

$$C_s = 0.202 + 1.109 \times 10^{-4} (T - 100) \quad \text{(C-2)}$$

where: C_o is the heat capacity of oil

C_s is the heat capacity of consolidated sand

T is the temperature, $^{\circ}F$.

Equation (C-1) is an empirical expression presented by Hougen and Watson (17). Equation (C-2) is presented by Davidson (39).

Mass Transport Properties

Capillary pressure, relative permeability, and viscosity data used with laboratory and field studies are presented in Figures 57 through 62.

Fluid State Properties

The fluid densities are presented in Figure 63.

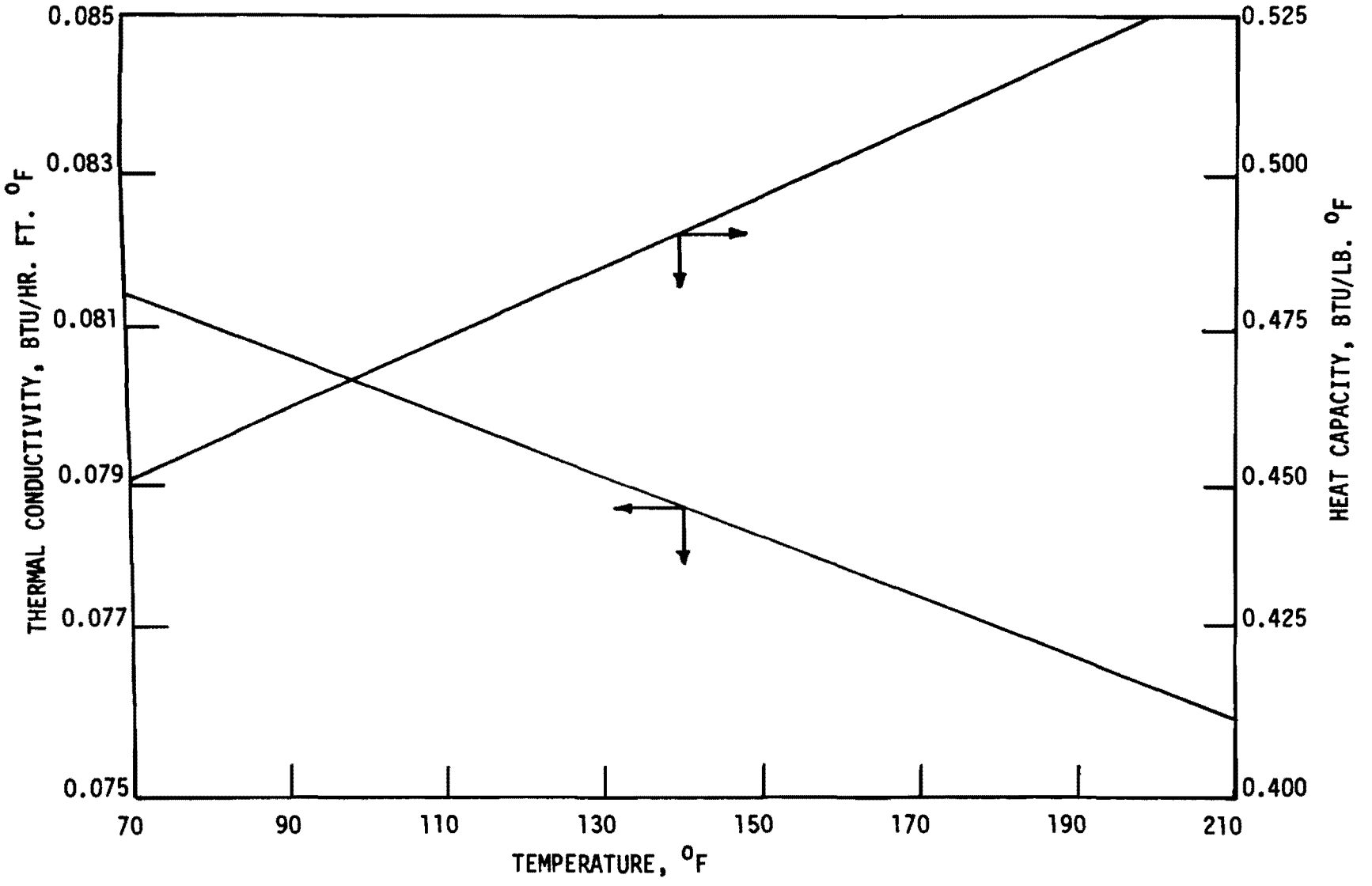

FIGURE 54. THERMAL PROPERTIES OF SYNTHETIC OIL (REFERENCE : 55)

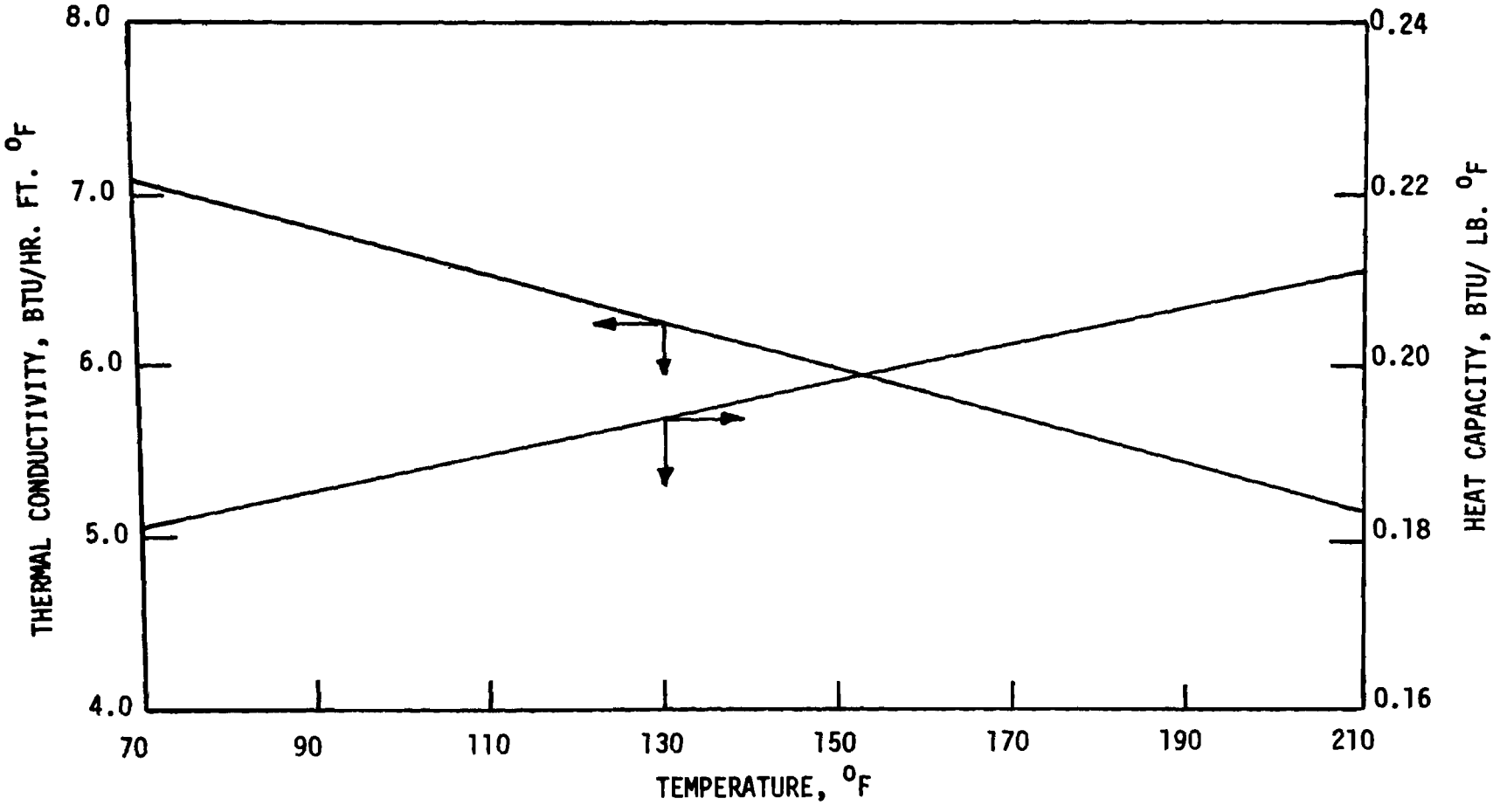

FIGURE 55. THERMAL PROPERTIES OF QUARTZ (SOURCE : REFERENCE 30)

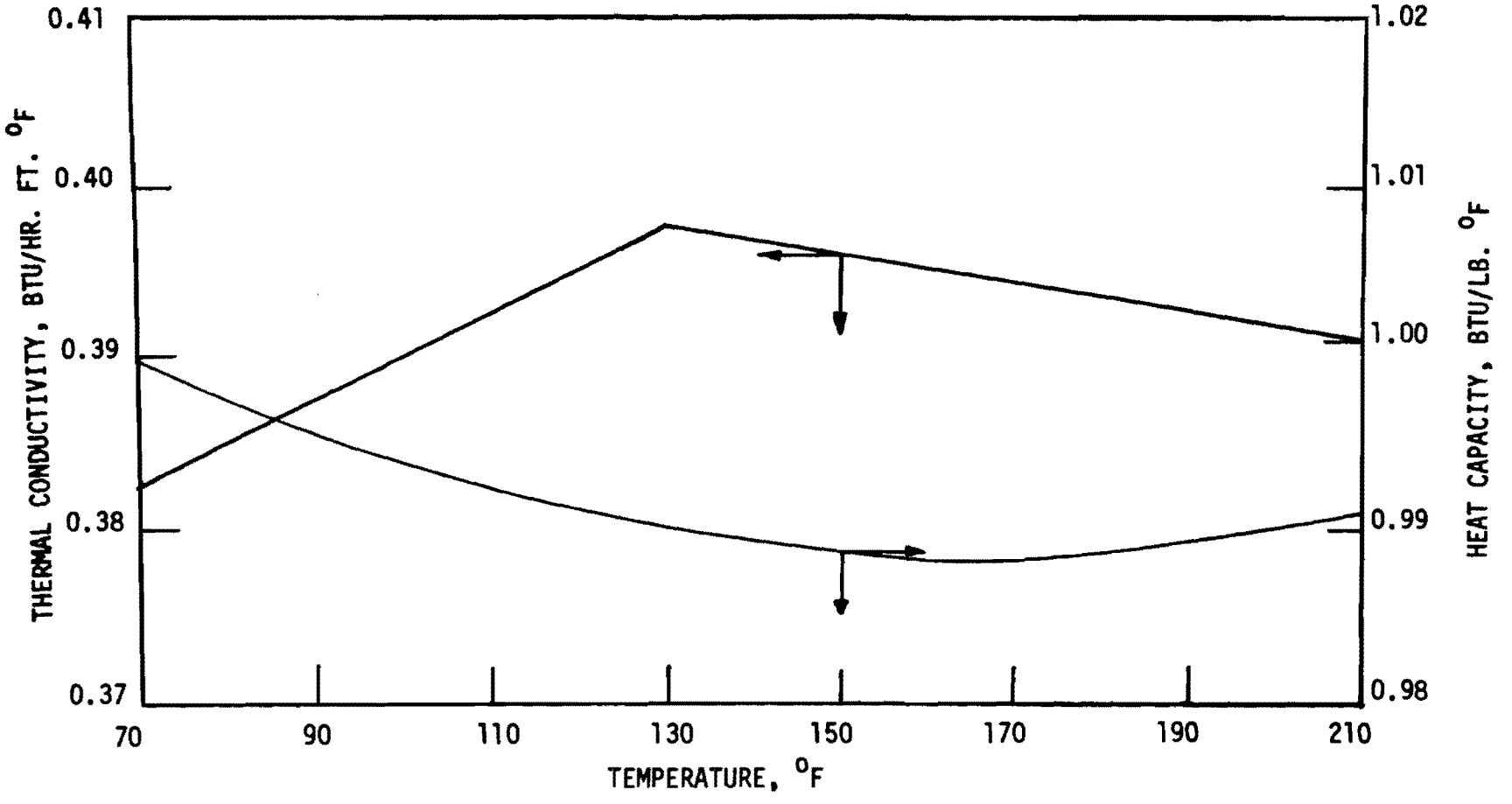

FIGURE 56. THERMAL PROPERTIES OF WATER (SOURCE : REFERENCE 30)

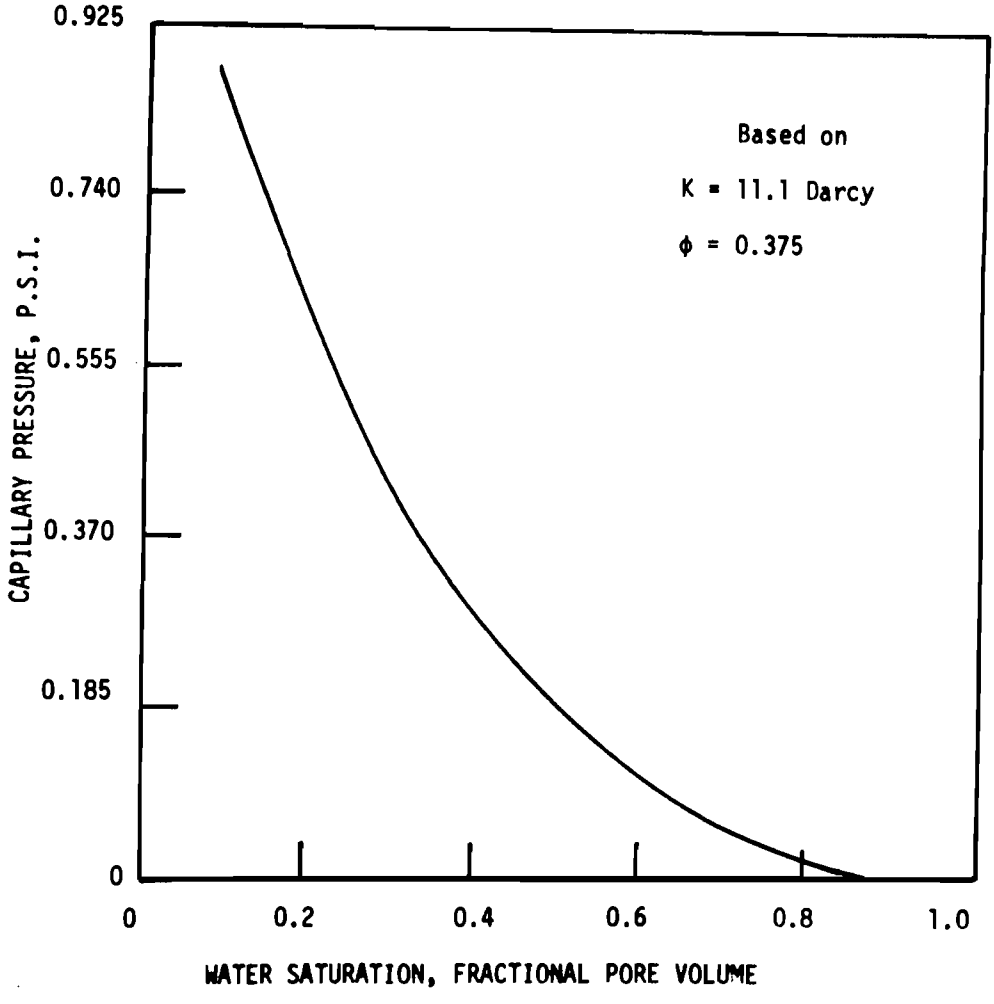

FIGURE 57. CAPILLARY PRESSURE DATA USED FOR FIVE-SPOT MODEL

(DATA SOURCE : REFERENCE 53)

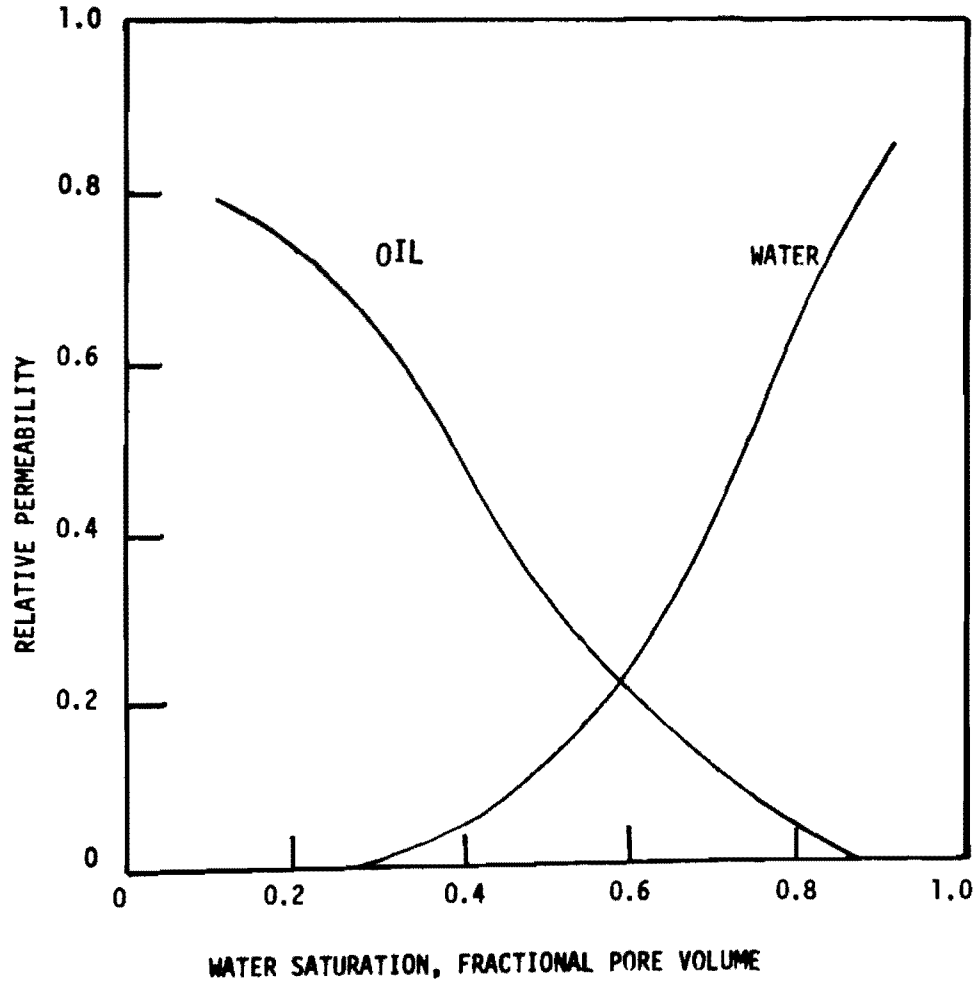

FIGURE 58. RELATIVE PERMEABILITY DATA USED FOR FIVE-SPOT MODEL

(DATA SOURCE : REFERENCE 53)

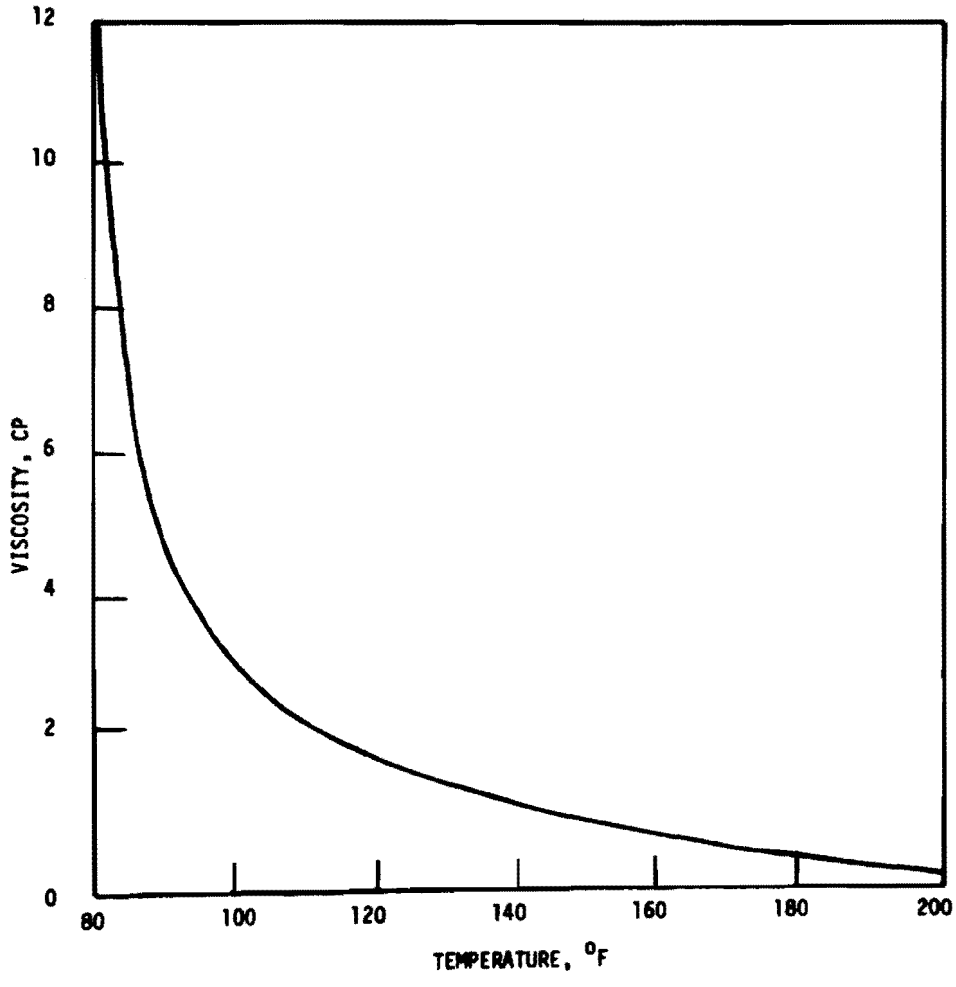

FIGURE 59. VISCOSITY TEMPERATURE CHART FOR SYNTHETIC OIL

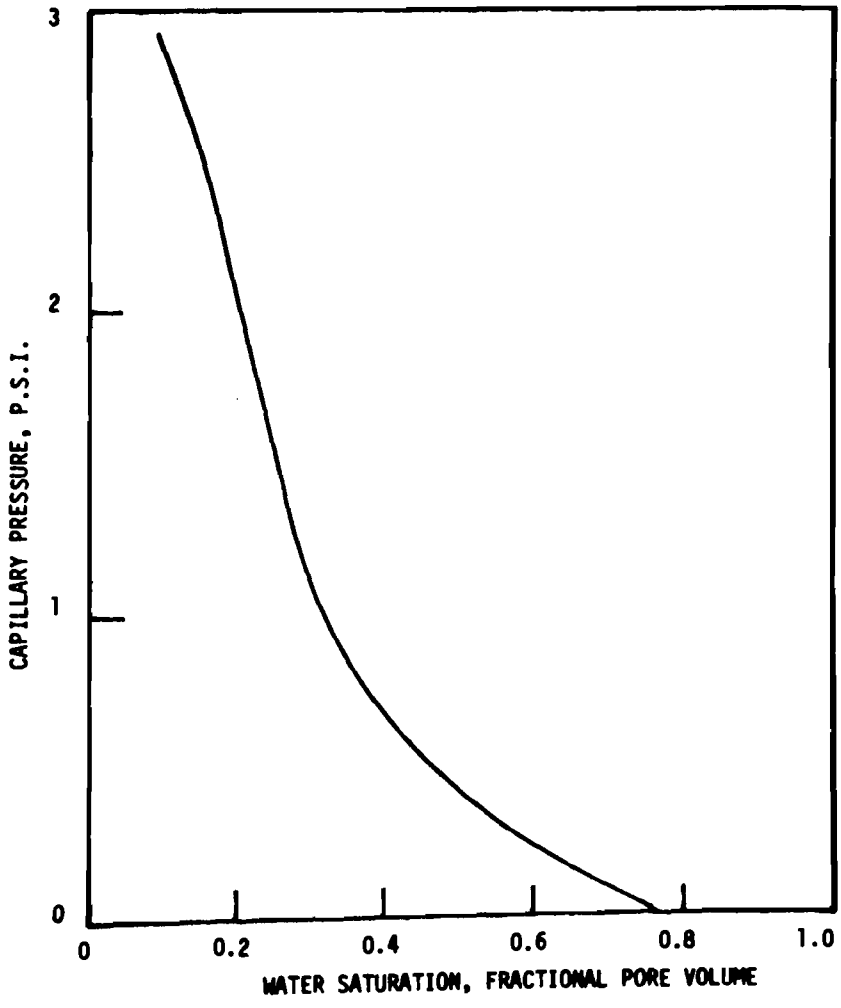

FIGURE 60. CAPILLARY PRESSURE DATA USED FOR FIELD CALCULATIONS

(DATA SOURCE : REFERENCE 53)

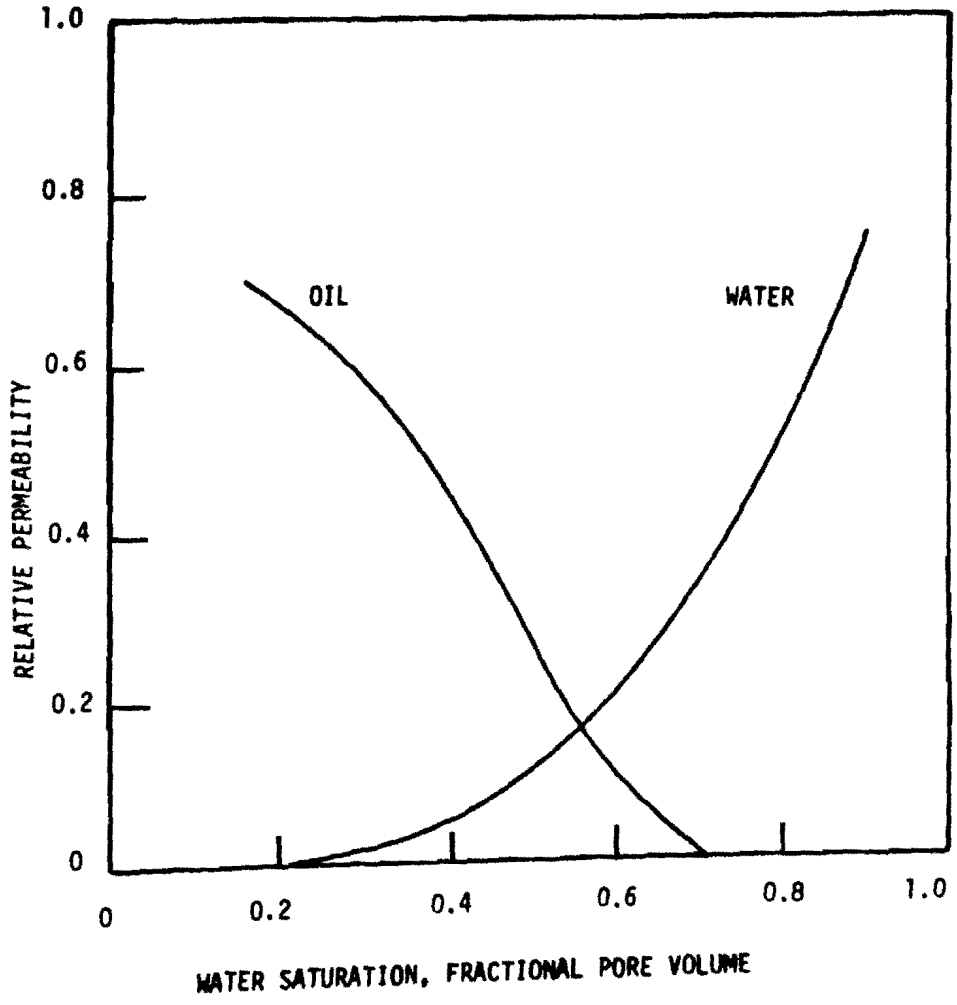

FIGURE 61. RELATIVE PERMEABILITY DATA USED FOR FIELD CALCULATIONS
(SOURCE : REFERENCE 53)

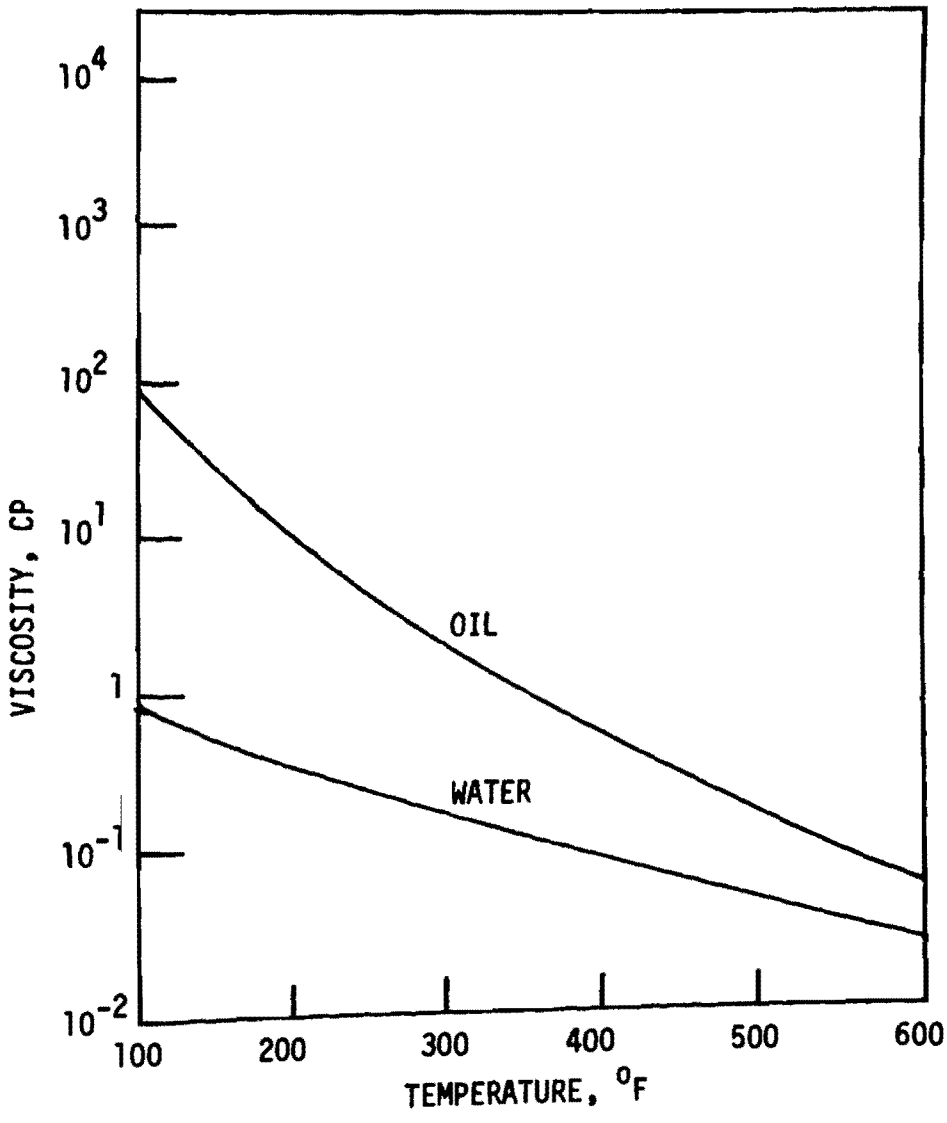

FIGURE 62. VISCOSITY CHANGE WITH TEMPERATURE FOR OIL AND WATER (SOURCE : REFERENCE 39)

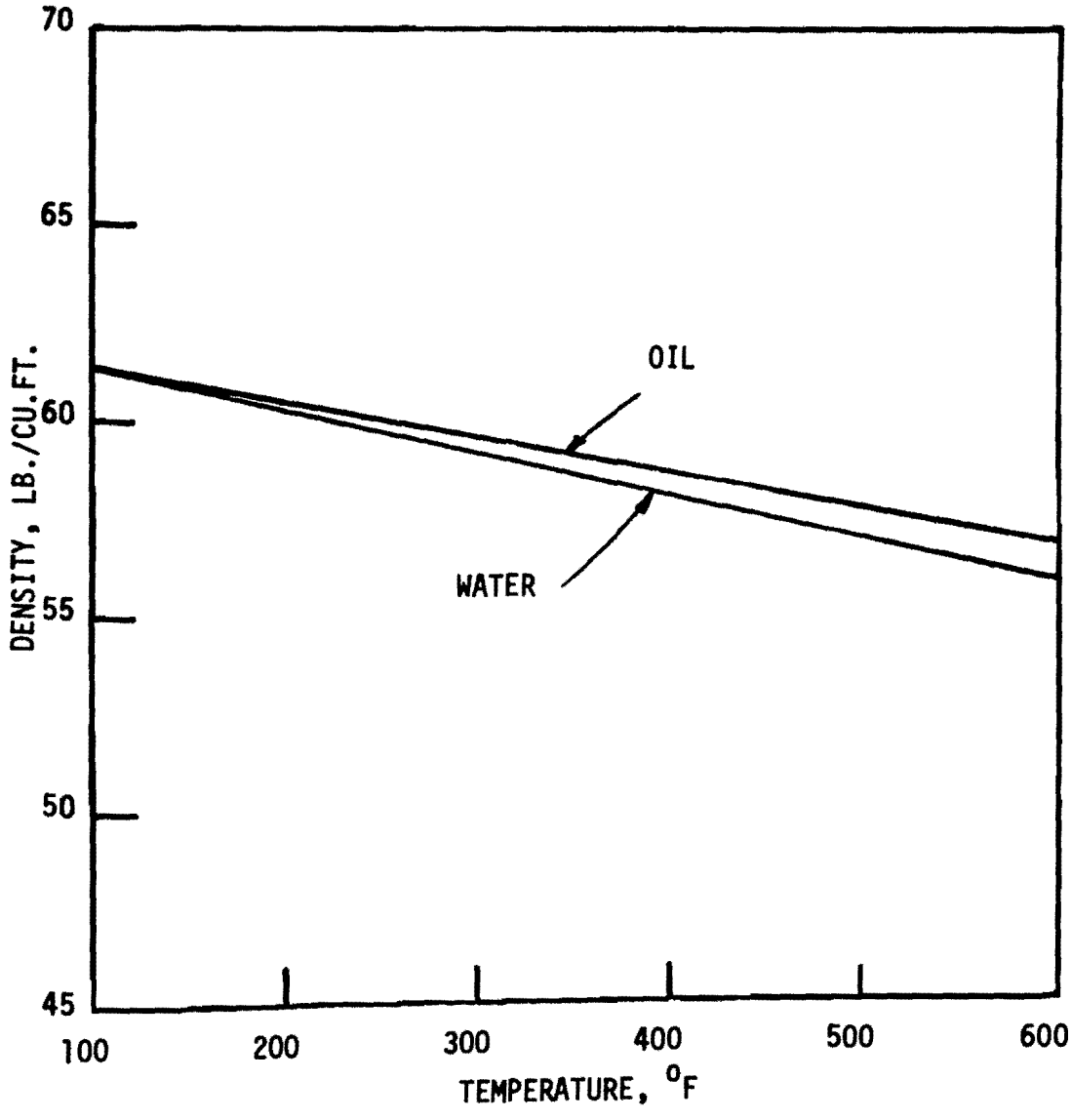

FIGURE 63. LIQUID DENSITIES VS. TEMPERATURE

(SOURCE : REFERENCE 39)

APPENDIX D

DERIVATION OF THE THERMAL ENERGY EQUATION

A general expression for the thermal energy of a substance may be obtained by developing an equation for the total energy (conservation of energy or the first law of thermodynamics) that describes the transport of energy in the substance, and substracting from it the mechanical energy equation. The following developments conform, in principle, to the analysis given by Bird, Stewart, and Lightfoot (54). The total energy of a substance, expressed on a unit volume basis, as a function of position and time may be described as:

$$\rho\frac{D}{Dt}(U_n+\Phi_n+1/2\ V^2) = -\ (\nabla\ .\ q_{th})\ -\ (\nabla\ .\ PV)\ -\ W_{fr} \qquad (D\text{-}1)$$

This is an equation of change for $E_n = U_n+\Phi_n+1/2\ V^2$, which we term the total energy.

where: U_n = internal energy per unit mass

Φ_n = potential energy defined by $g = -\ \nabla\Phi_n$

V = velocity

$-\ \nabla .\ q_{th}$ = rate of energy input per unit volume by conduction

$-\ \nabla .\ PV$ = rate of work done on the substance per unit volume by pressure forces

∇ = laplacian operator

W_{fr} = rate of friction work done on substance per unit volume

q_{th} = energy flux vector by conduction defined by

$$q_{th} = -\ K_t\frac{\partial T}{\partial x}\bar{i} - K_t\frac{\partial T}{\partial y}\bar{j}$$

$\frac{D}{Dt}$ = substantial derivative defined by $\frac{DT}{Dt} = \frac{\partial T}{\partial t} + V\ .\nabla\ T$

The equation of mechanical energy developed by Bird, Stewart, and Lightfoot may be written as:

$$\rho\frac{D}{Dt}(1/2\ V^2) = P(\nabla\ .\ \vec{V}) - (\nabla\ .\ \vec{PV}) - \rho\frac{D\Phi_n}{Dt} + E_{ivd} - W_{fr} \qquad (D\text{-}2)$$

where: E_{ivd} = irreversible rate of internal energy increase per unit volume by viscous dissipation.

Then, subtraction of equation (D-2) from equation (D-1) yields:

$$\rho\frac{DU_n}{Dt} = -(\nabla\ .\ q_{th}) - P(\nabla\ .\ V) - E_{ivd} \qquad (D\text{-}3)$$

where: $-P(\nabla\ .\ V)$ = reversible rate of internal energy increase per unit volume by compression.

Certain qualitative conclusions may be drawn regarding the order of magnitude of the irreversible rate of internal energy increase by viscous dissipation, E_{ivd}, and the reversible rate of internal energy increase by compression, $-P(\nabla\ .\ V)$, in a porous medium containing oil and water. For incompressible liquids, the term $(\nabla\ .\ V) = 0$. For slightly compressible liquids, this term would be quite small and can be neglected regarding the accuracy required in predicting the behavior of an oil reservoir. An examination of the magnitude of friction effects by Miller (41) suggests that the conversion from mechanical to thermal energy because of viscous dissipation may be neglected in our problem. Based upon the foregoing discussion equation (D-3) can be written as:

$$\rho\frac{DU_n}{Dt} = -\nabla\ .\ q_{th} \qquad (D\text{-}4)$$

It is convenient to have the equation of thermal energy in terms of temperature and heat capacity rather than the internal energy. By assuming that the thermal internal energy, U_n, is dependent on temperature only, we can write:

$$dU_n = C\,dT \tag{D-5}$$

the above expression is given in (45). For solids and liquids $C_p \approx C_v \approx C$. Now, ρ times the substantial derivative of U_n becomes:

$$\rho C \frac{DU_n}{Dt} = \rho C \frac{DT}{Dt} \tag{D-6}$$

Combining equation (D-6) and equation (D-4) yields:

$$\rho C \frac{DT}{Dt} = -\nabla \cdot q_{th} \tag{D-7}$$

Equation (D-7) is used to obtain the thermal energy equation for a porous medium containing oil and water. If it is assumed that the temperature is different in the solid and fluid phases, separate equations of the form (D-7) would be required for each phase. These equations would include a term accounting for transfer of thermal energy between the phases. In addition, the equation for the fluid mixture would contain a source term q to account for the thermal energy generated due to electric current flow in the connate water. The heat transfer from fluid to solid through a film may be described mathematically as: $\tilde{h}\,(T_f - T_s)$, where $\tilde{h}$ is the heat transfer film coefficient, T_f and T_s are the temperatures of the fluid and the solid phases respectively. In Part III, the development of the mathematical model, it is assumed that $\tilde{h}$ is very large so that at any point $T_s \approx T_f$. In terms of a unit reservoir

APPENDIX E

FORMULATION OF THE FINITE DIFFERENCE EQUATIONS

The Fluid Flow Equations

At standard temperature and pressure, equations (14) and (15) can be written in the following form:

$$\frac{\partial}{\partial x}\left(\frac{KK_{ro}}{\mu_o \beta_o}\frac{\partial P_o}{\partial x}\right) + \frac{\partial}{\partial y}\left(\frac{KK_{ro}}{\mu_o \beta_o}\frac{\partial P_o}{\partial y}\right) \pm \frac{q_{ov}}{\beta_o} = \frac{\partial}{\partial t}\left(\frac{\phi S_o}{\beta_o}\right) \qquad \text{(E-1)}$$

$$\frac{\partial}{\partial x}\left(\frac{KK_{rw}}{\mu_w \beta_w}\frac{\partial P_w}{\partial x}\right) + \frac{\partial}{\partial y}\left(\frac{KK_{rw}}{\mu_w \beta_w}\frac{\partial P_w}{\partial y}\right) \pm \frac{q_{wv}}{\beta_w} = \frac{\partial}{\partial t}\left(\frac{\phi S_w}{\beta_w}\right) \qquad \text{(E-2)}$$

where:

q_{ov} = oil volume (injected or produced) @ reservoir temperature and pressure per unit volume

q_{wv} = water volume (injected or produced) @ reservoir temperature and pressure per unit volume

This development of the fluid flow finite difference equations conforms, in principle, to that of M.D. Arnold (56), for a horizontal system. The time derivative of $\left(\frac{\phi S}{\beta}\right)$ can be expanded and the chain rule applied to yield:

$$\frac{\partial}{\partial t}\left(\frac{\phi S}{\beta}\right) = \frac{\phi S}{\beta}\left(\frac{1}{\phi}\frac{\partial \phi}{\partial P} - \frac{1}{\beta}\frac{\partial \beta}{\partial P}\right)\frac{\partial P}{\partial t} + \frac{\phi}{\beta}\frac{\partial S}{\partial t} \qquad \text{(E-3)}$$

The time derivative in equations (E-1) and (E-2) can be related to the time derivative of pressure by substituting the relation in (E-3) in equations (E-1) and (E-2). Then adding the two equations yields:

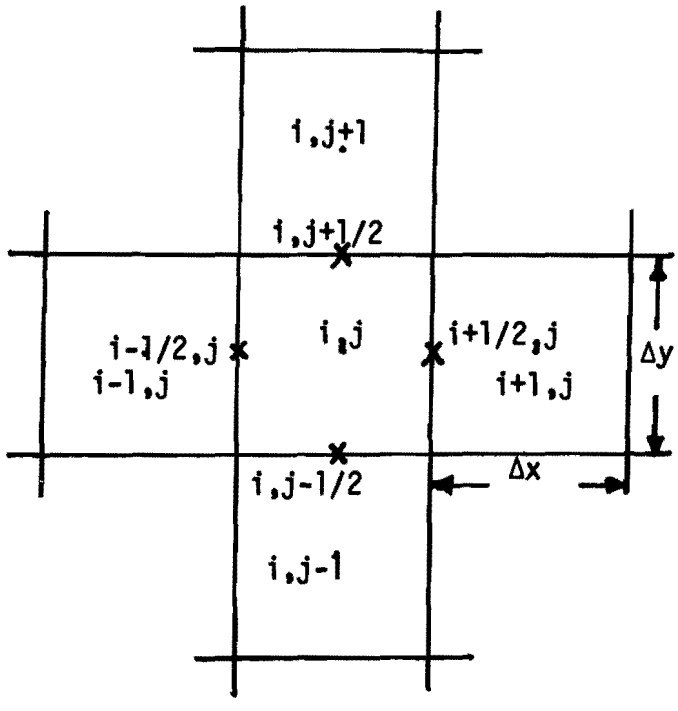

FIGURE 64. CALCULATION GRID

$$\beta_o \frac{\partial}{\partial x}\left(\frac{KK_{ro}}{\mu_o \beta_o}\frac{\partial P_o}{\partial x}\right) + \beta_w \frac{\partial}{\partial x}\left(\frac{KK_{rw}}{\mu_w \beta_w}\frac{\partial P_w}{\partial x}\right) + \beta_o \frac{\partial}{\partial y}\left(\frac{KK_{ro}}{\mu_o \beta_o}\frac{\partial P_o}{\partial y}\right) +$$

$$\beta_w \frac{\partial}{\partial y}\left(\frac{KK_{rw}}{\mu_w \beta_w}\frac{\partial P_w}{\partial y}\right) \pm q_{ovSTP}\beta_o \pm q_{wvSTP}\beta_w = \phi(S_o \dot{C}_o + S_o \dot{C}_r)\frac{\partial P_o}{\partial t} +$$

$$\phi\,(S_w \dot{C}_w + S_w \dot{C}_r)\,\frac{\partial P_w}{\partial t} + \phi\frac{\partial}{\partial t}\,(S_o + S_w) \qquad \text{(E-4)}$$

where:

$$\dot{C}_r = \frac{1}{\phi}\frac{\partial \phi}{\partial P}$$

$$\dot{C}_o = \frac{-1}{\beta o}\frac{\partial \beta_o}{\partial p}$$

$$\dot{C}_w = \frac{-1}{\beta_w}\frac{\partial \beta_w}{\partial p}$$

q_{wvSTP} = oil volume (injected or produced) @ standard temperature and pressure per unit volume

q_{wvSTP} = water volume (injected or produced) @ standard temperature and pressure per unit volume

Using the relation in (16), equation (E-4) reduces to:

$$\beta_o \frac{\partial}{\partial x}\left(\frac{KK_{ro}}{\mu_o \beta_o}\frac{\partial P}{\partial x}\right) + \beta_w \frac{\partial}{\partial x}\left(\frac{KK_{rw}}{\mu_w \beta_w}\frac{\partial}{\partial x}(P - P_{cow})\right) + \beta_o \frac{\partial}{\partial y}\left(\frac{KK_{ro}}{\mu_o \beta_o}\frac{\partial P}{\partial y}\right) +$$

$$\beta_w \frac{\partial}{\partial y}\left(\frac{KK_{rw}}{\mu_w \beta_w}\frac{\partial}{\partial y}\,(P - P_{cow})\right) \pm q_{ovSTP}\beta_o \pm q_{wvSTP}\beta_w =$$

$$-\phi\,(S_w \dot{C}_w + S_w \dot{C}_r)\,\frac{\partial P_{cow}}{\partial S_w}\frac{\partial S_w}{\partial t} + \phi(S_o \dot{C}_o + S_w \dot{C}_w + \dot{C}_r)\,\frac{\partial P}{\partial t} \qquad \text{(E-5)}$$

where: P is defined as pressure in the oil phase

For approximating the system of partial differential equations, a rectangular grid system shown in Figure 64 will be used. In applying the difference technique, the continuum of space and time is divided

into discrete intervals and values of the dependent variables are considered only at a finite set of points. Thus, the space coordinates for the difference system of constant Δx and Δy will be defined at the points (x_j, y_j) by the relationships:

$$x_i = (i - \tfrac{1}{2})\ \Delta x,\ 1 \leq i \leq I,$$

$$y_i = (j - \tfrac{1}{2})\ \Delta y,\ 1 \leq j \leq J,$$

and time is defined only at the discrete values given by

$$t_n = \sum_{m=1}^{n} \Delta t_m,$$

where the space intervals Δx, Δy as well as the sequence Δt_m are arbitrary and are chosen sufficiently small to limit the truncation error, that is, the error associated with the replacement of derivatives by difference quotients. The notation $P_{i,j,n}$ will mean $P(x_i, y_j, t_n)$.

Discretization of equation (E-5) with the coefficients evaluated at the new time level results in the implicit difference equation:

$$\beta_{oi,j}^{n+1}\left[\left(\frac{KK_{ro}}{\mu_o\beta_o}\right)_{i+\frac{1}{2},j}(P_{i+1,j}-P_{i,j})/(\Delta x_i)^2-\left(\frac{KK_{ro}}{\mu_o\beta_o}\right)_{i-\frac{1}{2},j}\right.$$

$$\left.(P_{i,j}-P_{i-1,j})/(\Delta x_i)^2\right]^{n+1}+\beta_{wi,j}^{n+1}\left[\left(\frac{KK_{rw}}{\mu_w\beta_w}\right)_{i+\frac{1}{2},j}\right.$$

$$(P_{i+1,j}-P_{cowi+1,j}-P_{i,j}+P_{cowi,j})/(\Delta x_i)^2-\left(\frac{KK_{rw}}{\mu_w\beta_w}\right)_{i-\frac{1}{2},j}$$

$$\left.(P_{i,j}-P_{cowi,j}-P_{i-1,j}+P_{cowi-1,j})/(\Delta x_i)^2\right]^{n+1}+\beta_{oi,j}^{n+1}$$

$$\left[\left(\frac{KK_{ro}}{\mu_o\beta_o}\right)_{i,j+\frac{1}{2}}(P_{i,j+1}-P_{i,j})/(\Delta y_j)^2-\left(\frac{KK_{ro}}{\mu_o\beta_o}\right)_{i,j-\frac{1}{2}}(P_{i,j}-P_{i,j-1})/\right.$$

$$\left.(\Delta y_j)^2\right]^{n+1}+\beta_{wi,j}^{n+1}\left[\left(\frac{KK_{rw}}{\mu_w\beta_w}\right)_{i,j+\frac{1}{2}}(P_{i,j+1}-P_{cowi,j+1}-P_{i,j}+\right.$$

$$P_{cowi,j})/(\Delta y_j)^2-\left(\frac{KK_{rw}}{\mu_w\beta_w}\right)_{i,j-\frac{1}{2}}(P_{i,j}-P_{cowi,j}-P_{i,j-1}+P_{cowi,j-1})$$

$$\left./(\Delta y_j)^2\right]^{n+1}+(q_{wvSTPi,j}\beta_{wi,j}+q_{ovSTPi,j}\beta_{oi,j})^{n+1}=$$

$$(\phi_{i,j}(S_o\dot{C}_o+S_w\dot{C}_w+\dot{C}_r))_{i,j}^{n+1}(P_{i,j}^{n+1}-P_{i,j}^{n})/\Delta t_{n+1}-(\phi_{i,j}(S_w\dot{C}_w+$$

$$S_w\dot{C}_r))_{i,j}^{n+1}\left(\frac{P_{cowi,j}^{n+1}-P_{cowi,j}^{n}}{\Delta t_{n+1}}\right) \qquad \text{(E-6)}$$

Equation (E-6) can be simplified in form to yield:

$$\left[A_{yi,j}P_{i,j-1} + A_{xi,j}P_{i-1,j} + B_{xi,j}P_{i,j} + C_{xi,j}P_{i+1,j} + C_{yi,j}\right.$$

$$\left.P_{i,j+1}\right]^{n+1} = D_{xi,j} \qquad \text{(E-7)}$$

where:

$$A_{yi,j} = \{(\frac{KK_{rw}}{\mu_w\beta_w})_{i,j-\frac{1}{2}}/(\Delta y_j)^2\}\ \beta_{wi,j} + \{(\frac{KK_{ro}}{\mu_o\beta_o})_{i,j-\frac{1}{2}}/(\Delta y_j)^2\}\ \beta_{oi,j}$$

$$A_{xi,j} = \{(\frac{KK_{rw}}{\mu_w\beta_w})_{i-\frac{1}{2},j}/(\Delta x_i)^2\}\ \beta_{wi,j} + \{(\frac{KK_{ro}}{\mu_o\beta_o})_{i-\frac{1}{2},j}/(\Delta x_i)^2\}\ \beta_{oi,j}$$

$$C_{xi,j} = \{(\frac{KK_{rw}}{\mu_w\beta_w})_{i+\frac{1}{2},j}/(\Delta x_i)^2\}\beta_{wi,j} + \{(\frac{KK_{ro}}{\mu_o\beta_o})_{i+\frac{1}{2},j}/(\Delta x_i)^2\}\ \beta_{oi,j}$$

$$C_{yi,j} = \{(\frac{KK_{rw}}{\mu_w\beta_w})_{i,j+\frac{1}{2}}/(\Delta y_j)^2\}\ \beta_{wi,j} + \{(\frac{KK_{ro}}{\mu_o\beta_o})_{i,j+\frac{1}{2}}/(\Delta y_j)^2\}\ \beta_{oi,j}$$

$$B_{xi,j} = \{-A_{xi,j} - A_{yi,j} - C_{xi,j} - C_{yi,j} - (\frac{\phi_{i,j}}{\Delta t_{n+1}})$$

$$(S_o\dot{C}_o + S_w\dot{C}_w + \dot{C}_{r\ i,j})^{n+1}\ \}$$

$$D_{xi,j} = -\left[\{(\frac{KK_{rw}}{\mu_w\beta_w})_{i+\frac{1}{2},j}\ (\frac{\beta_{wi,j}}{(\Delta x_i)^2})\ (P_{cowi,j} - P_{cowi+1,j})\ \}^{n+1} +\right.$$

$$\left.\{(\frac{KK_{rw}}{\mu_w\beta_w})_{i-\frac{1}{2},j}\ (\frac{\beta_{wi,j}}{(\Delta x_i)^2})\ (P_{cowi,j} - P_{cowi-1,j})\}^{n+1} + (\frac{KK_{rw}}{\mu_w\beta_w})_{i,j+\frac{1}{2}}\right.$$

$$\left(\frac{\beta_{wi,j}}{(\Delta y_j)^2}\right)\left(P_{cowi,j} - P_{cowi,j+1}\right)\Big\}^{n+1} + \left\{\left(\frac{KK_{rw}}{\mu_w \beta_w}\right)_{i,j-\frac{1}{2}}\left(\frac{\beta_{wi,j}}{(\Delta y_j)^2}\right)\right.$$

$$\left.\left(P_{cowi,j} - P_{cowi,j-1}\right)\Big\}^{n+1} + \left\{\left(q_{wvSTP}\beta_w + q_{ovSTP}\beta_o\right)_{i,j}\right\}^{n+1} +\right.$$

$$\left\{\frac{\phi_{i,j}}{\Delta t_{n+1}}\left(S_o\dot{C}_o + S_w\dot{C}_w + \dot{C}_r\right)^{n+1}_{i,j} P^n_{i,j}\right\} + \left\{\frac{\phi_{i,j}}{\Delta t_{n+1}}\left(S_w\dot{C}_w + S_w\dot{C}_r\right)^{n+1}_{i,j}\right.$$

$$\left.\left.\left(\frac{P^{n+1}_{cowi,j} - P^n_{cowi,j}}{\Delta t_{n+1}}\right)\right\}\right]$$

Equation (E-7) relates the pressure at a point (i,j) to the pressure at the four nearest grid points. Equations for the boundary points can also be put in the form of (E-7). For example, in order to eliminate flow across the Y = 0 boundary, the coefficient of $P_{i,j-1}$ in (E-7) should be set equal to zero yielding an equation similar to (E-7) but with one term missing. It is evident that at one corner of this boundary both the coefficients of $P_{i,j-1}$ and $P_{i-1,j}$ are zeros, and at the other corner the coefficients of $P_{i,j-1}$ and $P_{i+1,j}$ are zeros. Similar remarks apply at other boundaries.

Since one such equation exists for each grid block (i,j), there is a total of

$$N = I \times J$$

equations in the N unknown pressures. One such set arises at each time step. The set of equations is solved by the Strongly Implicit Procedure (SIP) developed by Stone (57).

Saturation Calculations

Discretization of equation (E-2) results in the following finite difference equation for the grid block (i,j):

$$\{ \left(\frac{KK_{rw}}{\mu_w\beta_w}\right)_{i+\frac{1}{2},j} (P_{wi+1,j} - P_{wi,j})/(\Delta x_i)^2 - \left(\frac{KK_{rw}}{\mu_w\beta_w}\right)_{i-\frac{1}{2},j} (P_{wi,j} - P_{wi-1,j})/(\Delta x_i)^2 + \left(\frac{KK_{rw}}{\mu_w\beta_w}\right)_{i,j+\frac{1}{2}} (P_{wi,j+1} - P_{wi,j})/(\Delta y_j)^2 - \left(\frac{KK_{rw}}{\mu_w\beta_w}\right)_{i,j-\frac{1}{2}} (P_{wi,j} - P_{wi,j-1})/(\Delta y_j)^2 + q_{wvSTP_{i,j}} \}^{n+1} = \frac{\left(\frac{\phi S_w}{\beta_w}\right)^{n+1}_{i,j} - \left(\frac{\phi S_w}{\beta_w}\right)^{n}_{i,j}}{\Delta t_{n+1}} \qquad \text{(E-8)}$$

Equation (E-8) can be arranged to yield

$$S^{n+1}_{wi,j} = S^{n}_{wi,j} \left(\frac{\phi^n}{\phi^{n+1}}\right)_{i,j} \left(\frac{\beta^{n+1}_w}{\beta^n_w}\right)_{i,j} + \Delta t_{n+1} \left(\frac{\beta_w}{\phi}\right)^{n+1}_{i,j} \Bigg[\left(\frac{KK_{rw}}{\mu_w\beta_w}\right)_{i+\frac{1}{2},j} (P_{wi+1,j}/(\Delta x_i)^2) + \left(\frac{KK_{rw}}{\mu_w\beta_w}\right)_{i-\frac{1}{2},j} (P_{wi-1,j}/(\Delta x_i)^2 + \left(\frac{KK_{rw}}{\mu_w\beta_w}\right)_{i,j+\frac{1}{2}} (P_{wi,j+1}/(\Delta y_j)^2 + \left(\frac{KK_{rw}}{\mu_w\beta_w}\right)_{i,j-\frac{1}{2}} (P_{wi,j-1})/(\Delta y_j)^2 - \left\{ \frac{\left(\frac{KK_{rw}}{\mu_w\beta_w}\right)_{i+\frac{1}{2},j} + \left(\frac{KK_{rw}}{\mu_w\beta_w}\right)_{i-\frac{1}{2},j}}{(\Delta x_i)^2} + \frac{\left(\frac{KK_{rw}}{\mu_w\beta_w}\right)_{i,j+\frac{1}{2}} + \left(\frac{KK_{rw}}{\mu_w\beta_w}\right)_{i,j-\frac{1}{2}}}{(y_j)^2} \right\} P_{wi,j} + q_{wvSTPi,j} \Bigg]^{n+1} \qquad \text{(E-9)}$$

Also,

$$S_{oi,j}^{n+1} = 1.0 - S_{wi,j}^{n+1} \qquad \text{(E-10)}$$

For calculating oil and water saturation distribution within the system, equations (E-9) and (E-10) are solved explicitly for each grid block in the system. This is possible because the sequence for solving the sets of equations involves solving the pressure equations before the saturation equations.

Salt Concentration Distribution

Since connate water is the electric current carrier and resistance heating element, brine, which may be saturated or relatively fresh, can be injected into the oil-bearing formation in order to control the resistivity of the water through which current flows at the desired level. In order to specify the heat generated within the system we must have a knowledge of two parameters:

i. a parameter determining the formation water resistivity. Salt concentration distribution within the system serves this purpose.

ii. a parameter determining the electric current flowing in the system due to the e.m.f. applied. Voltage distribution in the system serves this purpose.

The governing difference equation for the salt concentration distribution within the system is obtained by making a salt mass balance on a finite element of the system shown in Figure E-2.

The assumptions involved in the following development can be stated as follows:

i. transport of salt by diffusion due to salt concentration gradient between grid blocks is negligible (see Appendix B.)

ii. salt concentration in the finite element is uniform. Defining:

M_{salt} = mass of salt at time t in the finite element.

IN_{salt} = mass rate at which salt enters the finite element.

OUT_{salt} = mass rate at which salt leaves the finite element.

$\dot{M}_{salt}$ = mass of salt injected or produced.

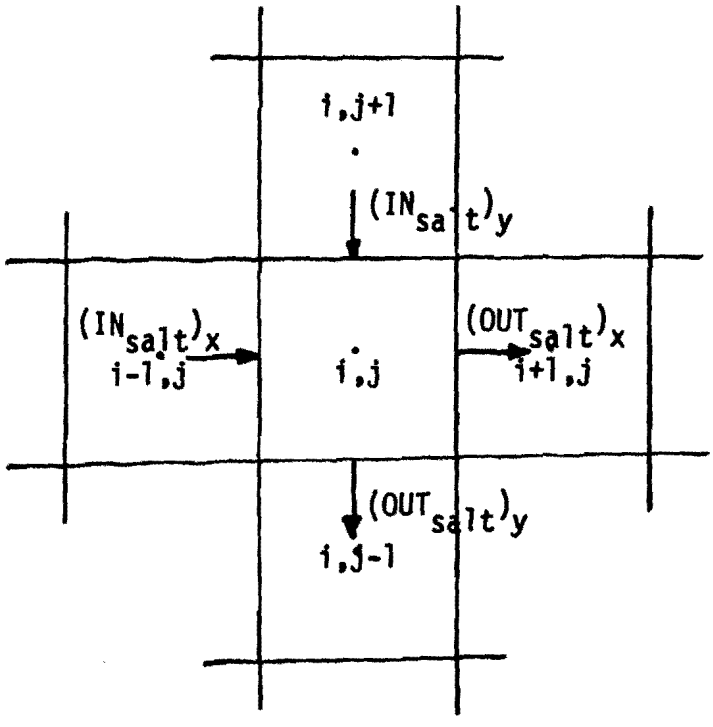

FIGURE 65. CONSTRUCTION USED TO DEVELOP A FINITE DIFFERENCE EQUATION FOR SALT CONCENTRATION DISTRIBUTION

we have at once the basic equation

$$\frac{dM_{salt}}{dt} \simeq IN_{salt} - OUT_{salt} \pm \dot{M}_{salt} \tag{E-11}$$

The direction of salt mass flow into and out of the finite element is governed by the flowing phase pressure distribution within the element and the four surrounding elements. For illustrative purpose, let the direction of salt mass flow be as shown in Figure 65, then

$$(IN_{salt})_{i,j} = \left(\frac{KK_{rw}}{\mu_w}\right)_{i-\frac{1}{2},j} (P_{wi-1,j} - P_{wi,j}) (Saltc)_{i-1,j}$$

$$\Delta y_j h/\Delta x_i + \left(\frac{KK_{rw}}{\mu_w}\right)_{i,j+\frac{1}{2}} (P_{wi,j+1} - P_{wi,j}) (Saltc)_{i,j+1}$$

$$\Delta x_i h/\Delta y_j \tag{E-12}$$

$$(OUT_{salt})_{i,j} = \left(\frac{KK_{rw}}{\mu_w}\right)_{i+\frac{1}{2},j} (P_{wi,j} - P_{wi+1,j}) (Saltc)_{i,j}$$

$$\Delta y_j h/\Delta x_i + \left(\frac{KK_{rw}}{\mu_w}\right)_{i,j-\frac{1}{2}} (P_{wi,j} - P_{wi,j-1}) (Saltc)_{i,j}$$

$$\Delta x_i h/\Delta y_j \tag{E-13}$$

$$\frac{dM_{salt}}{dt} \simeq \frac{(M_{salt})^{n+1}_{i,j} - (M_{salt})^{n}_{i,j}}{\Delta t_{n+1}} \tag{E-14}$$

Combining equations (E-11), (E-12), (E-13), and (E-14) a difference equation is obtained that allows use of known values of the dependent variable M_{salt} at a time level n to be used to determine the as yet unknown value of the dependent variable at time level n+1.

$$(M_{salt})^{n+1}_{i,j} = (M_{salt})^{n}_{i,j} + \Delta t_{n+1} \, (IN_{salt} - OUT_{salt})^{n}_{i,j} \pm$$

$$(\dot{M}_{salt})^{n}_{i,j} \, \Delta t_{n+1} \qquad \text{(E-15)}$$

The salt concentration in salt mass per unit water volume for the grid block (i,j) can be written as follows:

$$(Saltc)^{n+1}_{i,j} = \frac{(M_{salt})^{n+1}_{i,j}}{\Delta x_i \Delta y_j h \phi_{i,j} S^{n+1}_{wi,j}} \qquad \text{(E-16)}$$

Since salt enters and leaves the system via source terms, all exterior grid boundaries are treated as impermeable barriers. The computer program developed in this work is capable of utilizing any arbitrary initial salt concentration distribution.

In equation (E-15), known quantities are represented by the right hand side of the equation. Since one such equation exists for each grid block, there is a total of

$$N = I \times J$$

equations. The set of equations which arise at each time step is solved explicitly.

Voltage Distribution

Before formulating the finite difference scheme for the electric flow equation, let us consider the order of magnitude of the charge density. According to equation (27), the continuity relation between current density and charge density is

$$\nabla \cdot \tilde{J} = - \frac{\partial \rho_c}{\partial t} \qquad \text{(E-17)}$$

From Maxwell's equation (28,57)

$$\nabla \cdot D = \rho_c, \text{ and from } D = \varepsilon E$$

$$\nabla \cdot E = \frac{\rho_c}{\varepsilon} \qquad \text{(E-18)}$$

But $\tilde{J} = \sigma \tilde{E}$ so that (E-18) becomes

$$\nabla \cdot \tilde{J} = \frac{\rho \sigma}{\varepsilon} \qquad \text{(E-19)}$$

From (E-17) and (E-19) it follows that

$$\frac{\partial \rho_c}{\partial t} + \frac{\sigma}{\varepsilon} \rho_c = 0 \qquad \text{(E-20)}$$

A solution of this equation is

$$\rho_c = \rho_{cinitial} \, \bar{e}^{\,(\sigma/\varepsilon)t} \qquad \text{(E-21)}$$

as may be readily verified by taking the first diravative with respect to time and substituting in (E-20).

Let us put

$$\tilde{T}_r = \frac{\varepsilon}{\sigma}$$

The quantity $\tilde{T}_r$ is called the relaxation time.

In a perfect dielectric $\sigma = 0$ so that $\tilde{T}_r$ is infinite. Hence the charge maintains its original density indefinitely. On the other hand, for a conducting porous medium for which $\sigma = 0.04$ mhos per meter and $\varepsilon = 4.2 \times 10^{-11}$ farad per meter (see Part III for details), we find that

$$\tilde{T}_r = 1.05 \times 10^{-9} \text{ seconds}$$

The result of the short relaxation time is that the porous medium cannot maintain a charge configuration for long. It should be emphasized that the porous medium, under a high frequency A.C. current will behave as a dielectric. The exponential term in (E-21) becomes so very small in such a short time that its effect is soon practically negligible. According to the foregoing discussion equation (29) can be written as the form:

$$\frac{\partial}{\partial x}\left(\sigma\frac{\partial \psi}{\partial x}\right) + \frac{\partial}{\partial y}\left(\sigma\frac{\partial \psi}{\partial y}\right) = 0 \qquad \text{(E-23)}$$

Equation (E-23) can be discretized to yield the finite difference equation:

$$(\sigma)_{i+\frac{1}{2},j}(\psi_{i+1,j} - \psi_{i,j})/(\Delta x_i)^2 - (\sigma)_{i-\frac{1}{2},j}(\psi_{i,j} - \psi_{i-1,j})/(\Delta x_i)^2 + (\sigma)_{i,j+\frac{1}{2}}(\psi_{i,j+1} - \psi_{i,j})/(\Delta y_j)^2 - (\sigma)_{i,j-\frac{1}{2}}(\psi_{i,j} - \psi_{i,j-1})/(\Delta y_j)^2 = 0 \qquad \text{(E-24)}$$

Since electric current enters and leaves the system via source terms, all exterior grid boundaries are treated as insulating barriers

and equation (E-24) can be modified to account for the current source term yielding:

$$(\sigma)_{i+\frac{1}{2},j}\ (\psi_{i+1,j} - \psi_{i,j})/(\Delta x_i)^2 - (\sigma)_{i-\frac{1}{2},j}\ (\psi_{i,j} - \psi_{i-1,j})/(\Delta x_i)^2 + (\sigma)_{i,j+\frac{1}{2}}\ (\psi_{i,j+1} - \psi_{i,j})/(\Delta y_j)^2 - (\sigma)_{i,j-\frac{1}{2}}\ (\psi_{i,j} - \psi_{i,j-1})/(\Delta_j)^2 + \tilde{I} = 0 \qquad \text{(E-25)}$$

Equation (E-25) can be simplified in form to yield:

$$A_{xi,j}\psi_{i-1,j} + A_{yi,j}\psi_{i,j-1} + B_{xi,j}\psi_{i,j} + C_{xi,j}\psi_{i+1,j} + C_{yi,j}\psi_{i,j+1} = D_{xi,j} \qquad \text{(E-26)}$$

where: $\tilde{I}$ = Amps/unit volume

$$A_{xi,j} = (\sigma)_{i-\frac{1}{2},j}/(\Delta x_i)^2$$

$$A_{yi,j} = (\sigma)_{i,j-\frac{1}{2}}/(\Delta y_j)^2$$

$$C_{xi,j} = (\sigma)_{i+\frac{1}{2},j}/(\Delta x_i)^2$$

$$C_{yi,j} = (\sigma)_{i,j+\frac{1}{2}}/(\Delta y_j)^2$$

$$B_{xi,j} = -(A_{xi,j} + A_{yi,j} + C_{xi,j} + C_{yi,j})$$

$$D_{xi,j} = -\tilde{I}$$

In equation (E-25) known quantities are represented by the right hand side and the coefficients in the left hand side of the equation. Since one such equation arises for each grid block there is a total of

$$N = I \times J$$

equations. The set of equations is solved by successive over-relaxation. To obtain a value of the iteration parameter, $\tilde{\omega}$, which would produce near optimum rates of convergence, a series of computer runs were made using selected values of $\tilde{\omega}$ between 1 and 2. The number of iterations needed to reach a specified tolerance (0.01) was determined and plotted versus the value of $\tilde{\omega}$ at which the minimum occurred was selected for use. For the system studied, $\tilde{\omega}$ was found to be $\simeq 1.65$.

The value of the current source term is adjusted to yield the specified e.m.f. between the current electrodes by using linear interpolation between values of the current source term, i.e. two different values of the current source term give two different values for the e.m.f. applied (resistance of the system is considered constant during each time step), the current source term which corresponds to a specific e.m.f. at the current electrodes is calculated by linear interpolation between the previously calculated electric potential. Once the correct current source term has been specified, computation for the voltage distribution in the system is begun.

The power dissipated in any grid block due to electric current flow is calculated according to the equation:

$$(Hgen)_{i,j} = \tilde{I}^2 R_r \quad (3.413) \qquad \text{(E-27)}$$

The power factor is assumed to be equal to unity

$(Hgen)_{i,j}$: is the heat generation term in B.T.U. per hour in the element (i,j).

$\tilde{I}$: Total current flowing in the element, amps.

Temperature Distribution

Comparison of equations (14) or (15) with equation (31) shows that they are similar except for the presence of the convective transport term of equation (31). It has been reported by Spillette (59) that if finite difference approximations of the type applied to equations (14) and (15) are utilized when solving equation (31), the conduction term is very small and the convective term dominates the equation, causing artificial numerical dispersion. Davidson (39) has pointed out that the convective transport term dominates the temperature equation under high flow rates. As Fayers (60) has pointed out, this implies that the temperature equation is nearly hyperbolic; and implicit numerical computation schemes for systems of hyperbolic equations are stable and convergent (42, 61, 62). One further observation may be drawn regarding the validity of applying conventional finite difference approximations to the convective transport term. Figure 66, shows the directions of fluid flow into and out of the grid block (i,j) in a 15 x 15 grid mesh. Values of pressure in the grid block and the adjoining blocks are obtained from a computer run for solving the fluid flow equations for the system. It is clear that fluid flows into the grid block from three adjoining blocks and out of the block to the fourth adjoining block.

The net heat transfer by convection for the block (i,j) can be written as follows:

$$(Q_{convection})_{i,j} = \{(\rho C)_{i-1,j} V_{i-\frac{1}{2}} T_{i-1,j} + (\rho C)_{i,j+1} V_{i,j+\frac{1}{2}} T_{i,j+1} + (\rho C)_{i,j-1} V_{i,j-\frac{1}{2}} T_{i,j-1}\} - \{(\rho C)_{i,j} V_{i+\frac{1}{2},j} T_{i,j}\} \quad \text{(E-2)}$$

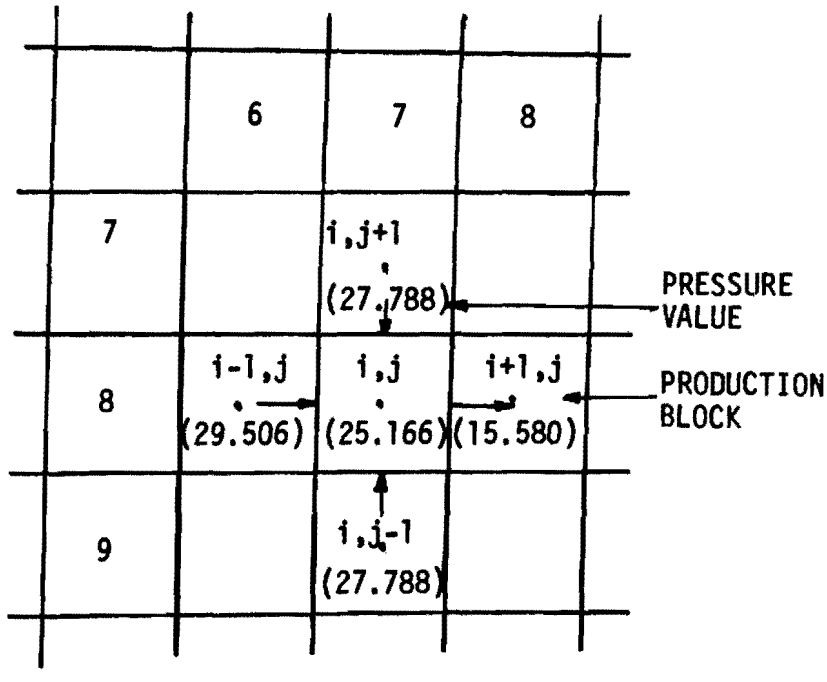

FIGURE 66. PART OF A 15 X 15 GRID MESH SHOWING DIRECTIONS OF FLUID FLOW INTO AND OUT OF GRID BLOCK (i,j)

which describes the net heat transfer by convection for that block in terms of the temperature of the three adjoining blocks from which fluid flow into the block under consideration. Let us consider discretization of the convective term in equation (31) for the grid block (i,j) and compare the obtained expression with the expression in (E-27). The convective transport term can be written in the form:

$$Q_{convection} = \left[\rho C \frac{\partial}{\partial x} (V_x T) + \rho C \frac{\partial}{\partial y} (V_y T)\right] dx$$

Discretizing the above expression yields:

$$(Q_{convection})_{i,j} = \left[(\rho C)_{i,j} (V_{i+1,j} T_{i+1,j} - V_{i,j} T_{i,j}) + (\rho C)_{i,j} (V_{i,j+1} T_{i,j+1} - V_{i,j} T_{i,j})\right] \quad \text{(E-28)}$$

Comparing the expressions in (E-27) and (E-28), shows that the expression in (E-27) describes the convective term for the grid block (i,j) more precisely than the expression in (E-28) does.

Equation (31) can be discretized, with the convective transport term evaluated as in (E-27), to yield the following difference equation:

$$\frac{(Q_{convection})^{n+1}_{i,j}}{\Delta x_i} = \frac{(\rho C)^{n+1}_{i,j} T^{n+1}_{i,j} - (\rho C)^{n}_{i,j} T^{n}_{i,j}}{\Delta t_{n+1}}$$

$$= (K_{te})^{n+1}_{i+\frac{1}{2},j} (T_{i+1,j} - T_{i,j})^{n+1} / (\Delta x_i)^2 - (K_{te})^{n+1}_{i-\frac{1}{2},j} (T_{i,j} - T_{i-1,j})^{n+1} / (\Delta x_i)^2 + (K_{te})_{i,j+\frac{1}{2}} (T_{i,j+1} - T_{i,j})^{n+1} / (\Delta y_j)^2 - (K_{te})_{i,j-\frac{1}{2}} (T_{i,j} - T_{i,j-1})^{n+1} / (\Delta y_j)^2 + \frac{\dot{q}^{n+1}_{i,j}}{\Delta x_i \Delta y_j h} + \frac{\dot{S}^{n}_{i,j}}{\Delta x_i \Delta y_j h} + \quad \text{(E-29)}$$

where:

$$(\rho C)_{i,j} = \{(\rho_o S_o C_o + \rho_w S_w C_w) + \rho_r C_r (1 - \phi)\}_{i,j}$$

Equation (E-29) can be arranged to yield:

$$(K_{te})^{n+1}_{i+\frac{1}{2},j} T^{n+1}_{i+1,j} + (K_{te})^{n+1}_{i-\frac{1}{2},j} T^{n+1}_{i-1,j} + (K_{te})^{n+1}_{i,j+\frac{1}{2}} T^{n+1}_{i,j+1} +$$

$$(K_{te})^{n+1}_{i,j-\frac{1}{2}} T_{i,j-1} - \{ (K_{te})_{i+\frac{1}{2},j} + (K_{te})_{i-\frac{1}{2},j} + (K_{te})_{i,j+\frac{1}{2}} +$$

$$(K_{te})_{i,j-\frac{1}{2}} + \frac{(\Delta x_i)^2}{\Delta t_{n+1}} (\rho C)_{i,j} \}^{n+1} T^{n+1}_{i,j} = -\{ (\rho C)^n_{i,j} \frac{(\Delta x_i)^2}{\Delta t_{n+1}} T^n_{i,j} +$$

$$\frac{\dot{q}_{i,j} (\Delta x_i)^2}{\Delta x_i \Delta y_{ih}} + \frac{(Q_{convection})^{n+1}_{i,j}}{\Delta x_i} (\Delta x_i)^2 + \frac{\dot{S}^n_{i,j}}{\Delta x_i \Delta y_j h} (\Delta x_i)^2 \qquad \text{(E-30)}$$

Equation (E-30) can be simplified in form to yield:

$$A^{n+1}_{yi,j} T^{n+1}_{i,j-1} + A^{n+1}_{xi,j} T^{n+1}_{i-1,j} + B^{n+1}_{xi,j} T^{n+1}_{i,j} + C^{n+1}_{xi,j} T^{n+1}_{i+1,j} +$$

$$C^{n+1}_{yi,j} T^{n+1}_{i,j+1} = D_{xi,j} \qquad \text{(E-31)}$$

where

$$A_{yi,j} = (K_{te})^{n+1}_{i,j-\frac{1}{2}}$$

$$A_{xi,j} = (K_{te})^{n+1}_{i-\frac{1}{2},j}$$

$$C_{xi,j} = (K_{te})^{n+1}_{i+\frac{1}{2},j}$$

$$C_{yi,j} = (K_{te})^{n+1}_{i,j+\frac{1}{2}}$$

$$B_{xi,j} = -\{ + A_{xi,j} + C_{xi,j} + A_{yi,j} + C_{yi,j} + \frac{(\Delta x_i)^2}{\Delta t_{n+1}} (\rho C)^{n+1}_{i,j}\}$$

$$D_{xi,j} = -\{(\rho C)^{n}_{i,j} \frac{(\Delta x_i)^2}{\Delta t_{n+1}} T^{n}_{i,j} + \frac{\dot{q}^{n+1}_{i,j}}{h} + \frac{\dot{S}^{n}_{i,j}}{h} +$$

$$(\Delta x_i)\ (Q_{convection})^{n+1}_{i,j}\ \} \qquad (\Delta x_i = \Delta y_i)$$

Equation (E-30) is in the same form as equation (E-7).

Calculation of the Heat Loss Term

Let k denote grid location in the vertical direction (adjacent stratum); L denotes the number of grid blocks, and ΔZ denotes the grid spacing. Discretization of equation (32) yields:

$$\frac{1}{\Delta Z_k} = \left(\frac{T^{n+1}_{ak+1} - T^{n+1}_{ak}}{\frac{\Delta Z_{k+1} + \Delta Z_k}{2}}\right) - \left(\frac{T^{n+1}_{ak} - T^{n+1}_{ak-1}}{\frac{\Delta Z_k + \Delta Z_{k-1}}{2}}\right) = \frac{\rho_r C_r}{K_{ta}} \left(\frac{T^{n+1}_{ak} - T^{n}_{ak}}{\Delta t_{n+1}}\right) \qquad \text{(E-32)}$$

$k = 1, 2, 3, \ldots\ldots, L$

Equation (E-32) can be simplified in form to yield:

$$A_k T^{n+1}_{ak-1} + B_k T^{n+1}_{ak} + C_k T^{n+1}_{ak+1} = D_k \qquad \text{(E-33)}$$

where:

$$A_k = 2/(\Delta Z_{k-1} + \Delta Z_k)\ \Delta Z_k$$

$$C_k = 2/(\Delta Z_{k+1} + \Delta Z_k)\ \Delta Z_k$$

$$B_k = -A_k - C_k - \frac{\rho_r C_r}{K_{ta}(\Delta t_{n+1})}$$

$$D_k = -\frac{\rho_r C_r\ T^n_{ak}}{K_{ta}\ \Delta t_{n+1}}$$

For grid block #1, $T_{ak-1} = T_{i,j}$. For grid block #L, $T_{ak+1} = T_{initial}$.

Equation (E-33) is solved for each grid block (i,j) for the evaluation of the temperature derivative $\frac{\partial T_a}{\partial Z} \Big| Z = h$

$$\frac{\partial T_a}{\partial Z} \Big| Z = h = \frac{T^n_{i,j} - T^n_{a,k=1}}{\Delta Z_{,k=1}}$$

The heat loss term is evaluated once the temperature derivative $\frac{\partial T_a}{\partial Z} \Big| Z = h$ is determined, according to the expression given in Part III.

Equation (E-34) relates the temperature at a point to the four nearest grid blocks. Equations for the boundaries can be written in the same way described in the discretization of the fluid flow equations. Since one such equation exists for each grid block, there is a total of

$$N = I \times J$$

equations in the N unknown temperatures. One such set arises each time step. The set of equations is solved by successive over-relaxation. The iteration parameter, $\tilde{\omega}$, was determined by the same method discussed in the solution of the electric flow equation. For the system studies, $\tilde{\omega}$ was found to be $\simeq 1.7$.

APPENDIX F

SUMMARY OF EXPERIMENTAL AND CALCULATED DATA

TABLE VI

EXPERIMENT 1

Measured Voltage:

Electrodes	Electric Potential Difference, Volts
1 and 2	13.0
2 and 3	9.5
3 and 4	8.5
4 and 5	10.5
5 and 6	14.5
6 and 7	12.5
7 and 8	29.5
8 and 9	15.5
7 and 10	19.0
10 and 11	12.0

Electric Potential Calculated from Above Data:

Electrode	Electric Potential, Volts
1	26.0
2	39.0
3	48.5
4	57.0
5	67.0
6	81.5
7	94.0
8	64.5
9	49.5
10	75.0
11	63.0

TABLE VII

MEASURED TEMPERATURE

EXPERIMENT 1

Thermocouple Number	Temperature Recorder Reading, m.v	Temperature, °F
1	3.8	154
2	1.9	89
3	1.7	81
4	1.7	81
5	1.9	89
6	1.7	81
7	1.7	81
8	1.7	81
9	1.9	89
10	1.8	85
11	1.7	81
12	1.65	80

Duration of heating = 4 minutes

TABLE VIII

EXPERIMENT 2

Measured Voltage:

Electrodes	Electric Potential Difference, Volts
1 and 2	13.0
2 and 3	9.5
3 and 4	8.0
4 and 5	9.5
5 and 6	14.0
6 and 7	11.0
7 and 8	30.0
8 and 9	14.0
7 and 10	18.0
10 and 11	13.0

Electric Potential Calculated from Above Data:

Electrode	Electrical Potential, Volts
1	28.0
2	41.0
3	50.5
4	58.5
5	68.0
6	82.0
7	93.0
8	63.0
9	49.0
10	75.0
11	62.0

TABLE IX

MEASURED TEMPERATURE

EXPERIMENT 2

Thermocouple Number	Temperature Recorder Reading, m.v.	Temperature °F
1	4.55	184
2	2.00	97
3	1.65	85
4	1.65	85
5	1.95	96
6	1.65	85
7	1.60	83
8	1.69	85
9	2.00	97
10	1.82	91
11	1.60	83
12	1.50	80

Duration of heating = 7 minutes

TABLE X

EXPERIMENT 3

Measured Voltage:

Electrodes	Electric Potential Difference, Volts
1 and 2	11.0
2 and 3	7.0
3 and 4	6.0
4 and 5	7.0
5 and 6	11.0
6 and 7	17.0
7 and 8	30.0
8 and 9	10.0
7 and 10	22.5
10 and 11	8.0

Electric Potential Calculated from Above Data:

Electrode	Electric Potential, Volts
1	34.0
2	45.0
3	52.0
4	58.0
5	65.0
6	76.0
7	93.0
8	63.0
9	53.0
10	70.5
11	62.5

TABLE XI

MEASURED TEMPERATURE

EXPERIMENT 3

Thermocouple Number	Temperature Recorder Reading, m.v.	Temperature °F
1	3.50	142.0
2	1.80	85.0
3	1.70	82.0
4	1.70	82.0
5	1.80	85.0
6	1.70	82.0
7	1.70	82.0
8	1.73	82.4
9	1.80	85.0
10	1.78	84.5
11	1.70	82.0
12	1.65	80.0

Duration of heating = 4.5 minutes

TABLE XII

POROUS MEDIUM AND OPERATING CHARACTERISTICS

EXPERIMENT 4

Porosity, fraction	0.379
Permeability, darcy	11.500
Pore Volume, c.c.	4,700.000
Initial Oil in Place, c.c.	4,060.000
Operating Temperature, °F	80.000
Oil Viscosity @ 80 °F, cp.	12.000
Initial Oil Saturation, Fractional Pore Volume	0.860
Initial Water Saturation, Fractional Pore Volume	0.136
Water Injection Rate in Model, c.c./min.	80.000

TABLE XIII

OIL RECOVERY BY COLD WATERFLOOD

EXPERIMENT 4

Volume Water Injected, c.c.	Cumulative Water Injected Fractional Pore Volume	Volume Oil Produced, c.c.	Cumulative Oil Produced, Fractional I.O.I.P.
1490.0	0.32	1490	0.367
100.0	0.34	70	0.384
110.0	0.36	60	0.400
100.0	0.38	48	0.411
100.0	0.40	42	0.420
100.0	0.43	39	0.430
100.0	0.45	32	0.440
101.0	0.47	30	0.446
105.0	0.49	27	0.453
102.0	0.51	26	0.455
105.0	0.53	24	0.465
101.5	0.56	23	0.471
100.0	0.58	20	0.476
102.0	0.60	20	0.480
103.0	0.62	19	0.485
101.5	0.64	19	0.490
106.0	0.67	19	0.494
103.5	0.69	18	0.500
102.0	0.71	16	0.503
103.0	0.73	15	0.507
123.5	0.76	17	0.511
100.0	0.78	14	0.515
102.0	0.80	13	0.518
102.0	0.82	13	0.522
101.0	0.84	12	0.525
100.0	0.86	12	0.528
100.0	0.88	11	0.531
104.0	0.91	10	0.533
108.0	0.93	10	0.536
130.0	0.96	16	0.538
103.0	0.98	10	0.542
102.0	1.00	9	0.545
100.0	1.02	8	0.547
100.0	1.04	8	0.550
100.0	1.07	8	0.551
100.0	1.09	8	0.553
105.0	1.11	8	0.555

TABLE XIII

OIL RECOVERY BY COLD WATERFLOOD

EXPERIMENT 4

(Continued)

Volume Water Injected, c.c.	Cumulative Water Injected Fractional Pore Volume	Volume Oil Produced, c.c.	Cumulative Oil Produced, Fractional I.O.I.P.
100.0	1.13	8	0.557
100.0	1.15	8	0.559
317.0	1.22	21	0.564
502.0	1.33	35	0.573
520.0	1.44	37	0.582
510.0	1.55	36	0.591
505.0	1.65	34	0.600
500.0	1.76	34	0.610
500.0	1.86	32	0.615
520.0	1.98	32	0.623
550.0	2.09	33	0.630
540.0	2.20	33	0.640
560.0	2.33	34	0.648
505.0	2.43	30	0.655
500.0	2.54	20	0.660
505.0	2.65	18	0.664
500.0	2.75	18	0.668
500.0	2.86	16	0.670
500.0	2.97	14	0.676

TABLE XIV

OIL RECOVERY BY THE ELECTROTHERMIC TECHNIQUE

EXPERIMENT 5

Volume Water Injected, c.c.	Cumulative Water Injected Fractional Pore Volume	Volume Oil Produced, c.c.	Cumulative Oil Produced, Fractional I.O.I.P.
1500	0.32	1500	0.370
480	0.42	175	0.410
490	0.53	145	0.450
500	0.63	96	0.472
510	0.74	134	0.505
475	0.84	102	0.530
500	0.95	109	0.556
520	1.06	80	0.576
490	1.16	78	0.595
475	1.26	78	0.615
500	1.37	76	0.634
500	1.48	80	0.653
505	1.58	80	0.673
510	1.69	80	0.692
520	1.80	70	0.710
470	1.90	55	0.720
485	2.01	30	0.730
490	2.11	20	0.736
500	2.22	20	0.741
475	2.32	15	0.744
500	2.42	10	0.747
500	2.53	10	0.749
505	2.64	9	0.751
485	2.74	9	0.754
520	2.85	9	0.756
550	2.97	10	0.759
500	3.10	9	0.761

TABLE XV

EXPERIMENT 5

Measured Voltage:

Electrodes	Electric Potential Difference, Volts
1 and 2	7
2 and 3	32
3 and 4	21
4 and 5	33
5 and 6	7
6 and 7	2
7 and 8	11
8 and 9	52
7 and 10	5
10 and 11	8

Electric Potential Calculated from Above Data:

Electrode	Electric Potential, Volts
1	5
2	12
3	44
4	65
5	98
6	105
7	107
8	96
9	44
10	102
11	94

Duration of Heating equals 0.15 minutes

TABLE XVI

EXPERIMENT 5

Measured Voltage:

Electrodes	Electric Potential Difference, Volts
1 and 2	11
2 and 3	25
3 and 4	10
4 and 5	25
5 and 6	11
6 and 7	5
7 and 8	19
8 and 9	32
7 and 10	9
10 and 11	12

Electric Potential Calculated from Above Data:

Electrode	Electric Potential, Volts
1	14
2	25
3	50
4	60
5	85
6	96
7	101
8	82
9	50
10	92
11	80

Duration of Heating Equals 9.5 minutes

TABLE XVII

EXPERIMENT 5

Measured Voltage:

Electrodes	Electric Potential Difference, Volts
1 and 2	13
2 and 3	18
3 and 4	8
4 and 5	18
5 and 6	13
6 and 7	9
7 and 8	24
8 and 9	25
7 and 10	13
10 and 11	16

Electric Potential Calculated from Above Data:

Electrode	Electric Potential, Volts
1	20
2	33
3	51
4	59
5	77
6	90
7	99
8	75
9	50
10	86
11	70

Duration of Heating equals 29.5 minutes

TABLE XVIII

MEASURED TEMPERATURE

EXPERIMENT 5

Thermocouple Number	Temperature Recorder Reading, m.v.	Temperature °F
1	5.20	208
2	4.50	185
3	3.30	144
4	3.10	138
5	5.10	205
6	3.20	142
7	3.15	140
8	3.00	137
9	4.60	189
10	4.20	175
11	3.00	135
12	2.50	120

Duration of heating = 30 minutes

TABLE XIX

MEASURED TEMPERATURE

EXPERIMENT 5

Thermocouple Number	Temperature Recorder Reading, m.v.	Temperature °F
1	1.30	80
2	1.75	96
3	3.35	150
4	3.40	152
5	1.40	83
6	2.85	135
7	3.25	147
8	3.40	152
9	1.80	97
10	2.60	124
11	3.70	160
12	3.50	155

Duration of Cold Water Injection = 34.5 minutes

TABLE XX

CALCULATED OIL RECOVERY BY COLD WATERFLOOD

RUN 4

Cumulative Water Injected c.c.	Cumulative Water Injected Fractional Pore Volume	Cumulative Oil Produced c.c.	Cumulative Oil Produced Fractional I.O.I.P.
2892	0.310	2892	0.360
3024	0.320	2987	0.370
5555	0.590	3802	0.470
7549	0.810	4159	0.510
8806	0.940	4318	0.530
10246	1.090	4476	0.550
11564	1.230	4601	0.570
12643	1.350	4694	0.580
13601	1.450	4770	0.590
14560	1.550	4841	0.600
15878	1.690	4932	0.610
15491	1.754	4972	0.612
17210	1.830	5017	0.618
18290	1.946	5081	0.626
20208	2.150	5186	0.639
22365	2.380	5290	0.650
25671	2.625	5393	0.664

TABLE XXI

CALCULATED WATER SATURATION AT BREAKTHROUGH

RUN 4

Grid Location, Y-Direction	Grid Location, X-Direction 1	2	3	4	5	6	7	8
1	85.0	72.8	64.2	57.2	51.9	42.9	33.5	13.6
2	72.8	67.3	60.6	56.0	51.5	42.8	33.3	13.6
3	64.2	60.6	57.5	54.6	51.0	43.0	33.3	13.6
4	57.2	56.0	54.6	53.2	50.65	43.6	33.8	13.6
5	51.9	51.5	51.0	50.6	50.4	45.0	35.7	13.6
6	42.9	42.8	43.0	43.6	45.0	48.6	41.8	28.5
7	33.5	33.3	33.3	33.8	35.7	41.8	44.8	39.7
8	13.6	13.6	13.6	13.6	13.6	28.5	39.7	37.8

TABLE XXII

CALCULATED WATER SATURATION DISTRIBUTION

RUN 4

Grid Location, Y-Direction	Grid Location, X-Direction							
	1	2	3	4	5	6	7	8
1	85.0	85.0	80.3	72.2	67.5	62.0	58.9	58.0
2	85.0	83.7	77.3	70.8	67.0	62.0	58.9	58.0
3	80.3	77.3	72.7	69.4	66.5	61.8	58.9	58.0
4	72.2	70.8	69.4	68.0	65.7	61.5	58.9	58.0
5	67.5	67.0	66.5	65.75	64.0	61.0	58.9	58.0
6	62.0	62.0	61.8	61.5	61.0	60.0	59.0	58.0
7	58.9	58.9	58.9	58.9	58.9	58.8	58.4	58.0
8	58.0	58.0	58.0	58.0	58.0	58.0	58.0	58.0

Cumulative water injected = 1.69 pore volumes

TABLE XXIII

CALCULATED ELECTRIC POTENTIAL DISTRIBUTION, VOLTS

RUN 1

Grid Location, Y-Direction	Grid Location, X-Direction 1	2	3	4	5	6	7	8
1	110.0	96.4	86.0	77.4	71.0	65.0	60.0	55.0
2	96.4	90.0	82.0	75.5	69.5	64.0	59.5	55.0
3	86.0	82.0	77.4	72.0	68.0	63.0	59.0	55.0
4	77.4	75.5	72.0	69.0	65.0	62.0	58.0	55.0
5	71.0	69.5	68.0	65.0	63.0	60.0	57.5	55.0
6	65.0	64.0	63.0	62.0	60.0	58.0	56.6	55.0
7	60.0	59.5	59.0	58.0	57.5	56.6	55.8	55.0
8	55.0	55.0	55.0	55.0	55.0	55.0	55.0	55.0

Duration of heating = 4 minutes

TABLE XXIV

CALCULATED TEMPERATURE DISTRIBUTION, °F

RUN 1

Grid Location, Y-Direction	1	2	3	4	5	6	7	8
1	181.0	117.0	95.0	87.4	84.4	83.0	82.4	82.1
2	117.0	104.0	93.0	87.6	85.0	83.0	82.0	81.9
3	95.0	93.0	90.0	86.4	84.0	83.0	82.0	81.5
4	87.4	87.6	86.4	85.0	83.3	82.0	81.5	81.0
5	84.4	85.0	84.0	83.3	82.0	81.6	81.0	80.6
6	83.0	83.0	83.0	82.0	81.6	81.0	80.6	80.3
7	82.4	82.0	82.0	81.5	81.0	80.6	80.3	80.1
8	82.1	81.9	81.5	81.0	80.6	80.3	80.1	80.0

TABLE XXV

CALCULATED ELECTRIC POTENTIAL DISTRIBUTION, VOLTS

RUN 2

Grid Location, Y-Direction	1	2	3	4	5	6	7	8
1	110.0	97.5	88.0	80.0	72.0	66.0	60.4	55.0
2	97.5	92.0	84.5	78.0	71.0	65.0	60.1	55.0
3	88.0	84.5	79.5	74.0	69.0	64.0	59.5	55.0
4	80.0	78.0	74.0	70.0	66.0	62.5	58.7	55.0
5	72.0	71.0	69.0	66.0	64.0	61.0	57.8	55.0
6	66.0	65.0	64.0	62.5	61.0	59.0	57.0	55.0
7	60.4	60.1	59.5	58.7	57.8	57.0	55.9	55.0
8	55.0	55.0	55.0	55.0	55.0	55.0	55.0	55.0

TABLE XXVI

CALCULATED TEMPERATURE DISTRIBUTION, °F

RUN 2

Grid Location, Y-Direction	Grid Location, X-Direction							
	1	2	3	4	5	6	7	8
1	199.0	161.0	118.0	98.0	90.0	87.0	85.0	84.7
2	161.0	134.0	111.0	98.0	91.0	87.0	85.2	84.2
3	118.0	111.0	102.0	94.0	89.5	86.0	84.5	83.4
4	98.0	98.0	94.0	91.0	87.5	85.0	83.4	82.4
5	90.0	91.0	89.5	87.5	85.0	84.0	82.4	81.5
6	87.0	87.0	86.0	85.0	84.0	82.5	81.5	80.8
7	85.0	85.2	84.5	83.4	82.4	81.5	80.8	80.4
8	84.7	84.2	83.4	82.4	81.5	80.8	80.4	80.3

Duration of heating = 7 minutes

TABLE XXVII

CALCULATED ELECTRIC POTENTIAL DISTRIBUTION, VOLTS

RUN 3

Grid Location, Y-Direction	Grid Location, X-Direction							
	1	2	3	4	5	6	7	8
1	110.0	94.0	82.0	74.0	68.0	63.5	59.1	55.0
2	94.0	86.0	79.0	73.0	67.0	63.0	58.8	55.0
3	82.0	79.0	74.0	70.0	66.0	62.0	58.4	55.0
4	74.0	73.0	70.0	67.0	64.0	61.0	57.8	55.0
5	68.0	67.0	66.0	64.0	61.5	59.0	57.1	55.0
6	63.5	63.0	62.0	61.0	59.0	58.0	56.4	55.0
7	59.1	58.8	58.4	57.8	57.1	56.4	55.6	55.0
8	55.0	55.0	55.0	55.0	55.0	55.0	55.0	55.0

TABLE XXVIII

CALCULATED TEMPERATURE DISTRIBUTION, °F

RUN 3

Grid Location, Y-Direction	Grid Location, X-Direction 1	2	3	4	5	6	7	8
1	168.0	132.0	97.0	86.0	83.0	82.0	81.8	81.6
2	132.0	107.0	92.0	86.0	84.0	82.0	81.7	81.4
3	97.0	92.0	88.0	85.0	83.0	82.0	81.5	81.1
4	86.0	86.0	85.0	84.0	82.5	82.0	81.1	80.8
5	83.0	84.0	83.0	82.5	82.0	81.2	80.8	80.5
6	82.0	82.0	82.0	82.0	81.2	80.8	80.5	80.2
7	81.8	81.7	81.5	81.1	80.8	80.5	80.2	80.1
8	81.6	81.4	81.1	80.8	80.5	80.2	80.1	80.1

Duration of heating = 4.5 minutes

TABLE XXIX

OPERATING CHARACTERISTICS FOR COMPUTER RUNS 1, 2, and 3

	RUN 1	RUN 2	RUN 3
Initial Salt Concentration Distribution, p.p.m.	75000	75000	Figure 16
Water Injection Rate, c.c./min.	0	40	40.0
E.M.F. Applied, Volt	110	110	110.0
Length of Heating Period, min.	4	7	4.5

TABLE XXX

CALCULATED SALT CONCENTRATION DISTRIBUTION,

THOUSAND P.P.M.

RUN 5

Grid Location, Y-Direction	Grid Location, X-Direction							
	1	2	3	4	5	6	7	8
1	1.0	1.0	1.0	1.1	1.9	4.5	8.9	16.5
2	1.0	1.0	1.0	1.2	2.3	5.2	9.6	16.5
3	1.0	1.0	1.1	1.5	2.9	5.9	10.1	16.5
4	1.1	1.2	1.5	2.2	3.7	6.6	10.5	16.5
5	1.9	2.3	2.9	3.7	5.1	7.5	10.7	16.5
6	4.5	5.2	5.9	6.6	7.5	9.0	11.2	13.3
7	8.9	9.6	10.1	10.5	10.7	11.2	12.6	14.5
8	16.5	16.5	16.5	16.5	16.5	13.3	14.5	16.5

Duration of fresh water injection = 18.5 minutes

TABLE XXXI

CALCULATED WATER SATURATION DISTRIBUTION

RUN 5

Grid Location, Y-Direction	Grid Location, X-Direction							
	1	2	3	4	5	6	7	8
1	85.0	77.5	69.0	62.0	56.0	50.0	42.0	39.0
2	77.5	71.0	67.0	60.0	55.5	50.0	42.0	39.0
3	36.0	67.0	63.0	59.0	55.0	50.0	43.0	39.0
4	62.0	60.0	59.0	57.0	55.0	50.5	43.0	40.0
5	56.0	55.5	55.0	55.0	59.0	51.0	44.0	41.0
6	50.0	50.0	50.0	50.5	51.0	52.0	46.5	41.0
7	42.0	42.0	43.0	43.0	43.0	44.0	46.5	41.0
8	39.0	39.0	39.0	40.0	41.0	41.0	41.0	45.0

Duration of salt saturated water injection = 14 minutes

TABLE XXXII

CALCULATED ELECTRIC CURRENT AND

POROUS MEDIUM AVERAGE TEMPERATURE

RUN 5

Time, minutes	Electric Current, Amps	Average Temperature, ^{o}F
0	0.88254	80.000
0.17	0.90196	80.087
1.00	1.02264	
1.83	1.14837	80.569
2.67	1.28918	81.728
3.50	1.42919	82.417
4.33	1.59541	83.188
5.17	1.76266	84.048
6.00	1.92541	85.001
6.83	2.08943	86.042
7.67	2.23623	87.159
8.50	2.41043	88.362
9.33	2.58056	89.662
10.33	2.78570	91.324
11.16	2.97062	92.829
12.00	3.16206	94.433
12.83	3.16206	96.140
13.66	3.52804	97.948
14.50	3.70399	99.841
15.33	3.90322	101.828
16.16	4.07446	103.911
17.00	4.24314	106.081
17.83	4.44812	108.352
18.66	4.65671	110.730
19.50	4.86889	113.215
20.33	4.08574	115.808
21.16	5.30898	118.513
22.00	5.53799	121.331
22.83	5.77328	124.265
23.66	6.01191	127.318
24.50	6.26101	130.490
25.33	6.51647	133.786
26.16	6.77680	137.207
27.00	7.03903	140.752
27.83	7.30723	144.426
28.66	7.56831	148.224
29.50	7.86126	152.157
30.33	8.16462	156.230

TABLE XXXIII

CALCULATED ELECTRIC POTENTIAL DISTRIBUTION, VOLTS

RUN 5

Grid Location, Y-Direction	Grid Location, X-Direction 1	2	3	4	5	6	7	8
1	110.0	106.9	104.6	102.5	100.1	95.9	84.0	55.0
2	106.9	105.4	103.7	101.9	99.5	95.2	82.9	55.0
3	104.6	103.7	102.4	100.7	98.2	93.7	81.1	55.0
4	102.5	101.9	100.7	98.8	96.0	91.2	78.7	55.0
5	100.1	99.5	98.2	96.0	92.8	87.3	75.4	55.0
6	95.9	95.2	93.7	91.2	87.3	81.3	70.7	55.0
7	84.0	82.9	81.1	78.7	75.4	70.7	63.6	55.0
8	55.0	55.0	55.0	55.0	55.0	55.0	55.0	55.0

Duration of heating = 0.17 minutes

TABLE XXXIV

CALCULATED SALT CONCENTRATION DISTRIBUTION,

THOUSAND P.P.M.

RUN 5

Grid Location, Y-Direction	Grid Location, X-Direction							
	1	2	3	4	5	6	7	8
1	200	200	198	181	131	64	20	10
2	200	199	192	167	114	53	17	10
3	198	192	177	143	93	43	15	10
4	181	167	143	109	70	34	13	9
5	131	114	93	70	47	26	12	8
6	64	53	43	34	26	17	10	8
7	20	17	15	13	12	10	8	7
8	10	10	10	9	8	8	7	7

Duration of salt saturated water injection = 14.17 minutes

TABLE XXXV

CALCULATED ELECTRIC POTENTIAL DISTRIBUTION, VOLTS

RUN 5

Grid Location, Y-Direction	Grid Location, X-Direction 1	2	3	4	5	6	7	8
1	110.0	102.9	97.7	93.1	88.6	83.3	74.4	55.0
2	102.9	99.6	95.7	91.7	87.5	82.4	73.7	55.0
3	97.7	95.7	92.8	89.3	85.4	80.6	72.4	55.0
4	93.1	91.7	89.3	86.2	82.6	77.95	70.5	55.0
5	88.6	87.5	85.4	82.6	79.0	74.4	67.7	55.0
6	83.3	82.4	80.6	77.95	74.4	70.1	64.2	55.0
7	74.4	73.7	72.4	70.5	67.7	64.2	60.0	55.0
8	55.0	55.0	55.0	55.0	55.0	55.0	55.0	55.0

Duration of heating = 9.33 minutes

TABLE XXXVI

CALCULATED SALT CONCENTRATION DISTRIBUTION,

THOUSAND P.P.M.

RUN 5

Grid Location, Y-Direction	Grid Location, X-Direction 1	2	3	4	5	6	7	8
1	200	200	200	198	186	143	72	26
2	200	200	200	197	182	136	68	24
3	200	200	199	194	175	129	65	24
4	198	197	194	185	164	122	65	25
5	186	182	175	164	145	113	68	30
6	143	136	129	122	113	96	68	40
7	72	68	65	65	68	68	59	48
8	26	24	24	25	30	40	48	46

Duration of salt saturated water injection = 23.33 minutes

TABLE XXXVII

CALCULATED ELECTRIC POTENTIAL DISTRIBUTION, VOLTS

RUN 5

Grid Location, Y-Direction	Grid Location, X-Direction 1	2	3	4	5	6	7	8
1	110.0	99.4	92.7	86.5	80.3	73.5	65.5	55.0
2	99.4	95.2	90.2	84.8	79.1	72.6	65.1	55.0
3	92.7	90.2	86.4	82.0	76.9	71.1	64.3	55.0
4	86.5	84.8	82.0	78.3	73.9	68.8	63.0	55.0
5	80.3	79.1	76.9	73.9	70.2	66.1	61.3	55.0
6	73.5	72.6	71.1	68.8	66.1	62.9	59.4	55.0
7	65.5	65.1	64.3	63.0	61.3	59.4	57.3	55.0
8	55.0	55.0	55.0	55.0	55.0	55.0	55.0	55.0

Duration of heating = 29.5 minutes

TABLE XXXVIII

CALCULATED SALT CONCENTRATION DISTRIBUTION,

THOUSAND P.P.M.

RUN 5

Grid Location, Y-Direction	Grid Location, X-Direction							
	1	2	3	4	5	6	7	8
1	200	200	200	200	200	196	168	108
2	200	200	200	200	200	196	168	108
3	200	200	200	200	200	196	169	110
4	200	200	200	200	199	195	171	115
5	200	200	200	199	199	195	175	127
6	196	196	196	195	195	193	179	144
7	168	168	169	171	175	179	176	160
8	108	108	110	115	127	144	160	159

Duration of salt saturated water injection = 43.5 minutes

TABLE XXXIX

CALCULATED TEMPERATURE DISTRIBUTION, ^{o}F

RUN 5

Grid Location, Y-Direction	Grid Location, X-Direction							
	1	2	3	4	5	6	7	8
1	189	213	205	183	158	142	141	155
2	213	219	208	186	162	145	141	151
3	205	208	198	179	160	144	138	145
4	183	186	179	167	154	141	134	136
5	158	162	160	154	145	135	129	128
6	142	145	144	141	135	129	123	121
7	141	141	138	134	129	123	119	117
8	155	151	145	136	128	121	117	116

Duration of heating period = 29.5 minutes

TABLE XL

CALCULATED TEMPERATURE DISTRIBUTION, ^{o}F

RUN 5

Grid Location, Y-Direction	1	2	3	4	5	6	7	8
1	80	80	84	98	122	144	151	150
2	80	82	89	106	130	149	153	151
3	84	89	101	120	142	155	155	151
4	98	106	120	138	153	160	156	152
5	122	130	142	153	161	162	157	152
6	144	149	155	160	162	161	157	153
7	151	153	155	156	157	157	155	153
8	150	151	151	152	152	153	153	153

Duration of cold water injection after heating = 34.33 minutes

TABLE XLI

CALCULATED TEMPERATURE DISTRIBUTION, ^{o}F

RUN 5

Grid Location, Y-Direction	Grid Location, X-Direction							
	1	2	3	4	5	6	7	8
1	80	80	80	82	88	103	122	135
2	80	80	81	83	91	105	124	136
3	80	81	82	86	94	109	127	138
4	82	83	86	91	100	114	130	140
5	88	91	94	100	109	120	133	141
6	103	105	109	114	120	127	136	142
7	122	124	127	130	133	136	139	142
8	135	136	138	140	141	142	142	142

Duration of cold water injection = 68.66 minutes

TABLE XLII

CALCULATED OIL RECOVERY BY THE ELECTROTHERMIC TECHNIQUE

RUN 5

Cumulative Water Injected c.c.	Cumulative Water Injected Fractional Pore Volume	Cumulative Oil Produced c.c.	Cumulative Oil Produced Fractional I.O.I.P.
5197	0.55	3719	0.46
6023	0.64	3903	0.48
6689	0.71	4038	0.50
7515	0.80	4197	0.52
8315	0.88	4343	0.53
8981	0.96	4464	0.55
10047	1.07	4661	0.57
11406	1.21	4917	0.61
12738	1.36	5147	0.63
13938	1.48	5336	0.66
15535	1.65	5546	0.68
17027	1.81	5696	0.70
18227	1.94	5794	0.71
19292	2.05	5866	0.72
19559	2.08	5883	0.72
21023	2.24	5965	0.73
21982	2.34	6009	0.74
23182	2.46	6056	0.74
24780	2.63	6106	0.75
26511	2.82	6149	0.75

TABLE XLIII

CALCULATED WATER SATURATION DISTRIBUTION

RUN 5

Grid Location, Y-Direction	Grid Location, X-Direction 1	2	3	4	5	6	7	8
1	85.0	85.0	85.0	82.4	78.4	75.0	73.0	72.4
2	85.0	85.0	85.0	82.0	78.0	75.0	73.0	72.5
3	85.0	85.0	84.0	81.0	78.0	75.0	73.5	73.0
4	82.4	82.0	81.0	79.0	77.0	75.5	74.0	73.0
5	78.4	78.0	78.0	77.0	77.0	76.0	74.0	73.0
6	75.0	75.0	75.0	75.5	76.0	76.0	74.0	73.0
7	73.0	73.0	73.5	74.0	74.0	74.0	74.6	74.0
8	72.4	72.5	73.0	73.0	73.0	73.0	74.0	74.0

Cumulative water injected = 2.62 pore volumes

TABLE XLIV

CALCULATED WATER SATURATION DISTRIBUTION

RUN 4

Grid Location, Y-Direction	Grid Location, X-Direction 1	2	3	4	5	6	7	8
1	85.0	85.0	84.5	78.0	71.0	67.0	64.0	62.6
2	85.0	85.0	83.0	76.5	70.0	67.0	64.0	62.6
3	84.5	83.0	79.0	74.0	70.0	67.0	64.0	62.6
4	78.0	76.5	74.0	71.0	69.0	67.0	64.0	62.7
5	71.0	70.0	70.0	69.0	68.0	67.0	64.0	63.0
6	67.0	67.0	67.0	67.0	67.0	66.0	64.0	63.0
7	64.0	64.0	64.0	64.0	64.0	64.0	64.0	63.0
8	62.6	62.6	62.6	62.7	63.0	63.0	63.0	63.0

Cumulative water injected = 2.62 pore volumes